SYRU/DECE/TR-83/2

RADIATION AND SCATTERING FROM ELECTRICALLY SMALL CONDUCTING BODIES OF ARBITRARY SHAPE

by

Ercument Arvas
Roger F. Harrington
Joseph R. Mautz

Department of
Electrical and Computer Engineering
Syracuse University
Syracuse, New York 13210

Technical Report No. 19

January 1983

Contract No. N00014-76-C-0225

Prepared for

DEPARTMENT OF THE NAVY
OFFICE OF NAVAL RESEARCH
ARLINGTON, VIRGINIA 22217

SYRU/DECE/TR-83/2

RADIATION AND SCATTERING FROM ELECTRICALLY SMALL CONDUCTING BODIES OF ARBITRARY SHAPE

by

Ercument Arvas
Roger F. Harrington
Joseph R. Mautz

Department of
Electrical and Computer Engineering
Syracuse University
Syracuse, New York 13210

Technical Report No. 19

January 1983

Contract No. N00014-76-C-0225

Approved for public release; distribution unlimited

Prepared for

DEPARTMENT OF THE NAVY
OFFICE OF NAVAL RESEARCH
ARLINGTON, VIRGINIA 22217

SECURITY CLASSIFICATION OF THIS PAGE (When Data Entered)

REPORT DOCUMENTATION PAGE		READ INSTRUCTIONS BEFORE COMPLETING FORM
1. REPORT NUMBER SYRU/DECE/TR-83/2	2. GOVT ACCESSION NO.	3. RECIPIENT'S CATALOG NUMBER
4. TITLE (and Subtitle) RADIATION AND SCATTERING FROM ELECTRICALLY SMALL CONDUCTING BODIES OF ARBITRARY SHAPE		5. TYPE OF REPORT & PERIOD COVERED Technical Report No. 19 6. PERFORMING ORG. REPORT NUMBER
7. AUTHOR(s) Ercument Arvas Roger F. Harrington Joseph R. Mautz		8. CONTRACT OR GRANT NUMBER(s) N00014-76-C-0225
9. PERFORMING ORGANIZATION NAME AND ADDRESS Dept. of Electrical & Computer Engineering Syracuse University Syracuse, New York 13210		10. PROGRAM ELEMENT, PROJECT, TASK AREA & WORK UNIT NUMBERS
11. CONTROLLING OFFICE NAME AND ADDRESS Department of the Navy Office of Naval Research Arlington, Virginia 22217		12. REPORT DATE January 1983 13. NUMBER OF PAGES 134
14. MONITORING AGENCY NAME & ADDRESS(if different from Controlling Office)		15. SECURITY CLASS. (of this report) UNCLASSIFIED 15a. DECLASSIFICATION/DOWNGRADING SCHEDULE

16. DISTRIBUTION STATEMENT (of this Report)

Approved for public release; distribution unlimited

17. DISTRIBUTION STATEMENT (of the abstract entered in Block 20, if different from Report)

18. SUPPLEMENTARY NOTES

This work was supported in part by the Digital Equipment Corporation, Marlboro, MA 01752

19. KEY WORDS (Continue on reverse side if necessary and identify by block number)

Apertures	Magnetostatic
Electrostatic	Polarizability
Discs	Radiation
Low frequency	Scattering

20. ABSTRACT (Continue on reverse side if necessary and identify by block number)

A simple moment solution is given for low frequency electromagnetic scattering and radiation problems. The problem is reduced to the corresponding electrostatic and magnetostatic problems. Each static problem is then solved using the Method of Moments. The surface of the perfectly conducting scatterer is modeled by a set of planar triangular patches. Pulse expansion functions and point maching testing are used to compute the charge density in the electrostatic problem. For the magnetostatic current a new set of charge-

DD FORM 1 JAN 73 1473 EDITION OF 1 NOV 65 IS OBSOLETE
S/N 0102-014-6601

UNCLASSIFIED
SECURITY CLASSIFICATION OF THIS PAGE (When Data Entered)

20. Abstract (continued)

free vector expansion functions is introduced. The problem is first formulated assuming the scatterer to be in an unbounded homogeneous region. Then the presence of an infinite ground plane is incorporated into the formulation. Scatterers of various shapes, such as the circular disc, the square plate, the sphere, and the cube are studied. Special attention is paid to a conducting box with a narrow slot. The computed results are the scattered fields, the induced charge and current distributions, and the induced electric and magnetic dipole moments. These are in close agreement with whatever published data are available. The electric polarizability of a small aperture in an infinite conducting screen is computed by solving the dual magnetostatic problem of a conducting disc. Five typical aperture shapes including the circle and the ellipse are considered. The results of computations agree well with available exact or measured data.

ABSTRACT

A simple moment solution is given for low frequency electromagnetic scattering and radiation problems. The problem is reduced to the corresponding electrostatic and magnetostatic problems. Each static problem is then solved using the Method of Moments. The surface of the perfectly conducting scatterer is modeled by a set of planar triangular patches. Pulse expansion functions and point matching testing are used to compute the charge density in the electrostatic problem. For the magnetostatic current a new set of charge-free vector expansion functions is introduced. The problem is first formulated assuming the scatterer to be in an unbounded homogeneous region. Then the presence of an infinite ground plane is incorporated into the formulation. Scatterers of various shapes, such as the circular disc, the square plate,the sphere, and the cube are studied. Special attention is paid to a conducting box with a narrow slot. The computed results are the scattered fields, the induced charge and current distributions, and the induced electric and magnetic dipole moments. These are in close agreement with whatever published data are available.

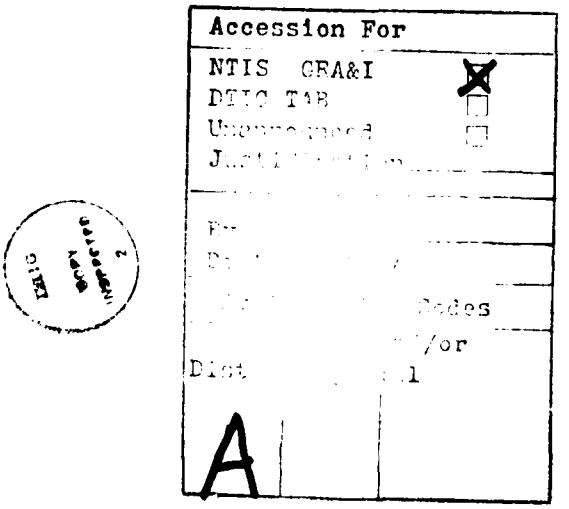

CONTENTS

Chapter 1

INTRODUCTION

Consider an arbitrarily shaped perfectly conducting body illuminated by an incident electromagnetic field ($\underline{E}^i$, $\underline{H}^i$). The problem is to find the scattered field ($\underline{E}^s$, $\underline{H}^s$) in the Rayleigh region. The Rayleigh region is defined [1] to be the range of frequencies for which the maximum dimension d of the body is much smaller than the wavelength λ. It has been shown by Rayleigh [2] that this low frequency scattering problem can approximately be solved by treating the corresponding electrostatic and magnetostatic problems separately. Also, it has been established that a small scatterer [1], (or a small aperture in a perfectly conducting screen [3]) may be approximated by radiating electric and magnetic dipoles. Exact values for the dipole moments are available in the literature only for simple shapes, such as the sphere and the circular or elliptical disc (or aperture)[3]-[6]. An extensive bibliography on the low frequency scattering problem is given in [1].

Our work formulates the electrostatic and the magnetostatic problems separately. An approximate solution is then obtained for each problem using the Method of Moments [7]. In the electrostatic problem an integral equation is solved for the induced charge density on the surface S of the body. Then the induced electric dipole moment is computed from the induced charge distribution. Similarly, in the magnetostatic problem an integral equation is solved for the induced current density on S. The induced magnetic dipole moment is computed using the induced current density.

In principle, this scattering problem can be handled by solving an electric field integral equation for the induced current on S. This is called an E-field solution. However, two static problems require, in general, less effort. Furthermore, although the E-field solutions give accurate results in the resonance region, where d is comparable to λ, they may begin to lose accuracy as the frequency decreases. Recently, Mautz and Harrington [8] have discussed this problem in detail, and have given a new E-field solution for bodies of revolution which gives accurate results in both the resonance region and the Rayleigh region.

The general formulation is presented in Chapter 2. The formulation of the electrostatic problem is known and has been used by various investigators [9]. The approach is to first model the surface S by planar triangular patches and then assume a constant charge density on each patch. An integral equation for the charge density is obtained by using the conditions that the total electrostatic potential on S is a constant and that the total charge is zero. This integral equation is solved approximately by the Method of Moments.

The same triangulated model of S is used in the magnetostatic problem. An integral equation for the induced magnetostatic current is obtained by using the condition that the component of the total magnetic field normal to the surface S is zero . This boundary condition is borrowed from the dynamic problem, but it holds for perfectly diamagnetic (μ =0) bodies in static fields as well. The surface divergence of the induced magnetostatic current must be zero. This is assured by introducing a set of charge-free vector expansion functions for the current.

To compute the scattered fields, space is divided into four regions; very close to the scatterer, the electric field is computed from the induced

charge only, and the magnetic field is computed using the induced current only. At a distance large compared to d, but small compared to λ, the electric field is computed using the static expression for the field of the induced electric dipole, and the magnetic field is computed using the static expression for the field of the induced magnetic dipole. In both of these near-zone cases the electric and magnetic fields are decoupled. For an intermediate region, where the distance from the scatterer is comparable to λ, the exact dynamic expressions are used to compute the fields from both dipoles. In the far-zone region, where the distance from the scatterer is large compared to both d and λ, far-field expressions are used for the dipole fields, and the fields are coupled.

In Chapter 3, the general formulation described in Chapter 2 is applied to various scatterers in free space. Open and closed surfaces are considered. The incident field is taken to be either a plane wave or is assumed to be produced by an oscillating electric or magnetic dipole placed near the scatterer. Special attention is paid to the case where an electric (magnetic) dipole is placed normally (tangentially) on a conducting sphere or on the face of a conducting cube.

Chapter 4 formulates the scattering problem in the presence of an infinite ground plane. In the first part of the chapter, the scatterer is assumed to be above the ground plane. In the remaining part, the special problem of a conducting box on a ground plane is considered.

Chapter 2

GENERAL FORMULATION

In Appendix A we describe how to approximate the problem of low frequency electromagnetic scattering by the corresponding electrostatic and magnetostatic problems. In this chapter we introduce the general procedure for the formulation and solution of these problems separately.

The main objective in an electrostatic problem is to determine the electric charge distribution induced on a perfectly conducting isolated body when it is placed in a specified impressed static electric field. Once the charge density is known, other quantities of interest, such as the induced electric dipole moment and the field produced by the induced charge , can readily be found.

In the magnetostatic part of the problem we are interested in determining the current distribution induced on a perfectly diamagnetic body when it is placed in a static impressed magnetic field. Once the current density is obtained, other related quantities can be solved for easily.

For each problem we obtain a different integral equation and use the Method of Moments to approximate this integral equation by a set of linear algebraic equations. These algebraic equations are then solved by the methods of linear algebra.

2.1. The Electrostatic Problem

The electrostatic problem has been studied extensively and the general formulation of the problem in terms of the Method of Moments is well-established [7,9]. We summarize the formulation here for the sake of complete-

ness and for quick reference. We will refer to it in the formulation of the magnetostatic problem in Section 2.2, and also in Chapter 4.

Consider a perfectly conducting body with an arbitrarily-shaped surface, which is originally charged to a net charge Q, and then is placed in an impressed field produced by external sources. The problem consists of finding the induced charge density on the surface.

2.1.1) The Electrostatic Integral Equation

Since the surface of the body defines an equipotential surface, the total potential produced by the induced and the external sources must be a constant V_o on the surface. Also, the net charge on the surface must still be equal to Q. The fundamental equations governing this electrostatic problem can be written as

$$\iint_S \frac{\sigma(\underline{r}')}{4\pi\varepsilon|\underline{r} - \underline{r}'|}\, ds' + \phi^i(\underline{r}) = V_0, \quad \underline{r} \text{ on } S \tag{2-1}$$

$$\iint_S \sigma(\underline{r}')\, ds' = Q \tag{2-2}$$

where

S denotes the surface of the body,

σ is the induced charge density on S,

$\phi^i(\underline{r})$ is the potential produced by the external sources alone, at a point $\underline{r}$,

$\underline{r}$ and $\underline{r}'$ denote the position vectors from an arbitrary origin to a field and a source point respectively, and

ε denotes the permittivity of the medium surrounding the body.

Equation (2-1) is an integral equation of the first kind for σ. It is to be solved by the Method of Moments, with the auxiliary condition (2-2).

2.1.2) The Expansion Functions for the Electrostatic Charge Density

To solve for σ, we approximate the surface S by planar triangular patches defined by a set of nodes and edges. The vertices of triangles are referred to as nodes and the sides are referred to as edges (Figure 2.1). We assume that the charge density is constant on each patch. In other words, we let

$$\sigma(\underline{r}) \cong \sum_{n=1}^{N} \sigma_n P_n(\underline{r}) \tag{2-3}$$

where

N is the number of triangular patches,

$\sigma_n, n = 1,2,\ldots,N,$ are the expansion coefficients to be determined, and

$P_n(\underline{r})$ is a pulse expansion function defined as follows.

$$P_n(\underline{r}) = \begin{cases} 1, & \underline{r} \text{ in } S^n \\ 0, & \text{otherwise} \end{cases} \tag{2-4}$$

Here S^n denotes the nth triangle. With this choice of expansion functions, σ_n directly gives the charge density on S_n, and (2-2) reads

$$\sum_{n=1}^{N} \sigma_n T^n = Q \tag{2-5}$$

where T^n denotes the area of the nth triangle. Substituting (2-3) into (2-1), we have

$$\sum_{n=1}^{N} \sigma_n \iint_{S_n} \frac{ds'}{|\underline{r} - \underline{r}'|} = 4\pi\epsilon V_o - 4\pi\epsilon\phi^i(\underline{r}), \quad \underline{r} \text{ on } S \tag{2-6}$$

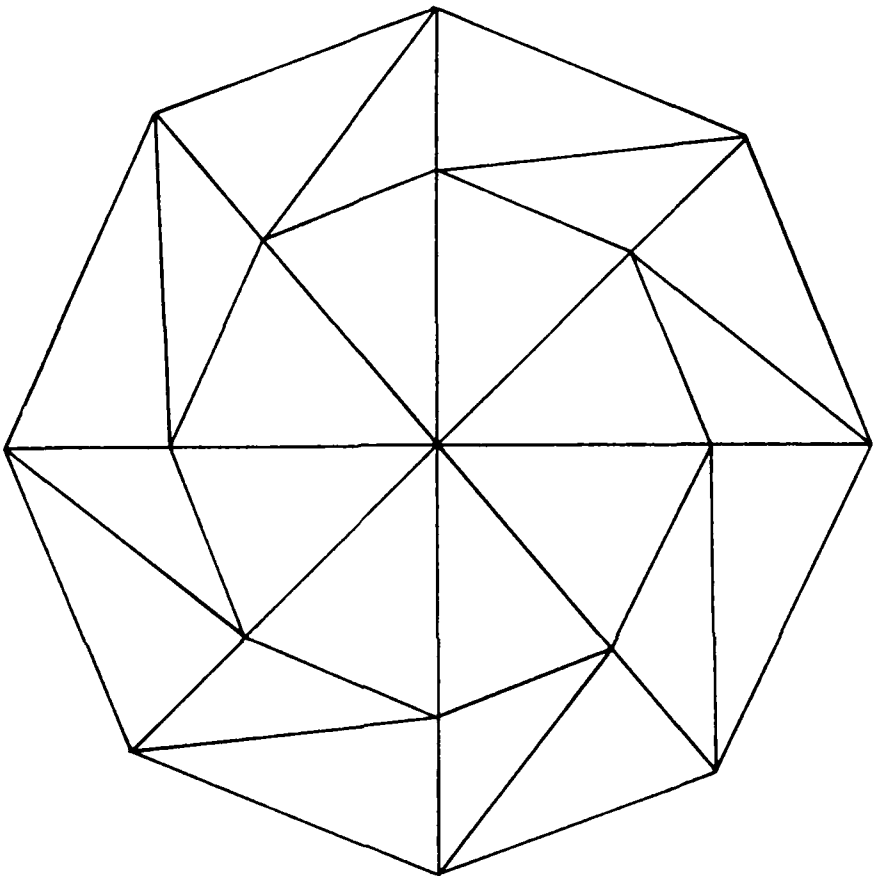

Fig. 2.1. A triangulated model of a circular disc. No. of the triangular patches=24, No. of nodes=17, No. of edges=40, No. of interior nodes=9.

We could have chosen some other types of expansion functions. For example, we could choose functions whose charge density is allowed to vary on each triangle. This might approximate the actual charge density more closely. We could also choose the expansion functions such that the total charge associated with each expansion function is zero. Then the condition (2-2) for Q = 0 would automatically be satisfied. Since we solve the electrostatic problem as one part of a low frequency scattering problem,we will take Q = 0.

The pulse expansion functions for the charge density have been successfully used by other investigators [9], and the results are readily available. We have the additional advantage that for this choice we can make use of the moment matrix obtained in the electrostatic problem to fill the moment matrix of the magnetostatic problem without additional integrations.

2.1.3) Testing Procedure for the Electrostatic Problem

For the reason mentioned above, and because of its simplicity, we choose point matching, i.e., we satisfy (2-6) at the centroid of each triangle, obtaining

$$\sum_{n=1}^{N} K_{mn}\sigma_n - 4\pi\varepsilon V_o = -4\pi\varepsilon\phi_m^i \quad , \quad m=1,2,\ldots,N \tag{2-7}$$

where

$$K_{mn} = \iint_{S_n} \frac{ds'}{|\underline{r}^m - \underline{r}'|} \quad , \tag{2-8}$$

$$\phi_m^i = \phi^i(\underline{r}^m) \tag{2-9}$$

Here $\underline{r}'$ is the position vector of the differential element of area ds' and $\underline{r}^m$ is the position vector to the centroid of the mth triangle S^m. The integral in (2-8) can be evaluated analytically and the result is given in [9].

2.1.4) The Moment Equation for the Electrostatic Problem

Using the Method of Moments, we reduce the integral equation (2-1) to the set of linear algebraic equations given in (2-7). Together with (2-5) we can write them in the form of matrices as

$$\left[\begin{array}{cccc|c} K_{11} & K_{12} \cdots & K_{1N} & -1 & \sigma_1 \\ K_{21} & K_{22} & K_{2N} & -1 & \sigma_2 \\ \vdots & & & & \\ K_{N1} & K_{N2} \cdots & K_{NN} & -1 & \sigma_N \\ \hline T^1 & T^2 \cdots & T^N & 0 & 4\pi\varepsilon V_o \end{array}\right] = \left[\begin{array}{c} -4\pi\varepsilon\phi_1^i \\ -4\pi\varepsilon\phi_2^i \\ \\ -4\pi\varepsilon\phi_N^i \\ \hline Q \end{array}\right] \tag{2-10}$$

or as

$$\left[\begin{array}{cc} [K_{mn}] & [-1] \\ [T^n] & 0 \end{array}\right] \left[\begin{array}{c} [\sigma_n] \\ 4\pi\varepsilon V_o \end{array}\right] = \left[\begin{array}{c} [-4\pi\varepsilon\phi_m^i] \\ Q \end{array}\right] \tag{2-11}$$

In matrix notation this is

$$P \vec{\sigma} = \vec{\phi} \tag{2-12}$$

where the moment matrix P is the square matrix of the order (N+1) × (N+1) on the left-hand side of (2-11), $\vec{\sigma}$ is the column vector on the left-hand

side of (2-11), and $\vec{\Phi}$ is the column vector on the right-hand side of (2-11). The solution of (2-12) gives both the charge density and the total potential of the body.

All types of electrostatic problems can be solved either by using (2-12) directly or by modifying it slightly. As an example, if Q is given and ϕ^i is zero, then one can obtain the charge distribution, the potential V_o, and the capacitance of the body by using (2-12) directly. In fact, it is easy to show that the capacitance of the body is given by

$$C = \frac{4\pi\varepsilon}{P^{-1}_{(N+1,\ N+1)}} \tag{2-13}$$

where $P^{-1}(N+1, N+1)$ is the element in the (N+1)th row and the (N+1)th column of the inverse of the matrix P. Another simple and practical application of the electrostatic problem formulated here is to find the magnetic polarizability tensor of a small aperture of arbitrary shape in an infinite conducting screen [10],[11].

As pointed out earlier, when we solve the electrostatic problem presented here as a part of a low frequency scattering problem, we take Q=0 in (2-11). Then, once the charge distribution is solved from (2-11), we obtain the induced electric dipole moment according to [12]

$$\underline{p}^{\text{ind}} = \iint_S \sigma(\underline{r}')\underline{r}'\, ds' \tag{2-14}$$

Here $\underline{r}'$ is the radius vector from an arbitrary origin to a source point on S. Since the charge density is constant on each triangle, (2-14) reads

$$\underline{p}^{\text{ind}} = \sum_{n=1}^{N} \sigma_n \iint_{S_n} \underline{r}'\, ds' \tag{2-15}$$

Working out the integral in (2-15), we have

$$\underline{p}^{ind} = \sum_{n=1}^{N} \sigma_n T^n \underline{r}^n \tag{2-16}$$

Here $\underline{r}^n$ is the radius vector to the centroid of the nth triangle and T^n is the area of the triangle.

The oscillating electric dipole which is used in computation of the scattered field is then given by

$$\underline{I}^{ind} = j\omega \, \underline{p}^{ind} \tag{2-17}$$

where ω is the angular frequency of the incident field. The details of the scattered field computations are given in Section 2.3.

This completes the general formulation of the electrostatic part of the problem, assuming the body is in an infinite homogeneous medium. Some applications are given in the following chapter. The formulation of the electrostatic problem in the presence of an infinite ground plane is given in Chapter 4.

2.2. The Magnetostatic Problem

As pointed out earlier, the electrostatic problem has been studied extensively by using the Method of Moments, and the results are available for an arbitrarily-shaped surface. However, as an approximation to the low frequency scattering problem, the magnetostatic problem has been applied to only very simple shapes. In fact, we are not aware of any such work using the Method of Moments. Hence, in this section we describe the formulation of the problem in more detail.

The magnetostatic problem can be stated as follows. Given a perfectly diamagnetic body placed in an impressed magnetic field $\underline{H}^{imp}$, we want to find the current distribution induced on the surface of the body such that the normal component of the total magnetic field is zero on the surface of the body and that the induced current density has zero surface divergence.

2.2.1) The Integral Equation for the Magnetostatic Problem.

Let the total magnetic field be the sum of the impressed field $\underline{H}^{imp}$ and the field $\underline{H}(\underline{J})$ produced by the induced surface current $\underline{J}$. Then we require that

$$\hat{n} \cdot (\underline{H}^{imp} + \underline{H}(\underline{J})) = 0 \qquad \text{on } S \tag{2-18}$$

where S denotes the surface of the body, and $\hat{n}$ is the unit (outward) normal vector to S. We also require that

$$\underline{\nabla}_s \cdot \underline{J} = 0 \tag{2-19}$$

where $\underline{\nabla}_s \cdot$ denotes the surface divergence operator.

We are here assuming a perfectly diamagnetic conductor. Otherwise the condition that the normal component of the magnetic field is zero does not hold on the conductor in a static field. One can interpret $\underline{J}$ in (2-19) as the zeroth order part of the total current density induced on an electrically small body when the latter is expressed in terms of a power series in k, where k is the wave number of the incident field [13, also refer to Appendix A].

Equivalently, we need to solve for $\underline{J}$ such that

$$H_n(J) = - H_n^{imp} \qquad \text{on } S \tag{2-20}$$

and (2-19) is also satisfied. The subscript n in (2-20) denotes the normal component. Equation (2-20) represents an integral equation of the first kind for $\underline{J}$ which will be solved by the Method of Moments.

2.2.2) The Expansion Functions for the Magnetostatic Current

To solve (2-20), we approximate the surface S by triangular patches. Although we are free to use any patching scheme, we prefer to use exactly the same patching scheme used in the electrostatic part. This allows us to use the same integrations computed in the electrostatic part to fill the moment matrix for the magnetostatic problem.

We let

$$\underline{J} = \sum_{i=1}^{N^b} C_i \underline{J}_i \qquad (2\text{-}21)$$

where

N^b is the number of the interior nodes for an open surface. For a closed surface N^b is equal to the total number of nodes minus one.

$\underline{J}_i$ is the vector expansion function associated with the ith interior (non-boundary) node, and C_i is the ith expansion coefficient to be determined.

The expansion function $\underline{J}_L$ associated with the Lth interior node is illustrated in Fig. 2.2. It has the following properties:

i) On each triangle attached to node L, the magnitude of $\underline{J}_L$ is constant. This magnitude is equal to the length of the edge opposite node L divided by the area of the triangle.

ii) On each triangle attached to node L, $\underline{J}_L$ is parallel to the edge opposite to node L. $\underline{J}_L$ circulates clockwise about the node L.

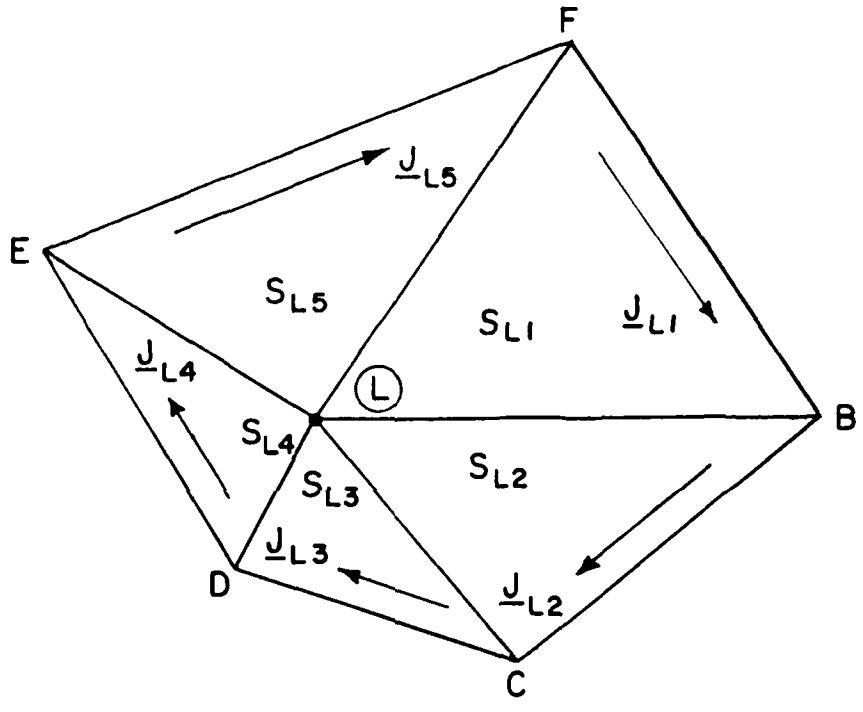

Fig. 2.2. The expansion function $\underline{J}_L$ associated with node L.

In Fig. 2.2 we have five triangles attached to node L. (Note that each triangle may be in a different plane.) The capital letters denote the nodes. On the first surface S_{L1} attached to node L, $\underline{J}_L$ is called $\underline{J}_{L1}$ and is given by

$$\underline{J}_{L1} = \frac{\overline{FB}}{T_{L1}} \tag{2-22a}$$

Here $\overline{FB}$ denotes the vector drawn from node F to node B, and T_{L1} is the area of the triangle S_{L1}. Similarly, on the fifth triangle S_{L5} attached to node L, $\underline{J}_L$ is called $\underline{J}_{L5}$ and is given by

$$\underline{J}_{L5} = \frac{\overline{EF}}{T_{L5}} \tag{2-22b}$$

Similar definitions hold for the other triangles.

iii) The component of $\underline{J}_L$ normal to an edge common to two triangles is continuous. Hence, no line charge accumulates on any edge. This component of $\underline{J}_L$ is given by

$$(\underline{J}_L)_n = 2/\ell_c \tag{2-23}$$

where ℓ_c is the length of the common edge between two triangles attached to node L.

iv) It is easy to show that

$$\underline{\nabla}_s \cdot \underline{J}_L = 0 \tag{2-24}$$

So that there is no charge associated with $\underline{J}_L$. Hence, by virtue of (2-21), we see that the necessary condition in (2-19) is already satisfied by this choice of expansion functions. Indeed it can be shown that [8,Appendix B]

$$\underline{J}_{Lk} = \hat{\underline{n}}_{Lk} \times \underline{\nabla}_s \psi_{Lk} \tag{2-25}$$

where $\hat{\underline{n}}_{Lk}$ is the unit normal vector to the kth triangle S_{Lk}, attached to node L. Here $\underline{\nabla}_s$ denotes the surface gradient operator, and ψ_{Lk} is a scalar function defined on S_{Lk}. ψ_{Lk} has a value equal to 2 at the node L, and linearly decreases to zero at the edge opposite to node L. ψ_{Lk} is discontinuous, because it suddenly drops to zero at the other two edges on S_{Lk}. Therefore $\underline{\nabla}_s \psi_{Lk}$ is impulsive at these edges. However, the composite function ψ_L consisting of ψ_{L1}, ψ_{L2},... is continuous so that its surface gradient is not impulsive. In fact, if all triangles attached to node L are in the same plane, then ψ_L defines a pyramid-like surface centered at node L, with height equal to 2. It has as many side surfaces as the number of triangles attached to node L. In Fig. 2.3 we have shown the part of ψ_L over two triangles, assuming both are in the xy plane. The encircled numbers in the figure denote the nodes.

On the first surface S_{L1} attached to node L, ψ_L is called ψ_{L1}, which is given by the planar surface passing through the points $(x_1,y_1,0)$, $(x_2,y_2,0)$, and $(0,0,2)$.

$$\psi_{L1} = 2\,\frac{x(y_2 - y_1) - y(x_2 - x_1) - x_1y_2 + y_1x_2}{(y_1x_2 - x_1y_2)} \tag{2-26}$$

Similarly, the equation of the plane passing through the points $(x_2,y_2,0)$, $(x_3,y_3,0)$, and $(0,0,2)$ defines ψ_{L2}.

$$\psi_{L2} = 2\,\frac{x(y_3 - y_2) - y(x_3 - x_2) - x_2y_3 + y_2x_3}{(y_2x_3 - x_2y_3)} \tag{2-27}$$

Then

$$\underline{J}_{L1} = \hat{\underline{n}}_{L1} \times \underline{\nabla}_s \psi_{L1} = \hat{\underline{z}} \times \underline{\nabla}_s \psi_{L1}$$

$$= \frac{(y_2 - y_1)}{(y_1x_2 - x_1y_2)/2}\,\underline{\hat{y}} + \frac{(x_2 - x_1)}{(y_1x_2 - x_1y_2)/2}\,\underline{\hat{x}} \tag{2-28}$$

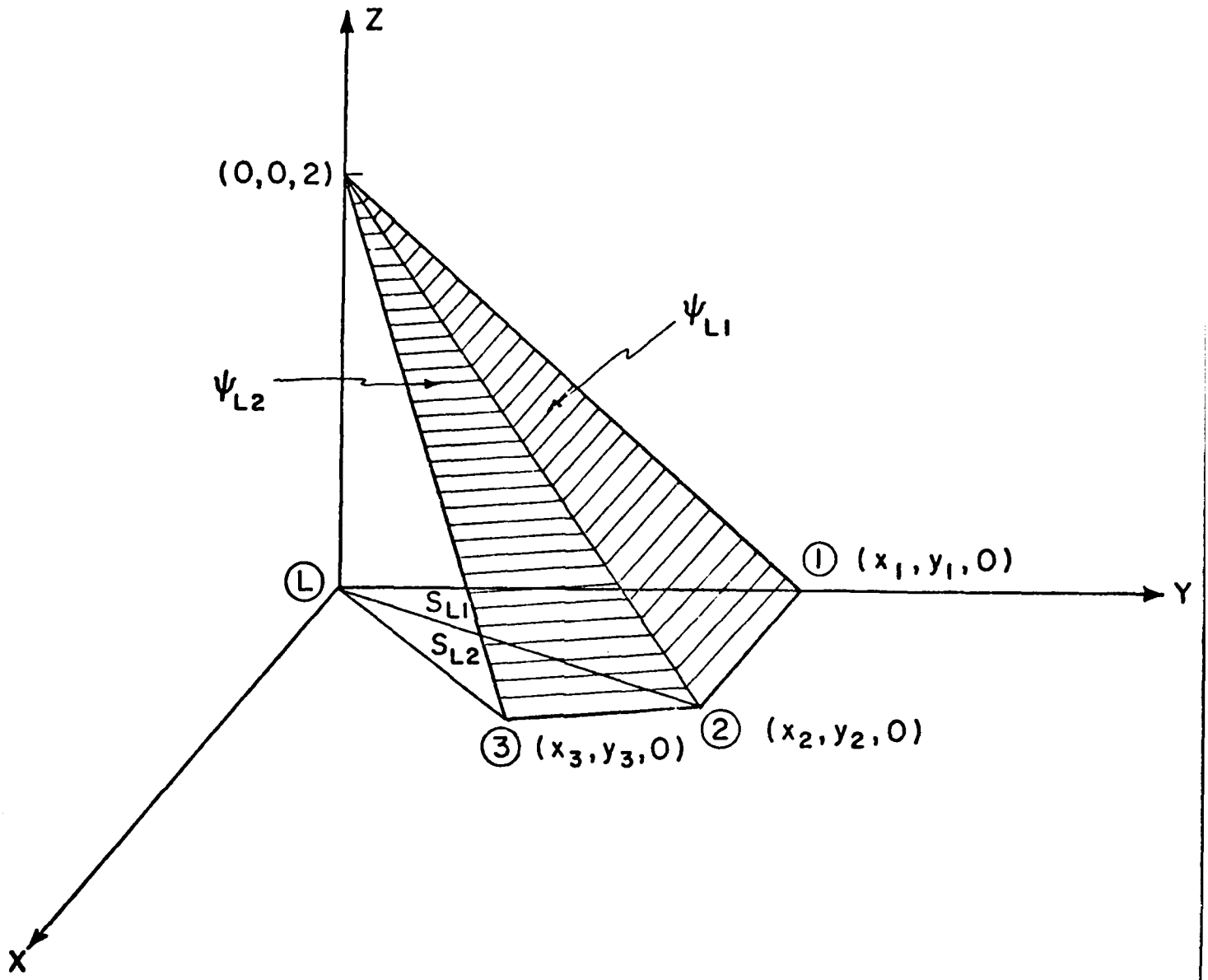

Fig. 2.3. Illustration of Ψ_L over two triangular surfaces.

where $\hat{\underline{x}}$, $\hat{\underline{y}}$, and $\hat{\underline{z}}$ denote the unit vectors along the coordinate axes. If the nodes 1, 2, 3,... encircle node L in the clockwise direction, as in Fig. 2.3, then $(y_1x_2 - x_1y_2)/2$ is the area of the triangle S_{L1}. As a result, (2-28) reduces to

$$\underline{J}_{L1} = \frac{\overline{12}}{T_{L1}} \tag{2-29a}$$

where $\overline{12}$ represents the vector drawn from node 1 to node 2, and T_{L1} is the area of the triangle S_{L1}. Similar results hold for $\underline{J}_{L2}$, $\underline{J}_{L3}$,...

However, if nodes 1,2,3,... were to encircle node L in the counterclockwise direction, then the area of the triangle S_{L1} would be $-(y_1x_2 - x_1y_2)/2$ and (2-28) would reduce to

$$\underline{J}_{L1} = -\frac{\overline{12}}{T_{L1}} \tag{2-29b}$$

It is evident from (2-29a) and (2-29b) that $\underline{J}_{L1}$ always flows clockwise about node L for $\hat{\underline{n}}_{L1}=\hat{\underline{z}}$. However,if $\hat{\underline{n}}_{L1}=-\hat{\underline{z}}$, then $\underline{J}_{L1}$, being proportional to $\hat{\underline{n}}_{L1}$, would flow counterclockwise about node L. Therefore, $\underline{J}_{L1}$ always encircles $\hat{\underline{n}}_{L1}$ in the left-hand sense. (A left-handed screw whose axis is parallel to $\hat{\underline{n}}_{L1}$ would advance in the direction of $\hat{\underline{n}}_{L1}$ when rotated in the direction of $\underline{J}_{L1}$.)

v) The expansion function $\underline{J}_L$ can be written as a linear combination of t_L expansion functions used in [14], where an expansion function is associated with each non-boundary edge. Here t_L denotes the number of triangles attached to node L. Usually the number of interior nodes is less than the number of interior edges, and hence we have fewer unknowns for the same patching scheme. On the other hand, each of our expansion functions is defined on at least three triangles, whereas each of those in [14] is defined on a pair of triangles. Furthermore, the expansion functions of [14] vary both in

magnitude and in direction on a triangle, but ours are constant there.

With such a choice for expansion functions, on each triangle there can be up to three expansion functions associated with the three nodes of the triangle. On a triangle which has a boundary edge only one expansion function can exist. In patching the surface S, care should be taken so that all triangles have at least one interior node. (For closed bodies this problem does not exist and there exist exactly three expansion functions on each triangle, except on those triangles attached to a specific node where there are exactly two expansion functions.)

vi) It can be shown that N^b expansion functions defined on an open surface form a linearly independent set. For closed surfaces the number of nodes N^n is equal to number of interior nodes. The set of N^n expansion functions forms a linearly dependent set, and when we remove one of them (arbitrarily) we are left with a linearly independent set. For this reason N^b in (2-21) is taken to mean the number of nodes minus one for a closed surface.

vii) The constant nature of the current flow with each basis function within a triangle may be at first disconcerting. Certainly for a large triangle modeling a curved section of the scattering surface, one would expect the direction and the magnitude of the actual current to vary within the triangle. In other words, one might ask, "Is a superposition of the basis functions within a triangle capable of representing a prescribed current flowing in an arbitrary way within the triangle?" Unfortunately the answer to such a question is "no", but we remind ourselves that this is a low-frequency scattering problem where we do not expect a fast variation of the current

except near the boundaries, or sharp edges, or on the regions very close to the source. Hence the problem can be overcome by choosing a large number of small triangular patches to model such regions of the scatterer. The same procedure should be used in solving the electrostatic problem. The expansion functions for the current are capable of representing an arbitrary but fixed direction and an arbitrary magnitude for the current within a non-boundary triangle. Near an edge (of an open surface) the component of the actual current normal to the edge must be zero anyway. With these basis functions, the current on a boundary triangle is guaranteed to be tangential to the edge.

Having decided on the expansion functions, we now take the usual steps in the Method of Moments technique. Substituting (2-21) into (2-20) we get

$$H_n\left(\sum_{i=1}^{N^b} C_i \underline{J}_i\right) = - H_n^{imp} \qquad \text{on S} \tag{2-30}$$

Using the linear property of the operator H_n, we have

$$\sum_{i=1}^{N^b} C_i H_{ni}(\underline{r}) = - H_n^{imp}(\underline{r}) \ , \quad \underline{r} \ \text{ on S} \tag{2-31}$$

Here, $H_{ni}(\underline{r})$ denotes the normal component of the magnetic field at a point $\underline{r}$ (on S), produced by the current basis function $\underline{J}_i$ associated with node i.

2.2.3) Testing Procedure and Moment Matrix for the Magnetostatic Problem

We assume a set u_j, $j=1,2,\ldots,N^b$ of scalar testing functions such that u_j is non-zero only over the triangles attached to node j. Then we define the symmetric product of u_j with any function f to be the integral of their product over the surface S, i.e.,

$$\langle u_j, f \rangle = \iint_S u_j f ds = \sum_{k=1}^{t_j} \iint_{S_{jk}} u_j f ds \tag{2-32}$$

Here t_j is the number of triangles attached to node j and S_{jk} denotes the surface of the kth triangle attached to node j. Taking the symmetric product of both sides of (2-31) with each of the testing functions u_j, $j=1,2,\ldots N^b$, and using the linearity property of the symmetric product defined in (2-32) we arrive at the following matrix equation.

$$Z \vec{I} = \vec{V} \tag{2-33}$$

where Z is an $N^b \times N^b$ square matrix such that

$$Z(j,i) = \iint_{S_j} u_j(\underline{r})\, H_{ni}(\underline{r})\, ds \qquad i,j=1,2,\ldots,N^b \,, \tag{2-34}$$

$\vec{I}$ is an $N^b \times 1$ column vector such that

$$I(i) = C_i \qquad i = 1,2,\ldots,N^b \,, \tag{2-35}$$

and $\vec{V}$ is an $N^b \times 1$ column vector such that

$$\begin{aligned} V(j) &= - \langle u_j, H_n^{imp} \rangle \\ &= - \iint_{S_j} u_j(\underline{r})\, H_n^{imp}(\underline{r})\, ds \end{aligned} \tag{2-36}$$

In (2-34) and (2-36), S_j denotes the union of the surfaces of all triangles attached to node j.

Assuming that node j has t_j triangles attached to it, we rewrite (2-34) as

$$Z(j,i) = \sum_{m=1}^{t_j} \iint_{S_{jm}} u_{jm}(\underline{r})\, \hat{\underline{n}}_{jm}(\underline{r}) \cdot \underline{H}_i(\underline{r})ds \tag{2-37}$$

Here, $\underline{H}_i(\underline{r})$ denotes the magnetic field produced by the expansion function $\underline{J}_i$ at a point $\underline{r}$, $\hat{\underline{n}}_{jm}(\underline{r})$ is the normal unit vector to the m th triangle S_{jm} which is attached to node j, and $u_{jm}(\underline{r})$ denotes the value of u_j at the point $\underline{r}$ on S_{jm}. Now using the relation

$$\underline{H} = \underline{\nabla} \times \underline{A} \tag{2-38}$$

where $\underline{A}$ is the magnetic vector potential, we have

$$Z(j,i) = \sum_{m=1}^{t_j} \iint_{S_{jm}} u_{jm}(\underline{r})\hat{\underline{n}}_{jm}(\underline{r}) \cdot (\underline{\nabla} \times \underline{A}_i(\underline{r}))ds \tag{2-39}$$

Here $\underline{A}_i(\underline{r})$ is the vector potential produced by $\underline{J}_i$, at the point $\underline{r}$.

Now, if we decide to choose u_{jm} to be identically equal to ψ_{jm} in (2-25) and make use of Stokes' theorem, we arrive at the following:

$$Z(j,i) = -\sum_{m=1}^{t_j} \iint_{S_{jm}} (\hat{\underline{n}}_{jm}(\underline{r}) \times \underline{\nabla}_s \psi_{jm}) \cdot \underline{A}_i(\underline{r})ds \tag{2-40}$$

Here we used the fact that the value of ψ_j is zero on the boundary of the surface S_j composed of t_j triangles attached to node j. Then using (2-25) in (2-40), we get

$$Z(j,i) = -\sum_{m=1}^{t_j} \iint_{S_{jm}} \underline{J}_{jm}(\underline{r}) \cdot \underline{A}_i(\underline{r})ds \tag{2-41}$$

Since $\underline{J}_{jm}$ is a constant vector which denotes the expansion function $\underline{J}_j$ on

the mth triangle attached to node j, we can take it outside the integral.

$$Z(j,i) = - \sum_{m=1}^{t_j} \underline{J}_{jm} \cdot \iint_{S_{jm}} \underline{A}_i(\underline{r}) ds \tag{2-42}$$

We now approximate the integrand in (2-42) by its value at the centroid of the triangle S_{jm} to get

$$Z(j,i) \cong - \sum_{m=1}^{t_j} (\underline{J}_{jm} \cdot \underline{A}_i(\underline{r}_{cjm})) \, T_{jm} \tag{2-43}$$

Here $\underline{A}_i(\underline{r}_{cjm})$ denotes the vector potential produced by $\underline{J}_i$ at the centroid $\underline{r}_{cjm}$ of the triangle S_{jm}, and T_{jm} is the area of S_{jm}.

Assuming that the node i has t_i triangles attached to it, we write $\underline{A}_i(\underline{r})$ as follows:

$$\begin{aligned} \underline{A}_i(\underline{r}) &= \frac{1}{4\pi} \iint_{S_i} \frac{\underline{J}_i(\underline{r}')}{|\underline{r} - \underline{r}'|} ds' \\ &= \frac{1}{4\pi} \sum_{\ell=1}^{t_i} \iint_{S_{i\ell}} \frac{\underline{J}_{i\ell}(\underline{r}')}{|\underline{r} - \underline{r}'|} ds' \\ &= \frac{1}{4\pi} \sum_{\ell=1}^{t_i} \underline{J}_{i\ell} \iint_{S_{i\ell}} \frac{ds'}{|\underline{r} - \underline{r}'|} \end{aligned} \tag{2-44}$$

The integral in (2-44) is the same as the electric scalar potential at a point $\underline{r}$, produced by a constant surface charge density on the triangular surface $S_{i\ell}$. This is the same integral we had in the electrostatic problem and its analytical evaluation is given in [9].

Substituting (2-44) into (2-43), we get

$$Z(j,i) \cong - \frac{1}{4\pi} \sum_{m=1}^{t_j} T_{jm} \underline{J}_{jm} \cdot \left(\sum_{\ell=1}^{t_i} \underline{J}_{i\ell} \iint_{S_{i\ell}} \frac{ds'}{|\underline{r}_{cjm} - \underline{r}'|} \right) \tag{2-45}$$

Comparing the integrals in (2-8) and (2-45), we finally have

$$Z(j,i) \cong -\frac{1}{4\pi} \sum_{m=1}^{t_j} T_{jm} \underline{J}_{jm} \cdot \left(\sum_{\ell=1}^{t_i} \underline{J}_{i\ell} K(jm, i\ell) \right) \tag{2-46}$$

Here $K(jm, i\ell)$ is the element in the row corresponding to the surface S_{jm} and in the column corresponding to the surface $S_{i\ell}$ of the matrix K used in the electrostatic problem (Eq. (2-11)). Hence the moment matrix P of the electrostatic problem provides the integrals that are required to fill the moment matrix Z of the magnetostatic problem.

Returning to (2-36), we have

$$V(j) = -\sum_{m=1}^{t_j} \iint_{S_{jm}} \psi_{jm}(\underline{r})\, H_n^{imp}(\underline{r}) ds \tag{2-47}$$

If we approximate $H_n^{imp}(\underline{r})$ by $H_n^{imp}(\underline{r}_{cjm})$, where $\underline{r}_{cjm}$ denotes the centroid of the triangle S_{jm}, then

$$V(j) \cong -\sum_{m=1}^{t_j} H_n^{imp}(\underline{r}_{cjm}) \iint_{S_{jm}} \psi_{jm}(\underline{r}) ds \tag{2-48}$$

The integral in (2-48) is equal to the volume of the pyramid-like object of height 2. Hence,

$$V(j) \cong -\frac{2}{3} \sum_{m=1}^{t_j} T_{jm}\, H_n^{imp}(\underline{r}_{cjm}) \tag{2-49}$$

The moment equation (2-33) with the defining relations (2-46), (2-35), and (2-49) is solved to obtain the unknown expansion coefficients, and the induced current density $\underline{J}$ is found by (2-21). Once the current distribution is known, the induced magnetic dipole moment can be obtained [12] from

$$\underline{M}^{ind} = \frac{1}{2} \iint_S \underline{r} \times \underline{J}(\underline{r}) ds \tag{2-50}$$

If we have N triangular surfaces and denote by J^n the total current on nth triangle, (2-50) reads

$$\underline{M}^{ind} = \frac{1}{2} \sum_{n=1}^{N} \iint_{S^n} \underline{r} \cdot \underline{J}^n(\underline{r}) ds$$

$$= -\frac{1}{2} \sum_{n=1}^{N} \underline{J}^n \cdot \iint_{S^n} \underline{r}\, ds \qquad (2\text{-}51)$$

Here S^n denotes the surface of the nth triangular patch. Working out the integral in (2-51), we have

$$\underline{M}^{ind} = \frac{1}{2} \sum_{n=1}^{N} (\underline{r}^n \times \underline{J}^n) T^n \qquad (2\text{-}52)$$

Here $\underline{r}^n$ is the position vector of the centroid of S^n, and T^n is the area of S^n.

The oscillating magnetic dipole used in computation of the scattered field is then given by

$$\underline{K\ell}^{ind} = j\omega\mu\, \underline{M}^{ind} \qquad (2\text{-}53)$$

where ω is the angular frequency of the incident field, and μ is the permeability of the medium surrounding the scatterer.

This completes the formulation of the magnetostatic problem, assuming the scatterer is in an infinite homogeneous medium. The formulation of the magnetostatic problem in the presence of an infinite screen is given in Chapter 4.

Some applications of the magnetostatic problem formulated here will appear in the next chapter. A simple and practical application of the problem is to find the electric polarizability of a small aperture in an infinite conducting screen.

2.3. Computation of the Scattered Field

To compute the scattered fields $\underline{E}^s$ and $\underline{H}^s$, we divide the space into four regions.

i) Very close to the scatterer we compute $\underline{E}^s$ directly from the induced static charge distribution σ as follows

$$\underline{E}^s = \frac{1}{4\pi\varepsilon} \iint_S \frac{\sigma(\underline{r}')\ (\underline{r} - \underline{r}')}{|\underline{r} - \underline{r}'|^3}\, ds'$$

$$\cong \frac{1}{4\pi\varepsilon} \sum_{n=1}^{N} \sigma_n \iint_{S^n} \frac{(\underline{r} - \underline{r}')\, ds'}{|\underline{r} - \underline{r}'|^3}$$

$$\cong \frac{1}{4\pi\varepsilon} \sum_{n=1}^{N} \sigma_n T^n \frac{(\underline{r} - \underline{r}^n)}{|\underline{r} - \underline{r}^n|^3} \qquad (2\text{-}54)$$

Here $\underline{r}$ denotes the position vector of the field point, $\underline{r}'$ denotes the position vector of the differential element of area ds', S^n denotes the surface of the nth triangular patch, T^n is the area of S^n, σ_n is the computed charge density on S^n, and $\underline{r}^n$ denotes the position vector to the centroid of S^n.

Similarly we compute the scattered magnetic field $\underline{H}^s$ from the induced magnetostatic current $\underline{J}$ as follows:

$$\underline{H}^s = \frac{1}{4\pi} \iint_S \frac{\underline{J} \times (\underline{r} - \underline{r}')}{|\underline{r} - \underline{r}'|^3}\, ds'$$

$$= \frac{1}{4\pi} \sum_{n=1}^{N} \iint_{S^n} \frac{\underline{J}^n \times (\underline{r} - \underline{r}')}{|\underline{r} - \underline{r}'|^3}\, ds'$$

$$\cong \frac{1}{4\pi} \sum_{n=1}^{N} T^n \frac{\underline{J}^n \times (\underline{r} - \underline{r}^n)}{|\underline{r} - \underline{r}^n|^3} \qquad (2\text{-}55)$$

Here $\underline{J}^n$ denotes the total induced current density on the nth triangular patch S^n.

ii) At a distance large compared to the maximum linear dimension d of the scatterer, but small compared to the wavelength λ, we compute $\underline{E}^s$ from the induced static electric dipole $\underline{P}^{ind}$ and $\underline{H}^s$ from the induced static magnetic dipole $\underline{M}^{ind}$. The induced dipoles are placed at the origin, and the scattered fields at a point defined by the radius vector $\underline{r}$ are given by the following:

$$\underline{E}^s(\underline{r}) = \frac{3\,\hat{\underline{r}}(\underline{P}^{ind} \cdot \hat{\underline{r}}) - \underline{P}^{ind}}{4\pi\varepsilon\, r^3} \quad , \tag{2-56}$$

$$\underline{H}^s(\underline{r}) = \frac{3\,\hat{\underline{r}}(\underline{M}^{ind} \cdot \hat{\underline{r}}) - \underline{M}^{ind}}{4\pi\, r^3} \tag{2-57}$$

where

$$r = |\underline{r}| \tag{2-58}$$

and

$$\hat{\underline{r}} = \frac{\underline{r}}{r} \tag{2-59}$$

iii) At a distance large compared to d, but comparable with λ, the scattered fields are computed by replacing the scatterer by the oscillating electric and magnetic dipoles of (2-17) and (2-53). The exact dynamic expressions are used to compute the fields produced by them at a point $\underline{r}$ [refer to Appendix B].

$$\underline{E}^s(\underline{r}) = \frac{e^{-jkr}}{j\omega 4\pi\varepsilon r}\left[k^2(\hat{\underline{r}} \times \underline{I}\ell^{ind}) \times \hat{\underline{r}} + (3\hat{\underline{r}}(\hat{\underline{r}} \cdot \underline{I}\ell^{ind}) - \underline{I}\ell^{ind})\left(\frac{1}{r^2} + \frac{jk}{r}\right)\right.$$

$$\left. - j\omega\mu(\underline{K}\ell^{ind} \times \hat{\underline{r}})\left(jk + \frac{1}{r}\right)\right] \tag{2-60}$$

and

$$\underline{H}^s(\underline{r}) = \frac{e^{-jkr}}{j\omega 4\pi\mu r}\left[k^2(\hat{\underline{r}} \times \underline{K}\ell^{ind}) \times \hat{\underline{r}} + (3\hat{\underline{r}}(\hat{\underline{r}} \cdot \underline{K}\ell^{ind}) - \underline{K}\ell^{ind})\left(\frac{1}{r^2} + \frac{jk}{r}\right)\right.$$

$$\left. + j\omega\varepsilon(\underline{I}\ell^{ind} \times \hat{\underline{r}})\left(jk + \frac{1}{r}\right)\right] \tag{2-61}$$

where r and $\hat{r}$ are as defined in (2-58) and (2-59).

iv) For the far field, we use the far-field expressions for the dipole fields, neglecting the terms that vanish faster than 1/r, i.e.,

$$\underline{E}^s(\underline{r}) = \frac{e^{-jkr}}{j\omega 4\pi\varepsilon r} k\, \hat{r} \times [k(\underline{I}^{ind} \times \hat{r}) - \omega\mu \underline{K}^{ind}] \tag{2-62}$$

$$\underline{H}^s(\underline{r}) = \frac{e^{-jkr}}{j\omega 4\pi\mu r} k\, \hat{r} \times [k(\underline{K}^{ind} \times \hat{r}) + \omega\varepsilon \underline{I}^{ind}] \tag{2-63}$$

Note that while the near field problem (cases (i) and (ii)) is "decoupled," that is, $\underline{E}^s$ and $\underline{H}^s$ are determined completely independently, the field at large distances from the scatterer is not decoupled. In general, the electric dipole contributes to both the electric and the magnetic far field, and so does the magnetic dipole. Expressions (2-60) and (2-61) for the fields in region iii are also valid in regions ii and iv. That is, if $kr \ll 1$, (2-60) and (2-61) reduce to (2-56) and (2-57), and, if $kr \gg 1$, (2-60) and (2-61) reduce to (2-62) and (2-63).

Chapter 3

SCATTERING FROM SMALL BODIES IN FREE SPACE

In this chapter we use the procedure described in the previous chapter to compute the distribution of the charge and the current induced on the surface of a small conducting body when it is illuminated by an electromagnetic wave. We assume the body is placed in free space (ϵ_o, μ_o) and the incident field is either a plane wave or is produced by an oscillating electric or magnetic dipole placed near the scatterer.

Given the incident field $(\underline{E}^i, \underline{H}^i)$, we find ϕ^i such that

$$\underline{E}_o^i = -\nabla\phi^i \tag{3-1}$$

where

$$\underline{E}_o^i = \lim_{k\to 0} \underline{E}^i \tag{3-2}$$

and ∇ denotes the gradient operator. We use ϕ^i of (3-1) as the applied potential in the electrostatic problem (eq. (2-1)). Similarly we let

$$\underline{H}^{imp} = \lim_{k\to 0} \underline{H}^i \tag{3-3}$$

and use $\underline{H}^{imp}$ in (2-18) to solve the magnetostatic problem.

If the source of the incident field is an oscillating electric dipole $\underline{I\ell}$ placed close to the scatterer, then we only need to solve the corresponding electrostatic problem. We obtain the electrostatic problem by replacing $\underline{I\ell}$ with a quasi-static electric dipole $\underline{P}$ such that

$$\underline{I\ell} = j\omega\, \underline{P} \tag{3-4}$$

Here ω is the angular frequency of the incident wave in the original

problem. We do not solve any magnetostatic problem because close to an oscillating electric dipole the magnetic field vanishes in the limit $k \to 0$. That is, H^{imp} as defined by (3-3) is zero in this case. By a similar argument we solve only the magnetostatic problem if the source is an oscillating magnetic dipole $\underline{K\ell}$ placed close to the scatterer. We obtain the magnetostatic problem by replacing $\underline{K\ell}$ with a quasi-static magnetic dipole $\underline{M}$ such that

$$\underline{K\ell} = j\omega\mu \underline{M} \tag{3-5}$$

and assuming the scatterer to be perfectly diamagnetic.

3.1. Plane Wave Scattering from a Small Sphere

The exact results for this problem are summarized in Appendix A. To apply the method described in the previous chapter, we take the following steps:

i) For convenience the sphere is assumed to be of radius 1 meter and is placed at the center of a spherical coordinate system.

ii) To approximate the spherical surface with triangular patches, the surface is first divided uniformly into N_ϕ slices in the ϕ-direction, then each of these slices is divided into N_θ +1 patches. The poles (θ=0° and θ = 180°) are taken to be two nodes. Hence, in each ϕ-slice we have two triangular and N_θ -1 quadrilateral patches. The addition of diagonals to all quadrilaterals completes the triangulation of the spherical surface. The resulting model of the spherical surface is shown in Figure 3.1. We have a total of $2N_\theta N_\phi$ triangular patches modeling the surface. The total number of unknowns for the electrostatic problem is then $2N_\theta N_\phi + 1$. The number of nodes is $N_\theta N_\phi + 2$. Therefore, the number of unknowns in the

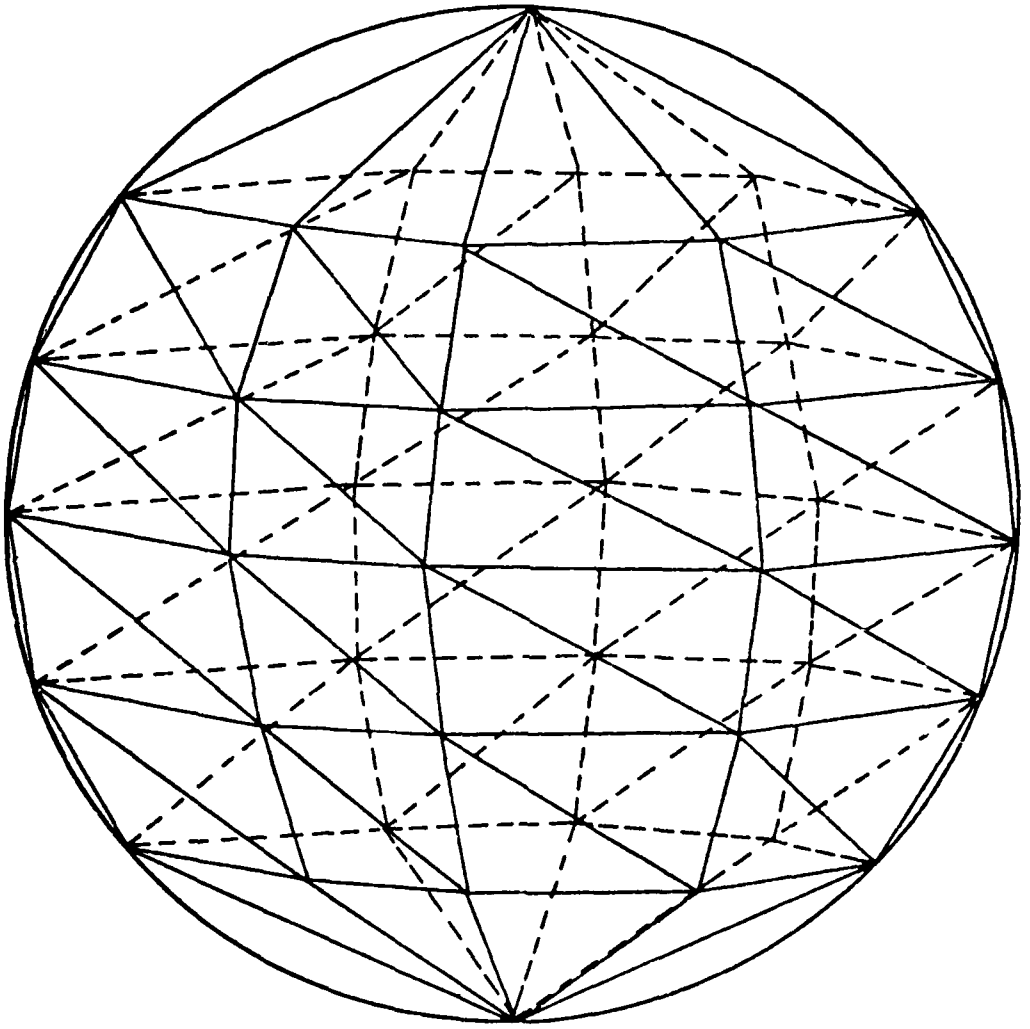

Fig. 3.1. A triangulated model of a spherical surface. N_ϕ=8, N_θ=5, No. of patches=80, No. of nodes=42.

magnetostatic problem is $N_\theta N_\phi + 1$. In this grid scheme the triangulated sphere is always inscribed inside the actual sphere, because the nodes are taken to be on the actual surface. To get a partially inscribed model we simply take the nodes to be slightly outside the actual sphere, obtaining a better representation of the actual surface. Obviously it is impossible to patch a spherical surface exactly by using a finite number of triangular patches. However the triangular patches are better than the rectangular patches in terms of adequately modeling an arbitrary surface, and they are better than quadrilateral patches in terms of computer description.

For an axially incident plane wave described by

$$\underline{E}^i = 120\pi\, e^{-jkz}\, \underline{x} \qquad \text{(V/m)},$$

$$\underline{H}^i = e^{-jkz}\, \underline{\hat{y}} \qquad \text{(A/m)}$$

we have

$$\phi^i = -\,120\pi x \qquad \text{(V)} \qquad (3\text{-}6)$$

$$\underline{H}^{imp} = 1\, \underline{\hat{y}} \qquad \text{(A/m)} \qquad (3\text{-}7)$$

Figure 3.2 shows the computed current density for this case. Also shown in the figure is the exact magnetostatic result for comparison. The agreement is good. As we noted earlier, the computed current is a constant vector on each triangular patch. Hence for $\phi = 0°$, as we change θ, J_θ varies on the triangular surface. However for $\phi = 90°$, $J_\phi = -J_x$, which is fixed on each patch. This is the reason why we have steps in the curve for J_ϕ of Figure 3.2. To observe the influence of the patching scheme on the results, we changed the direction of $\underline{E}^i$ and $\underline{H}^i$. The change in the results indicated that the influence of the triangulation scheme is negligible. Figure 3.3 shows the computed charge density for

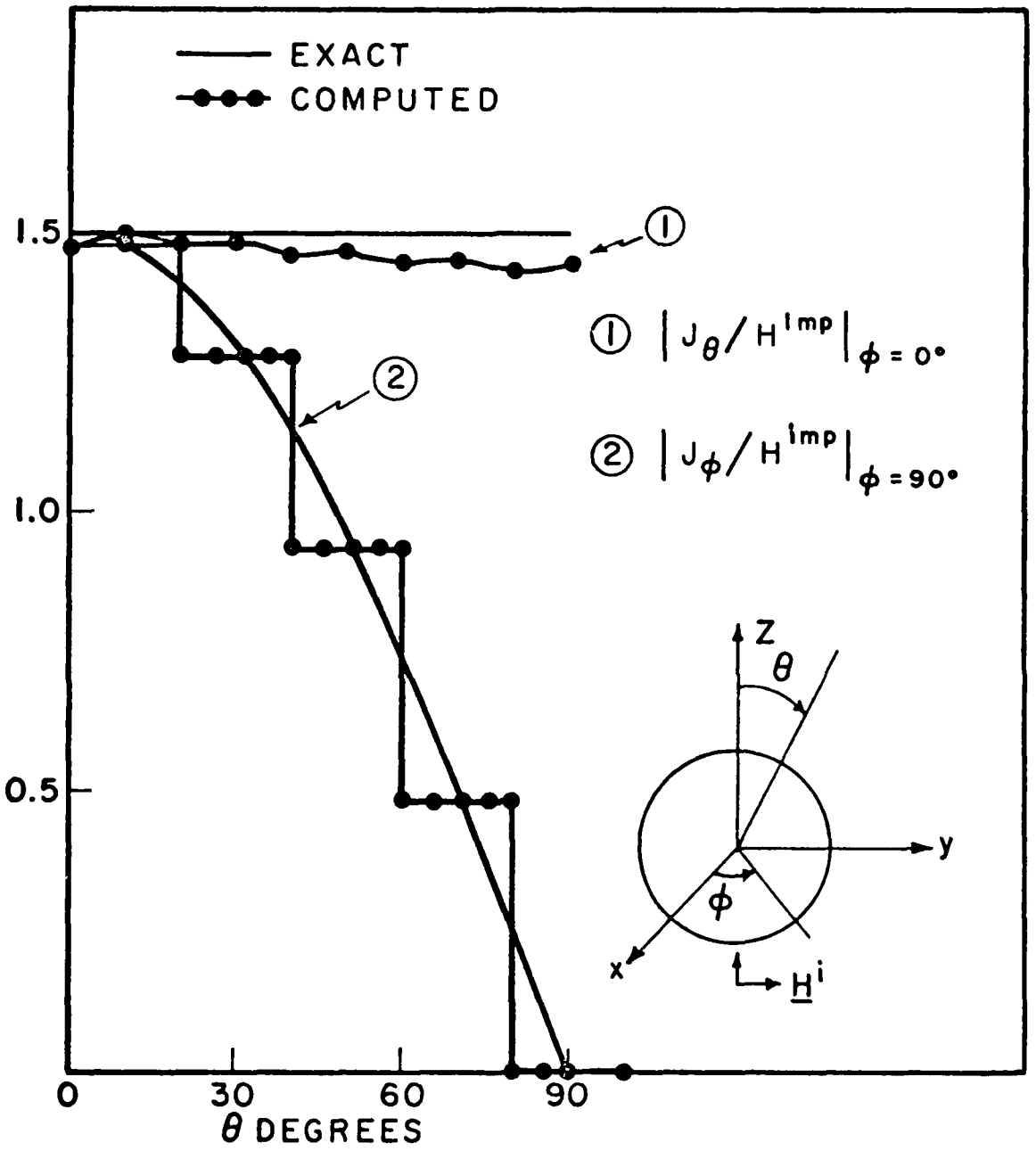

Fig. 3.2. Induced current distribution on a sphere due to an axially incident plane wave. No. of unknowns = 97.

$$\phi^i = -120\pi z \quad (V) \tag{3-8}$$

The exact result [15] is also shown.

For an impressed magnetic field $\underline{H}^{imp} = 1\ \hat{\underline{z}}$ (A/m), the magnitude of the exact current at $\theta = 90^\circ$ is 1.5 (A/m), and the computed value is 1.46 (A/m).

With an inscribed model of the surface, the computed dipole moments are less than the exact values. As we slightly increase the radius of the triangulated sphere to have a partially inscribed model, we notice that the induced charge and current distributions do not change, but the induced dipole moments get closer to the exact values. This is to be expected, since the dipole moments are proportional to the cube of the radius, whereas the current and charge density do not depend on the radius. Table 3.1 compares the computed dipole moments with the exact values. Note that as the radius of the model surface is increased from 1.0 to 1.01 (or 1.02), the computed dipole moments increase by a factor $(1.01)^3$ (or $(1.02)^3$). Table 3.2 shows the progression of the solution as the number of unknowns is increased.

Since the scattered far field is completely defined by the induced dipoles, we do not need a pattern plot. From the result we have for the induced dipole moments (the third line of Table 3.1) , the relative error between the exact and computed far field will be at most three percent.

3.2. Dipole Near a Small Sphere

Figure 3.4a represents an arbitrarily oriented oscillating dipole near a conducting sphere. The exact results, together with some low frequency approximations for this scattering problem, are summarized in Chapter 10 of [16]. We first consider a radially directed electric dipole near the sphere. Next we solve the problem of a magnetic dipole placed tangentially on the sphere.

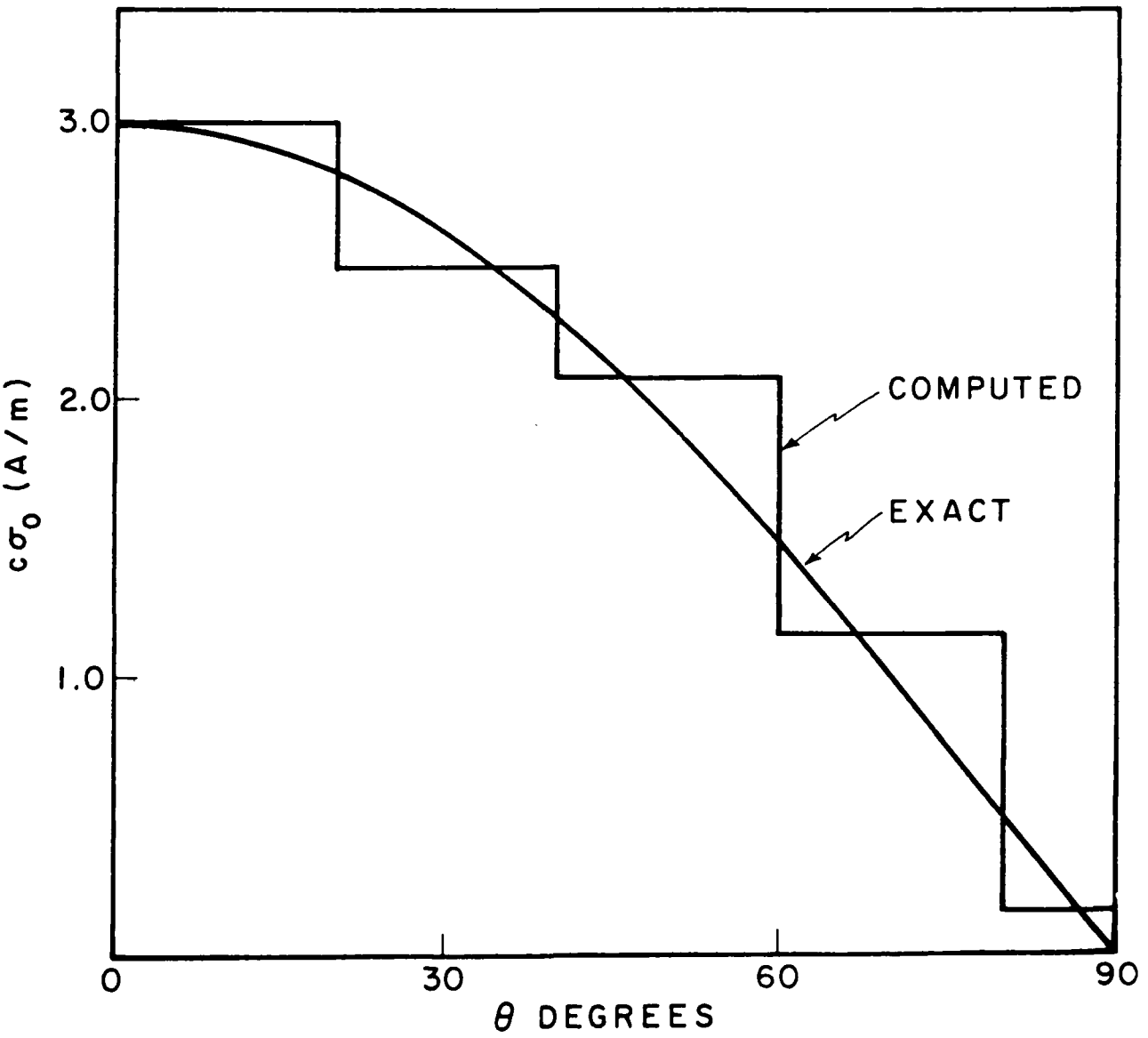

Fig. 3.3. Induced charge distribution on a sphere due to a z-polarized incident plane wave. No. of unknowns = 193 , c = the speed of light , $\underline{E}_0^i = 377\ \hat{z}$ (V/m).

Table 3.1. Comparison of the computed and exact dipole moments for a sphere, plane wave incidence. $N_\theta = 8$, $N_\phi = 12$, No. of unknowns in magnetostatic problem = 97, No. of unknowns in electrostatic problem = 193. Exact area = 4π, $|\underline{E}^i| = 120\pi$.
Exact $|M^{ind}| = 2\pi$, Exact $|P^{ind}| = 4.18879 \times 10^{-8}$.

Radius of Patched Sphere	Computed Area	Relative % Error	Computed $\lvert M^{ind} \rvert$	Relative % Error	Computed $\lvert P^{ind} \rvert$	Relative % Error
1.0	12.09759	3.73	5.7818	7.98	3.9276×10^{-8}	6.23
1.01	12.34075	1.79	5.9569	5.19	4.0466×10^{-8}	3.39
1.02	12.5863	-0.16	6.1354	2.35	4.1680×10^{-8}	0.49

Table 3.2. Progression of the computed dipole moments for a sphere, with plane wave incidence, as the number of unknowns is increased. Radius of patched sphere is taken to be 1m.
NS = No. of unknowns in electrostatic problem.
NM = No. of unknowns in magnetostatic problem.

N_θ	N_ϕ	Computed Area	Relative % Error	NM	$\lvert \underline{M}^{ind} \rvert$ Computed	Relative % Error	NS	$\lvert P^{ind} \rvert$ Computed	Relative % Error
5	8	11.525	8.28	41	5.202	17.2	81	3.3706×10^{-8}	19.5
7	8	11.70675	6.8	57	5.3898	14.2	113	3.4883×10^{-8}	16.7
7	12	12.0456	4.14	85	5.7249	8.88	169	3.769×10^{-8}	10
8	12	12.09759	3.73	97	5.7818	7.98	193	3.927×10^{-8}	6.23

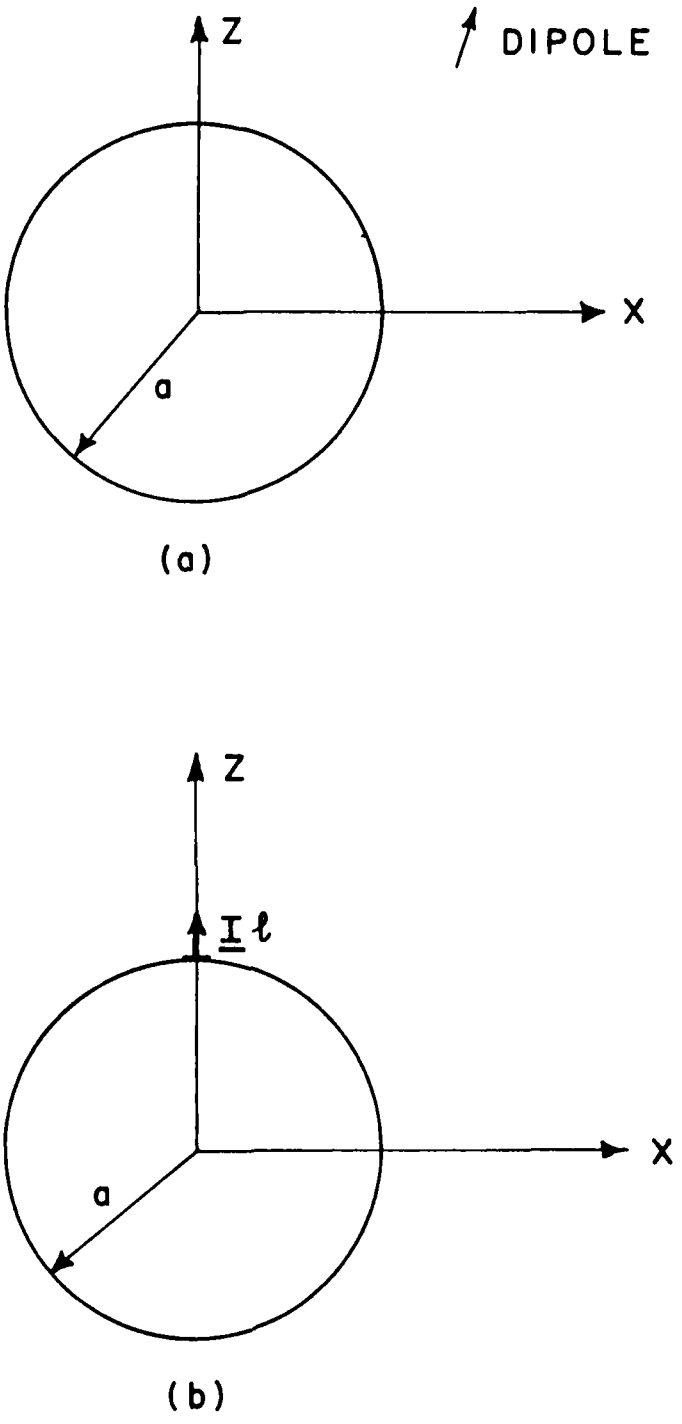

Fig. 3.4. a)An arbitrarily oriented oscillating electric (or magnetic) dipole near a conducting sphere. b) A radially directed oscillating electric dipole on a small conducting sphere.

3.2.1) Electric Dipole Near a Conducting Sphere

Figure 3.4b shows a radially oriented oscillating electric dipole $I\ell$ on a perfectly conducting sphere. In the limit ka → 0, it is stated in [16] that the induced dipole moment is twice that of the source dipole. In fact, the first term in the exact expression for the total far field is the field of $3I\ell$ placed at the origin (Eq. (6-118) of [4]). Hence the far field can be computed by replacing the system in Fig. 3.4b by an electric dipole of moment $3I\ell$ placed at the origin. The moment of this dipole is independent of the radius of the sphere, as long as ka is very small.

To get more information about the induced dipole moment and the induced charge density, we used image theory to solve the electrostatic problem depicted in Figure 3.5a. Here we have a radially oriented static electric dipole near a perfectly conducting sphere. To apply the method of images, we assume that the dipole is composed of two point charges of opposite sign displaced a small distance d such that

$$\lim_{d\to 0} Qd = P \tag{3-9}$$

The values and the positions of the image charges are shown in Figure 3.5b. Q_3 is used to maintain charge neutrality. In the limit d → 0, we have the following results

$$\sigma = \frac{P}{4\pi a}\left[-\frac{1}{Z_1^2} + \frac{Z_1(Z_1^2 - 5a^2) + a(Z_1^2 + 3a^2)\cos\theta}{(Z_1^2 + a^2 - 2Z_1 a\cos\theta)^{5/2}}\right] \tag{3-10}$$

$$V_o = \frac{-P}{4\pi\varepsilon Z_1^2} \tag{3-11}$$

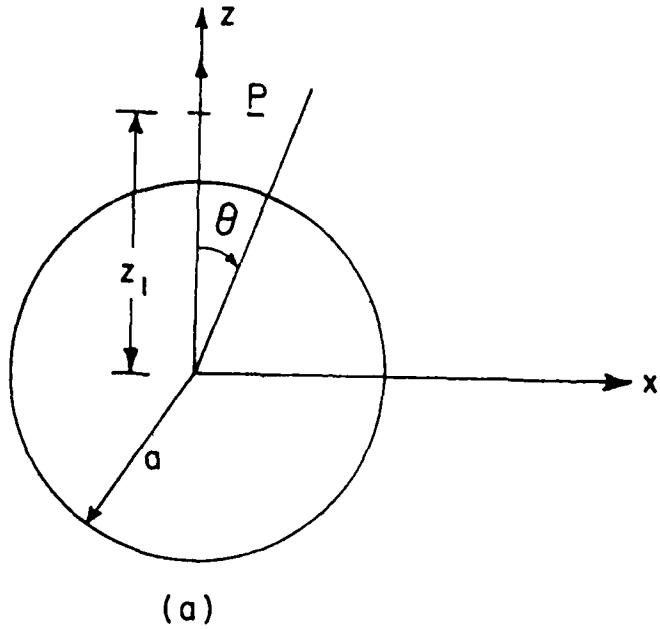

(a)

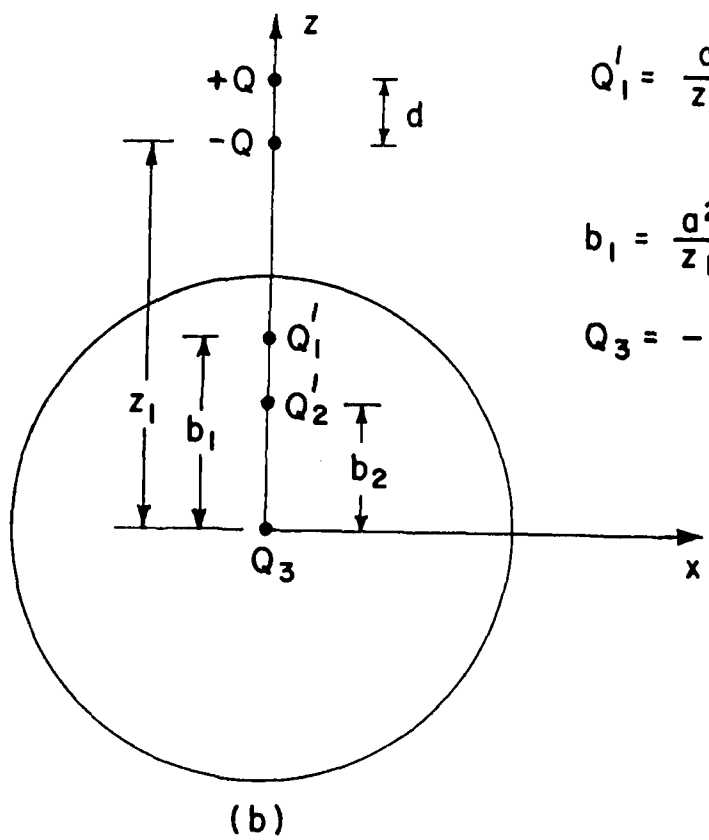

$$Q_1' = \frac{a}{z_1} Q \,, \quad Q_2' = -\frac{a}{(z_1+d)} Q$$

$$b_1 = \frac{a^2}{z_1} \,, \quad b_2 = \frac{a^2}{(z_1+d)}$$

$$Q_3 = -(Q_1' + Q_2')$$

(b)

Fig. 3.5. a)A radially oriented static electric dipole near a conducting sphere. b)An approximate representation of the problem in (a) , in terms of the method of images.

$$P^{ind} = 2\left(\frac{a}{Z_1}\right)^3 P \qquad (3\text{-}12)$$

Here σ is the induced charge density on the sphere, V_o is the potential of the sphere, and P^{ind} is the induced dipole moment. Notice from (3-12) that for $Z_1 \gg a$ the induced dipole moment is twice that of source dipole, independent of the radius a.

To compute an approximate solution for the electrostatic problem of Fig. 3.5a we patch the spherical surface non-uniformly. By this we mean the density of triangular patches is increased in the region close to the source. Since the incident potential varies rapidly in that region, the induced charge density is expected to do so also. The case where the dipole is just on the sphere ($Z_1 \to a$) is treated later. For $Z_1 > a$ we have taken

$$\underline{P} = 4\pi\varepsilon_o \hat{\underline{z}} \qquad (3\text{-}13)$$

So that the incident potential is given by

$$\phi^i = \frac{z - Z_1}{((z - Z_1)^2 + x^2 + y^2)^{3/2}} \quad . \qquad (3\text{-}14)$$

Figure 3.6 shows the induced charge density on the sphere when a = 2 meters and Z_1 = 3 meters. Also shown in the figure is the exact result of (3-10) for comparison. The agreement is good. Figure 3.7 shows the variation of the computed potential of the sphere as the dipole moves away from the sphere. The exact result of (3.11) is also shown. The agreement between both results is again good. Figure 3.8 shows the variation of the induced dipole moment with the location of the source dipole. The exact result of (3-12) shows very good agreement with the computed one.

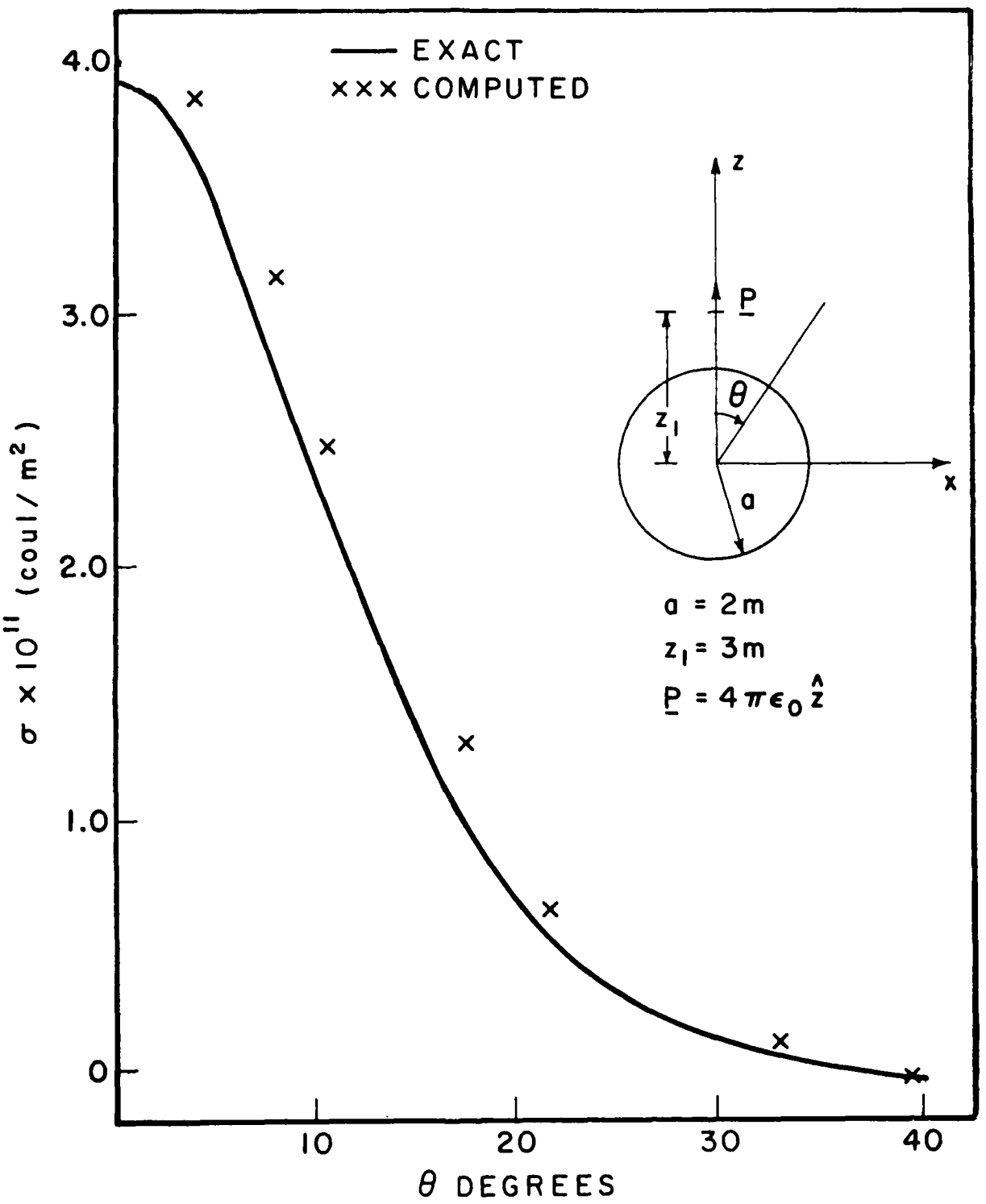

Fig. 3.6. Induced charge distribution on a sphere near an electric dipole.

No. of unknowns = 193.

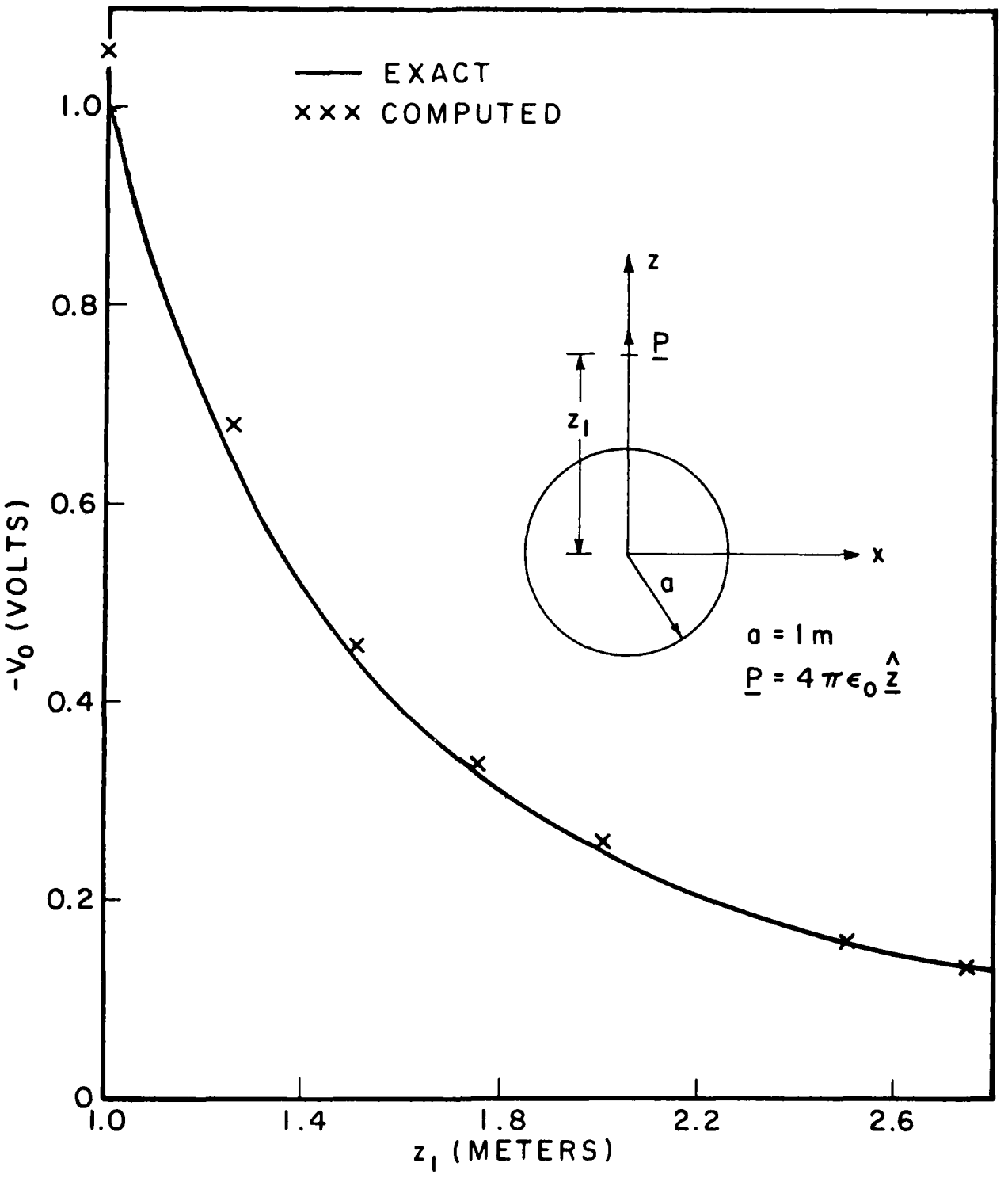

Fig. 3.7. The variation of the potential of the sphere with the distance Z_1.

No. of unknowns = 193.

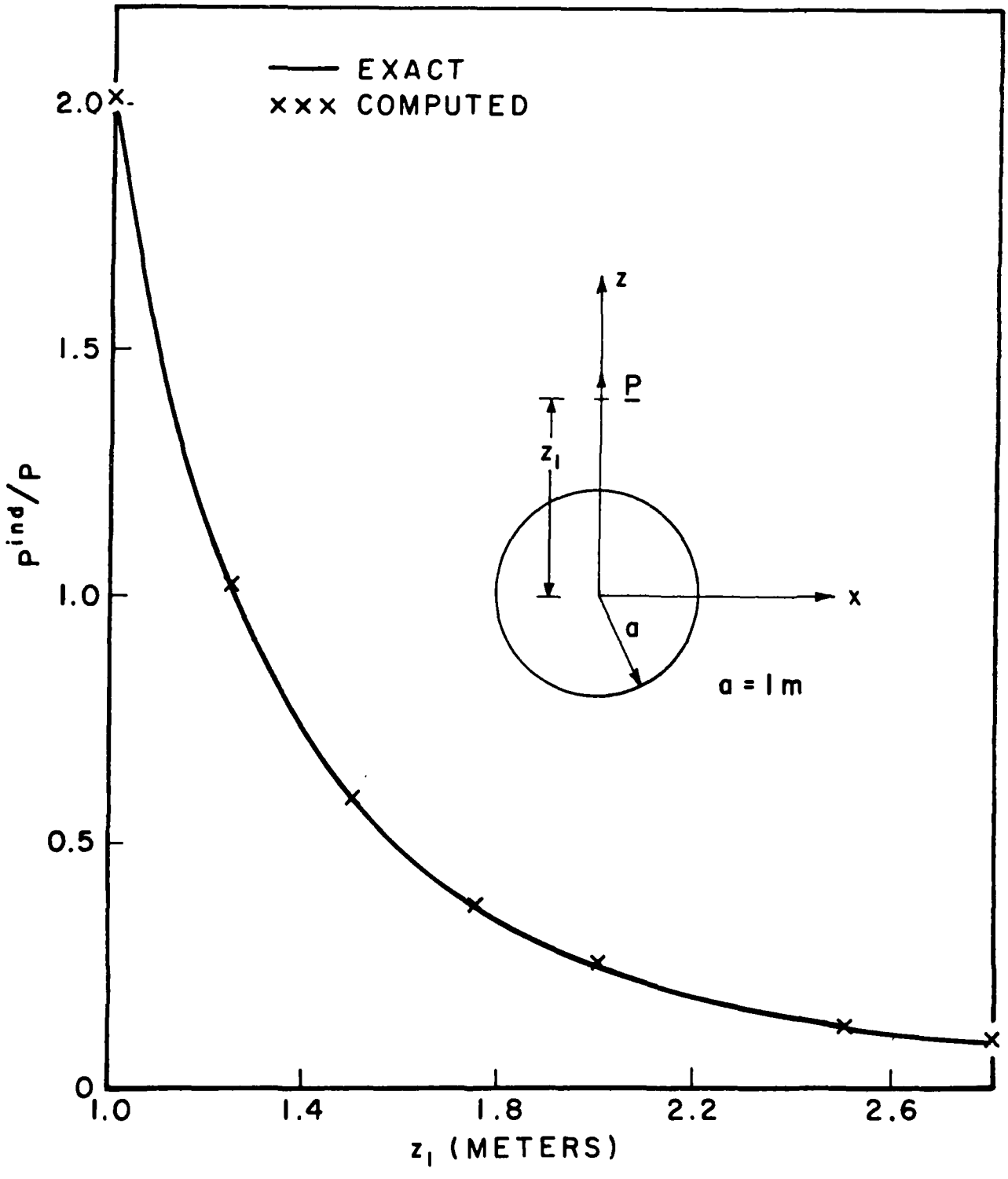

Fig. 3.8. Variation of the induced dipole moment with the distance Z_1.

No. of unknowns = 193.

When the dipole is just on the sphere (i.e., $Z_1 \to a$), the incident potential is very large and is changing rapidly over the region close to the dipole. Hence, the direct use of the point matching scheme does not give good results. To overcome this difficulty due to the singularity in the incident potential, we solve an equivalent problem. Here another dipole is placed just inside the sphere, below the original source dipole. Figure 3.9 shows the configuration. It is clear that the total potential produced by the original and the pseudo-image dipole will be approximately zero on a small region defined by θ_o on the spherical surface (Fig. 3.9b). The total incident potential outside this small region will be twice that produced by the original source dipole, and will vary slowly. The induced charge distribution in this equivalent problem is obviously different from the one in the original problem. The total potential at any exterior point will be the same in each case, that is

$$\phi^T = \phi^i(\underline{P}) + \phi(\sigma) \tag{3-15}$$

or

$$\phi^T = \phi^i(2\underline{P}) + \phi(\sigma_e) = 2\phi^i(\underline{P}) + \phi(\sigma_e) \tag{3-16}$$

Here ϕ^T denotes the total potential at an exterior point, σ and σ_e are the charge distributions in the original and equivalent problems respectively, $\phi^i(\underline{P})$ denotes the incident potential due to an electric dipole $\underline{P}$, and $\phi(\sigma)$ and $\phi(\sigma_e)$ denote the potentials produced by the induced charges in the original and equivalent problems , respectively. The induced dipole moments are related as follows:

$$\underline{P}^{ind} = \underline{P}_e^{ind} + \underline{P} \tag{3-17}$$

where $\underline{P}^{ind}$ is the induced dipole in the original problem, $\underline{P}_e^{ind}$ is the induced dipole in the equivalent problem and $\underline{P}$ is the source dipole in the original problem.

We assumed θ_o to be five degrees and patched the dashed region of Fig. 3.9b by twelve triangular patches. Hence, the twelve elements of the excitation vector $\vec{\Phi}$ of (2-12) corresponding to these triangles are set to zero. For a = 2 meters and $\underline{P} = 4\pi\varepsilon_o \hat{\underline{z}}$, the computed results are as follows:

$$\underline{P}^{ind} = 2.01125\ \underline{P}$$

$$V_o = -\ 0.2695$$

The exact results are given by the following

$$\underline{P}^{ind} = 2\ \underline{P}$$

$$V_o = -\ 0.25$$

The relative errors in the computed results are 0.56 and 7.8 percent respectively.

As pointed out earlier, the exact result for the problem shown in Fig. 3.4b is given in [4]. Figure 3.10 compares the total computed and exact fields at various distances. The computed field is produced by an oscillating electric dipole of moment $3\underline{I}^{\ell}$ at the origin. The diameter of the sphere is taken to be 2 meters and the wavelength is 50 meters. The exact result is obtained by taking the first seven terms of the eigenfunction series given in (6-120) of [4]. Note that the fields in the figure are normalized with respect to the same constant. That is, the actual fields are $|\eta I^{\ell}/4^{-}jk|$ times the values shown in the figure. It is seen that even at a distance equal to a half-wavelength the agreement between the two results is very good.

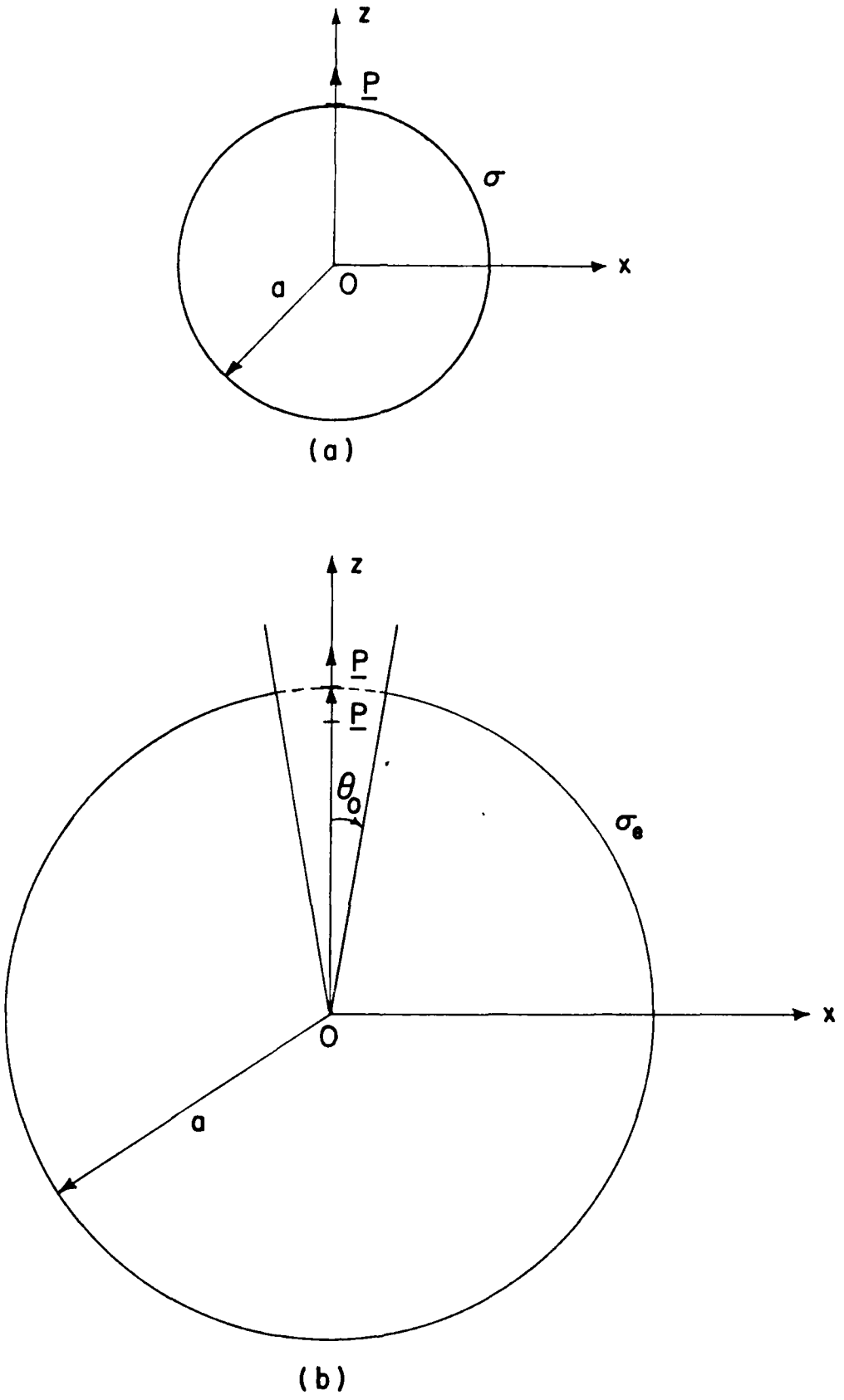

Fig. 3.9. a) Original problem. b) An equivalent problem for the exterior region. The total incident potential is approximately zero over the dashed region. For small θ_0 the dashed region is approximately a planar surface.

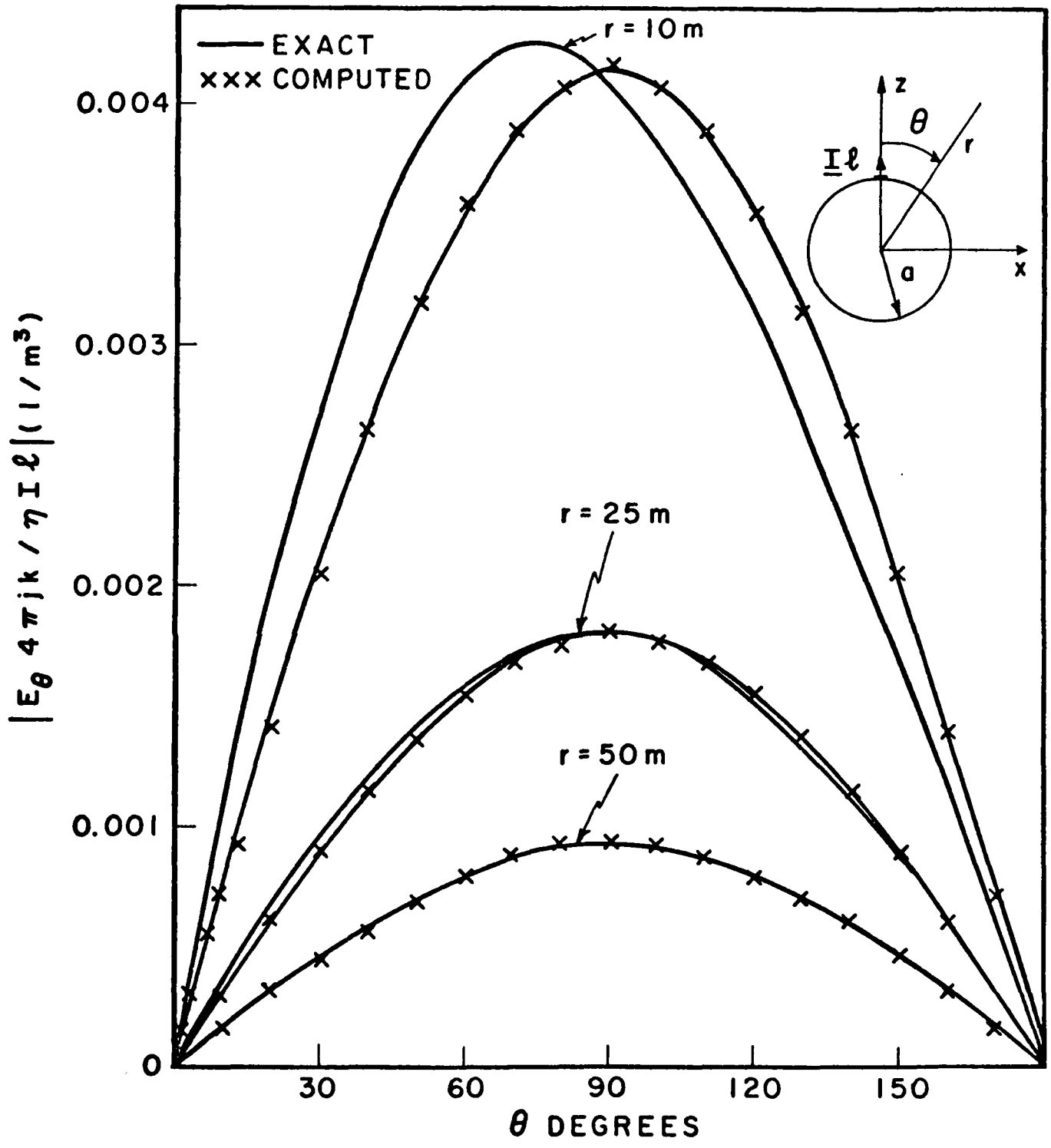

Fig. 3.10. The total field for the problem of Fig. 3.4b .

a=1m. , λ=50m.

Figure 3.11 compares the far fields for two different radii. The radius of the sphere is taken to be 2 meters or 5 meters. The wavelength is fixed at 50 meters, and the source dipole $I\ell$ is assumed to be on the sphere. For both radii the exact induced dipole is $2I\ell$. Hence the far field computed by replacing the system of Fig. 3.4b with $3I\ell$ placed at the origin will be the same whether the radius is 2 meters or 5 meters. This is why we have only one curve for the dipole field in the figure. For the exact far field, the first ten terms of the eigenfunction series are summed for a = 5 meters and eight terms are taken for a = 2 meters. The curves shown in the figure are normalized, that is, the true values are $\eta I\ell\ e^{-jkr}/r$ times the values shown in the figure. It is seen that if the diameter/wavelength ratio is more than 0.2, the dipole representation is not good, even for the far-field computations.

3.2.2) Magnetic Dipole on a Small Sphere

Figure 3.12a represents an oscillating magnetic dipole $K\ell$ tangentially placed on a small conducting sphere. It is stated in chapter 10 of [16] that the induced dipole moment for this problem (in the limit as ka → 0) is $K\ell/2$. (The problem depicted in Fig. 3.12a may represent an equivalent problem for computation of the field transmitted through a short and narrow slot on the conducting sphere.) To solve the corresponding magnetostatic problem, we use the technique described earlier, that is, we place a pseudo-image magnetic dipole just below the original one, inside the sphere, and patch the region near these dipoles densely. If θ_o is small enough, then the normal component of the total magnetic field produced by both dipoles is approximately zero on the dashed region of Fig. 3.12b. Hence

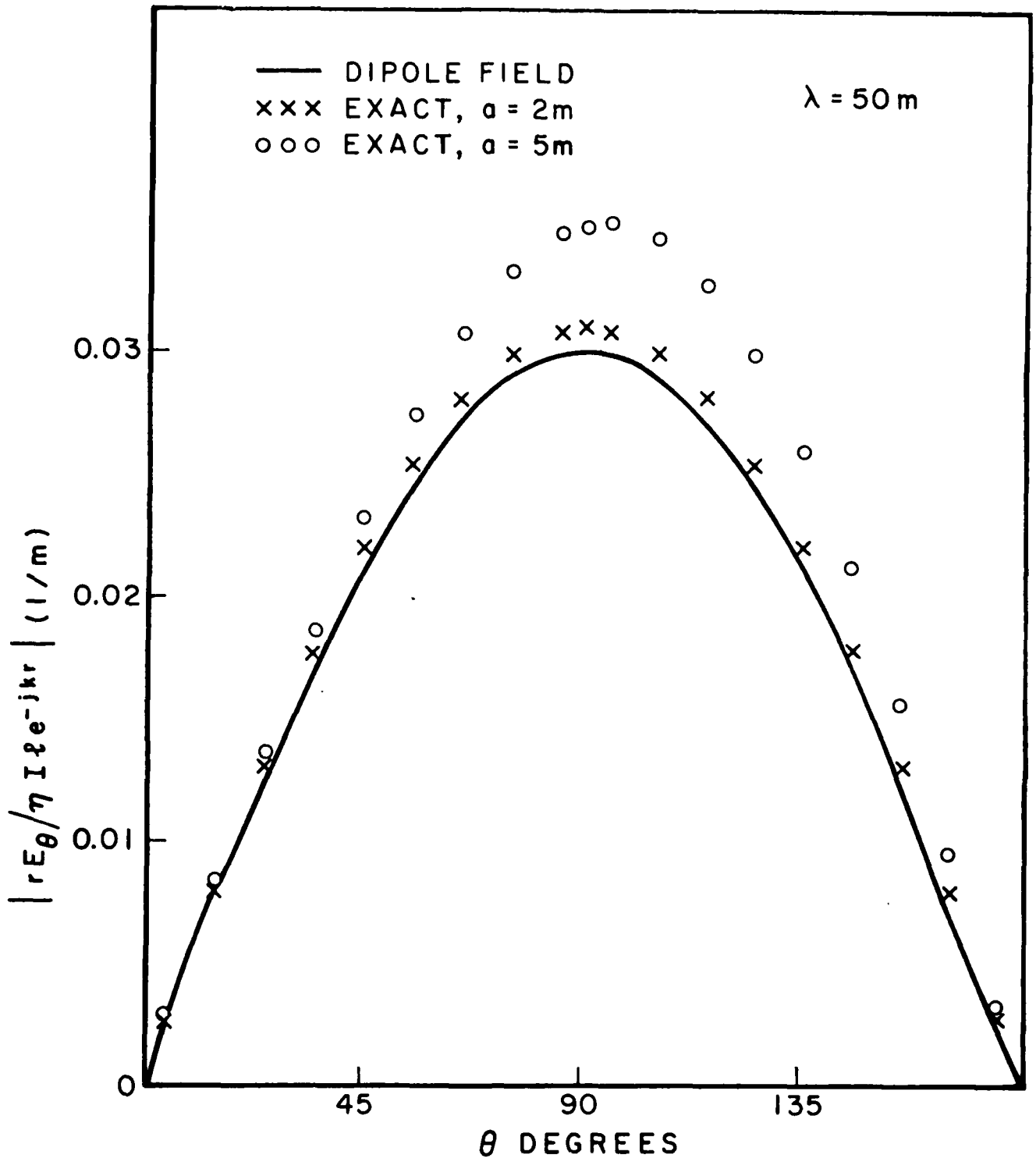

Fig. 3.11. The far field for two different radii in the problem of Fig. 3.4b.

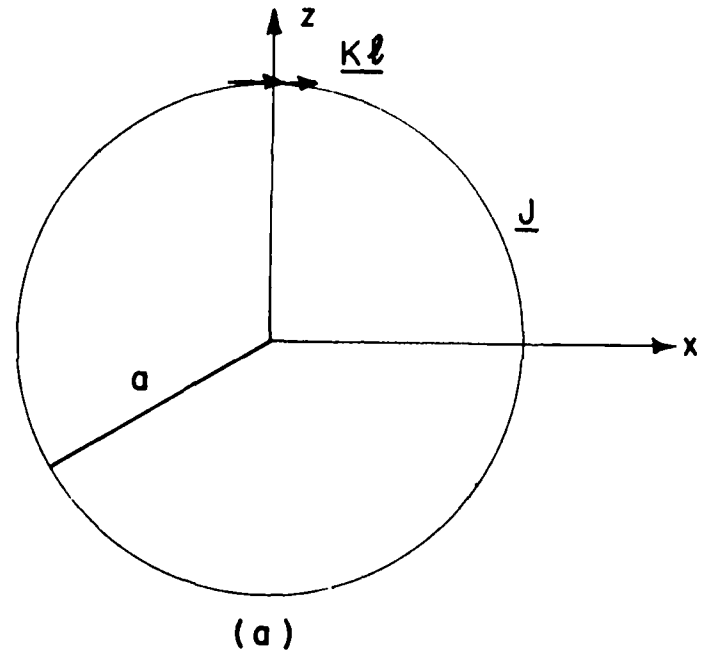

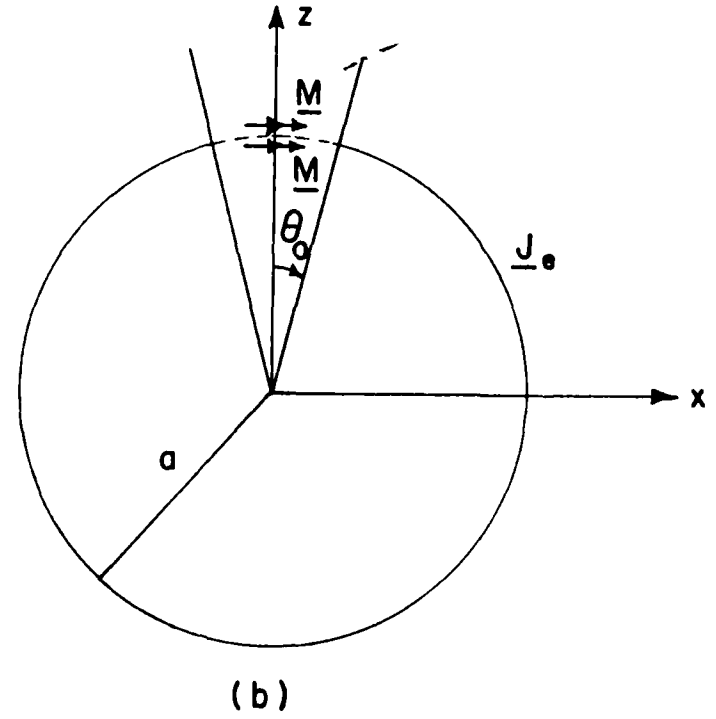

Fig. 3.12. a)An oscillating magnetic dipole placed tangentially on a small sphere. b) An approximately equivalent magnetostatic problem.

the element of the excitation vector $\vec{V}$ in (2-49) corresponding to the node at the pole ($\theta = 0°$) is set to zero, and there is no contribution from the triangles in the dashed region to the elements of (2-49) corresponding to the nodes on the boundary of the dashed region. We failed to obtain reasonable answers even to this equivalent problem. We believe this is due to the fact that the singularity of the magnetic field of the magnetic dipole is of the third order. Hence the variation of the incident magnetic field is too fast and the approximation of (2-47) by (2-48) is not valid in this case. (In the electric dipole case the singularity of the incident potential was of second order, and we could obtain reasonable results for the equivalent problem shown in Fig. 3.9b.)

Notice that the singularity of the electric field produced by a magnetic dipole is of the second order. Hence we use Maxwell's equations and some vector calculus to express the excitation vector for the magnetostatic problem (Eq.(2-47)) in terms of the incident electric field. From (2-47), we have

$$V(j) = -\sum_{m=1}^{t_j} \iint_{S_{jm}} \psi_{jm}(\underline{r})\, \hat{\underline{n}}_{jm} \cdot \underline{H}^{imp}(\underline{r})\, ds$$

$$= \sum_{m=1}^{t_j} \iint_{S_{jm}} \psi_{jm}(\underline{r})\, \hat{\underline{n}}_{jm} \cdot \frac{\nabla \times \underline{E}^{imp}}{j\omega\mu}\, ds$$

$$= -\frac{1}{j\omega\mu} \sum_{m=1}^{t_j} \iint_{S_{jm}} (\hat{\underline{n}}_{jm} \times \nabla_s \psi_{jm}) \cdot \underline{E}^{imp}\, ds$$

$$\simeq \frac{-1}{j\omega\mu} \sum_{m=1}^{t_j} (\underline{J}_{jm} \cdot \underline{E}^{imp}(\underline{r}_{cjm}))\, T_{jm} \qquad (3\text{-}18)$$

For the dipole of Fig. 3.12a, we have

$$\underline{E}^{imp} = \frac{j\omega\mu M}{4\pi} e^{-jkr} \left(\frac{jk}{r^2} + \frac{1}{r^3}\right)(\hat{y}(z-a) - \hat{z}\, y) \tag{3-19}$$

where

$$r = \sqrt{x^2 + y^2 + (z-a)^2} \tag{3-20}$$

and

$$j\omega\mu\underline{M} = \underline{K}\ell \tag{3-21}$$

Substituting (3-19) into (3-18) and taking the limit $k \to 0$, we have

$$V(j) \cong \frac{-M}{4\pi} \sum_{m=1}^{t_j} T_{jm}\, \underline{J}_{jm} \cdot \left(\frac{\hat{y}\,(z_{cjm} - a) - \hat{z}\, y_{cjm}}{r_{cjm}^3}\right) \tag{3-22}$$

Here z_{cjm} and y_{cjm} represent the coordinates of the centroid of the triangle S_{jm}, and r_{cjm} is the distance from the dipole to this centroid. Using (3-22) instead of (2-49) for the excitation vector, we solve the magnetostatic problem shown in Fig. 3.12b. With dipole moment $\underline{M} = 0.4\pi\hat{x}$, a=1 meter, and $\theta_o = 5$ degrees (Fig. 3.12b) the computed ratio of the induced to original dipole moment is 0.4889. The exact result for this ratio is 0.5. The relative error is 2.2 percent. The number of unknowns used for this problem is 97. We have also observed that the computed ratio does not depend on the radius of the sphere.

3.3. The Circular Disc

Figure 3.13a represents a conducting circular disc lying in the xy plane. The other parts of the figure show various types of electromagnetic illumination of the disc. The disc problem has been studied extensively and a summary of the results can be found in Chapter 14 of [16].

Figure 3.14 shows the induced magnetostatic current density on the disc due to an incident plane wave, as shown in Fig. 3.13b. The radius of

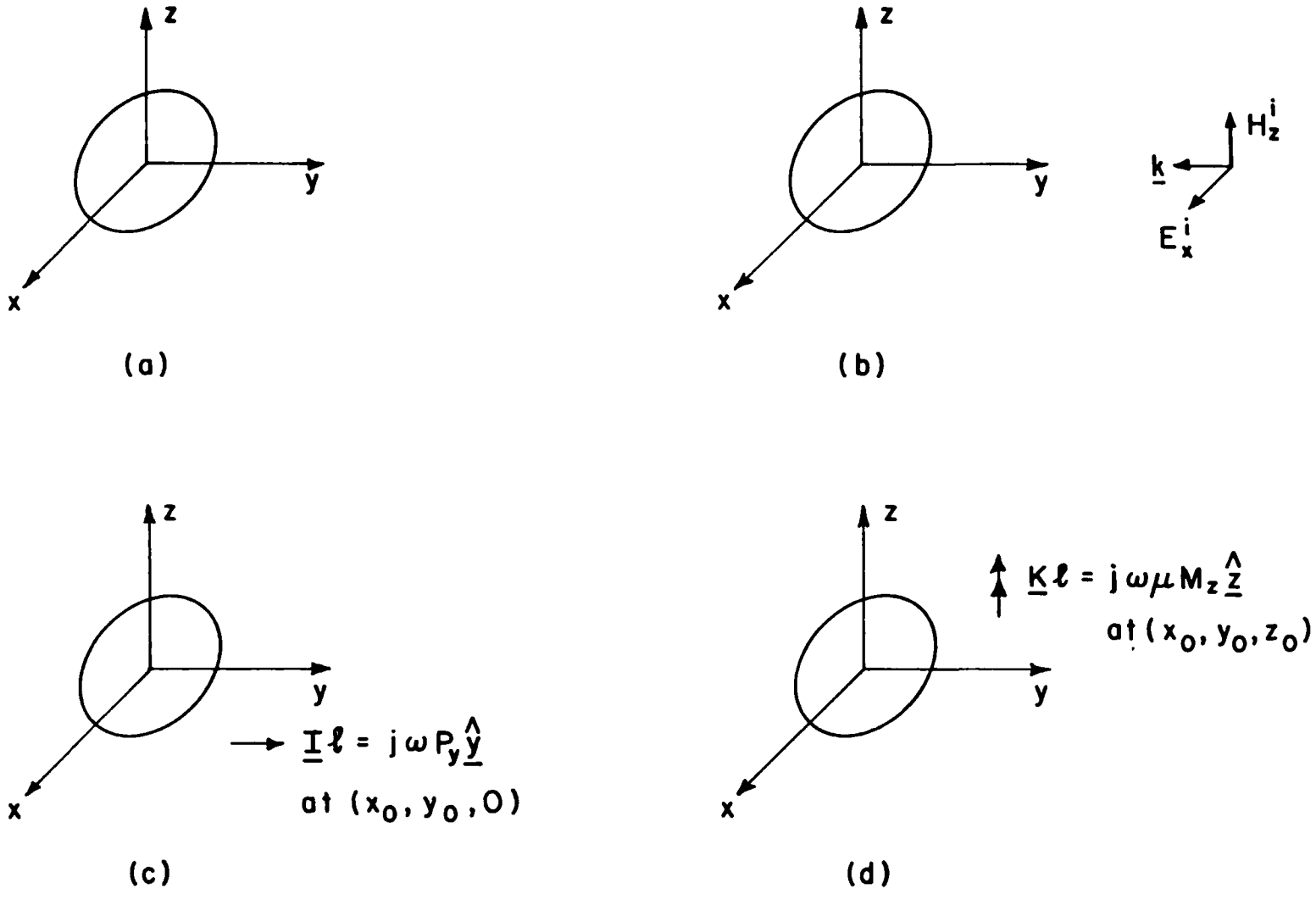

Fig. 3.13. a) The circular disc in the xy plane. b)Edge-on plane wave incidence. c)An electric dipole in the xy plane. d)A magnetic dipole perpendicular to the plane of the disc.

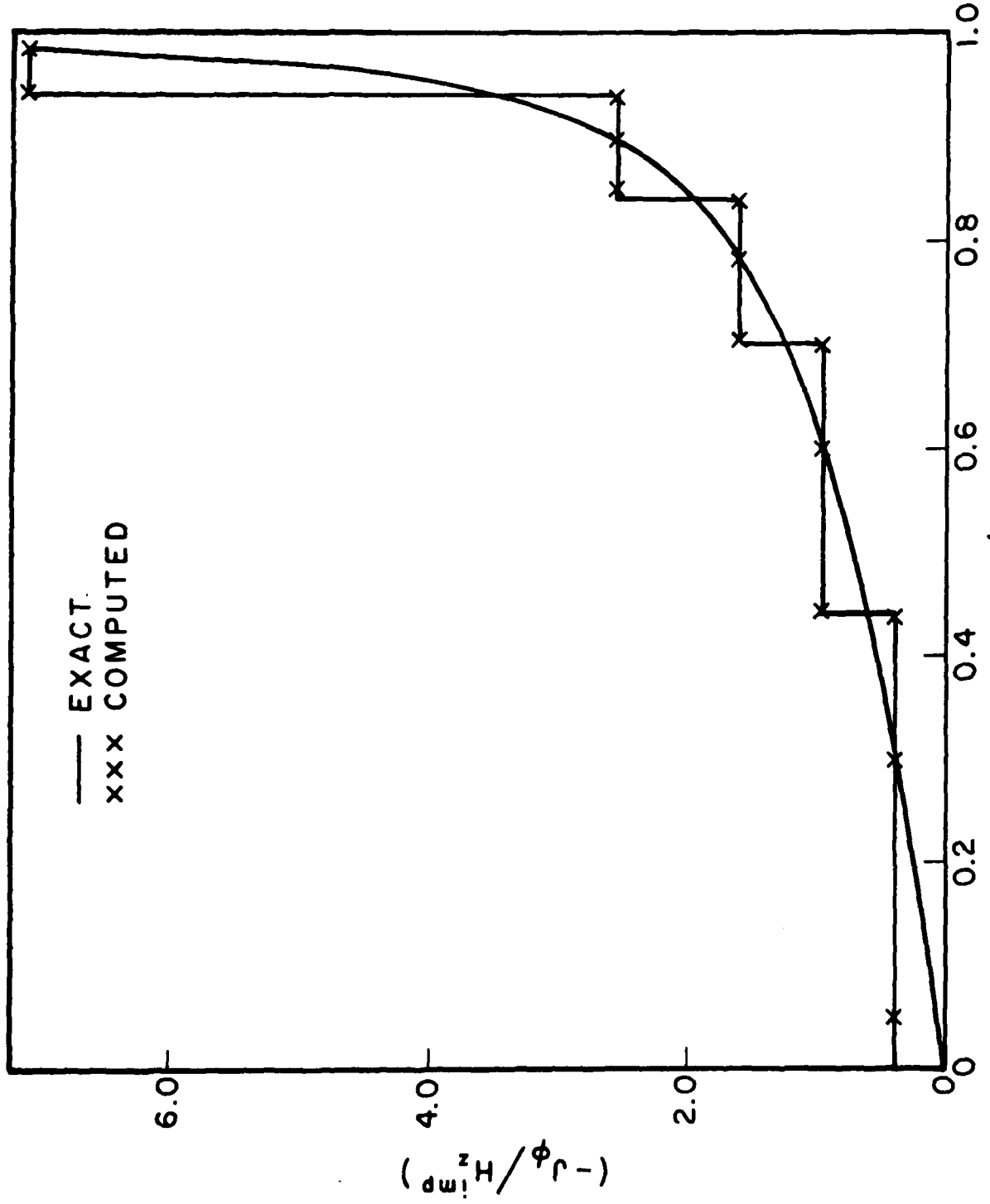

Fig. 3.14. Current induced on the disc of Fig. 3.13b.

the disc is taken to be 1 meter, and the number of unknowns used to compute the current density is 81. The exact result is taken from [17]. It is seen that the computed result is a good step approximation to the exact one.

Tables 3.3 to 3.5 summarize the results concerning the induced dipole moments for the disc problem. The exact results are obtained using the equations (14.185),(14.187),(14.188),and (14.193) of [16].

3.4. The Square Plate and the Bent Plate

Figure 3.15 shows the induced current density on a square plate of 1 meter side length, for two different incident plane waves. The plate is placed in the xy plane. Also shown in the figure is the result obtained using the E-field solution program written by Rao [14], where we let the wavelength be 56 meters. It is seen from the figure that the magnetostatic part is dominant in the total induced current, even for θ = 20 degrees. At θ = 0 degrees (normal incidence) the magnetostatic current vanishes.

Figure 3.16 shows the induced magnetostatic current density on a bent square plate of side length 1.5 meters. The bend is located at a distance of one third the width from an edge, and a plane wave with the magnetic field polarized perpendicular to the larger section of plate is incident. The smaller plate section is bent through an angle of 50 degrees away from the direction of propagation, which is parallel to the larger section of the plate.

Table 3.3. Induced dipole moments for the problem of Fig. 3.13b. $E_x^i = 377$ (V/m), $H_z^i = 1$ (A/m); N, N^b = No. of unknowns, exact $\underline{M}^{ind} = -2.66\ \hat{\underline{z}}$, exact $\underline{P}^{ind} = 0.178 \times 10^{-7}\ \hat{\underline{x}}$.

N^b	Computed M_z^{ind}	Relative % Error	N	Computed P_x^{ind}	Relative % Error
37	-2.2853	14.3	85	0.1539×10^{-7}	13.5
49	-2.3407	12.2	109	0.1574×10^{-7}	12
81	-2.5162	5.6	181	0.1685×10^{-7}	5.3

Table 3.4. Induced electric dipole moment for the problem of Fig. 3.13c. No. of unknowns = 109, source dipole $\underline{P} = 4\pi\epsilon_o\hat{\underline{y}}$ at (x_o, y_o, z_o).

x_o	y_o	z_o	Computed P_y^{ind}	Exact P_y^{ind}	% Error
0	1.5	0	$0.335\ 10^{-10}$	0.3544×10^{-10}	5.5
1.2	1.2	0	$0.602\ 10^{-11}$	0.63404×10^{-11}	5

Table 3.5. Induced magnetic dipole moment for the problem of Fig. 3.13d. No. of unknowns = 49, source dipole $\underline{M} = 4\pi\hat{\underline{z}}$ at (x_o, y_o, z_o)

x_o	y_o	z_o	Computed M_z^{ind}	Exact M_z^{ind}	% Error
1.2	1.2	0	0.671	0.678	1.06
0	0	2	-0.456	-0.466	2.2

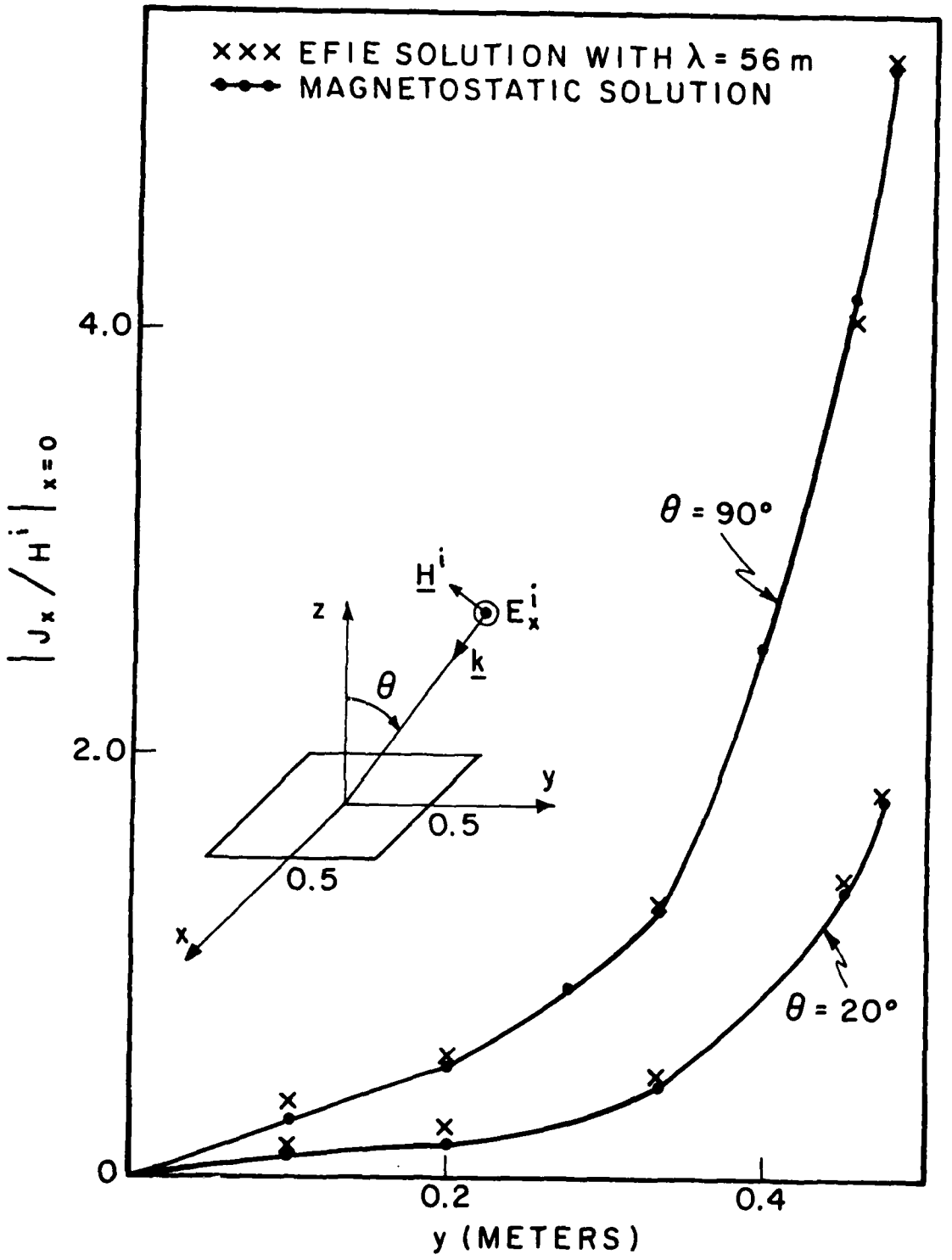

Fig. 3.15. Induced current on a square plate due to two different incident plane waves.

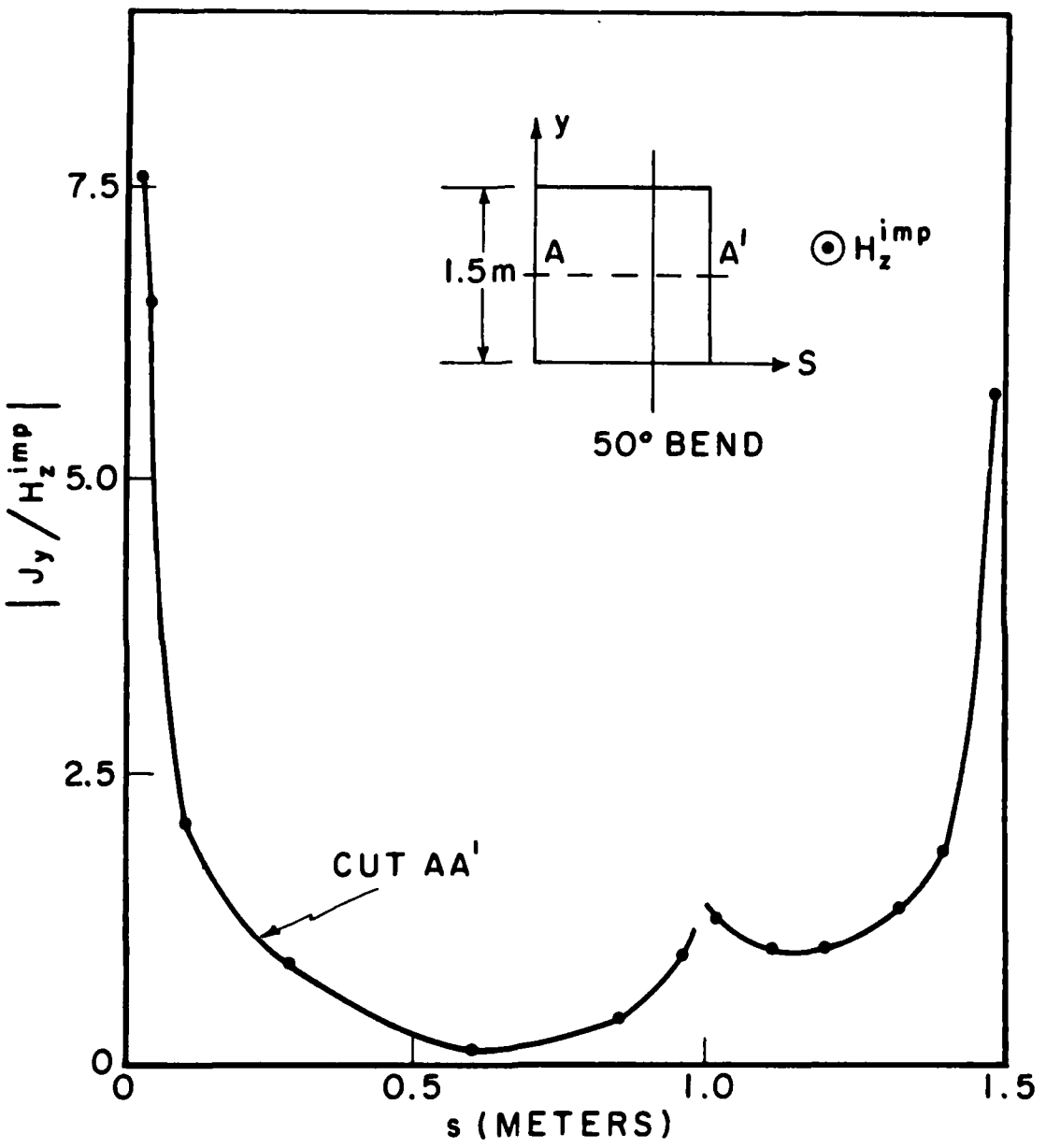

Fig. 3.16. Distribution of the magnetostatic current on a bent square plate.

No. of unkowns = 77.

3.5. The Small Conducting Cube

3.5.1) Plane Wave Incidence

Figure 3.17a represents a conducting cube of side length 0.1λ illuminated by a plane wave. Figure 3.18 shows the induced current density on the right face, computed using the magnetostatic formulation. Figure 3.19 shows the induced current on the top face. Also shown are the results obtained by using Rao's [14] E-field solution. Close agreement between the two results is not expected, since the maximum dimension of the cube is 0.17λ in this case. Our result also has some similarity with the result of [18] obtained using rectangular patches, but a precise comparison was not possible. Although the current distribution is not in close agreement with the two results mentioned above, the computed radar cross section does agree very well with published data. If E_x^i of Fig. 3.17a is taken to be 120π (V/m), then the computed induced dipoles for the cube of side length one meter are given by $\underline{P}^{ind} = 0.115\times10^{-7}\hat{\underline{x}}$ (C-m) and $\underline{M}^{ind} = -1.57\ \hat{\underline{z}}$ (A-m^2). The radar cross section obtained using these dipoles as the source of the scattered field is $0.0031\lambda^2$. This result agrees with the experimental and computational results mentioned in [18]-[19]. In fact, we have observed that the radar cross section obtained using these dipoles agrees (within less than ten percent) with the published results [19] even for a side length of 0.2λ. Note that in this case the maximum dimension of the cube is as large as 0.35λ.

Finally, we have observed that the induced dipole moments are proportional to the volume of the cube. This is expected , since the induced charge and current distributions do not depend on the size of the cube.

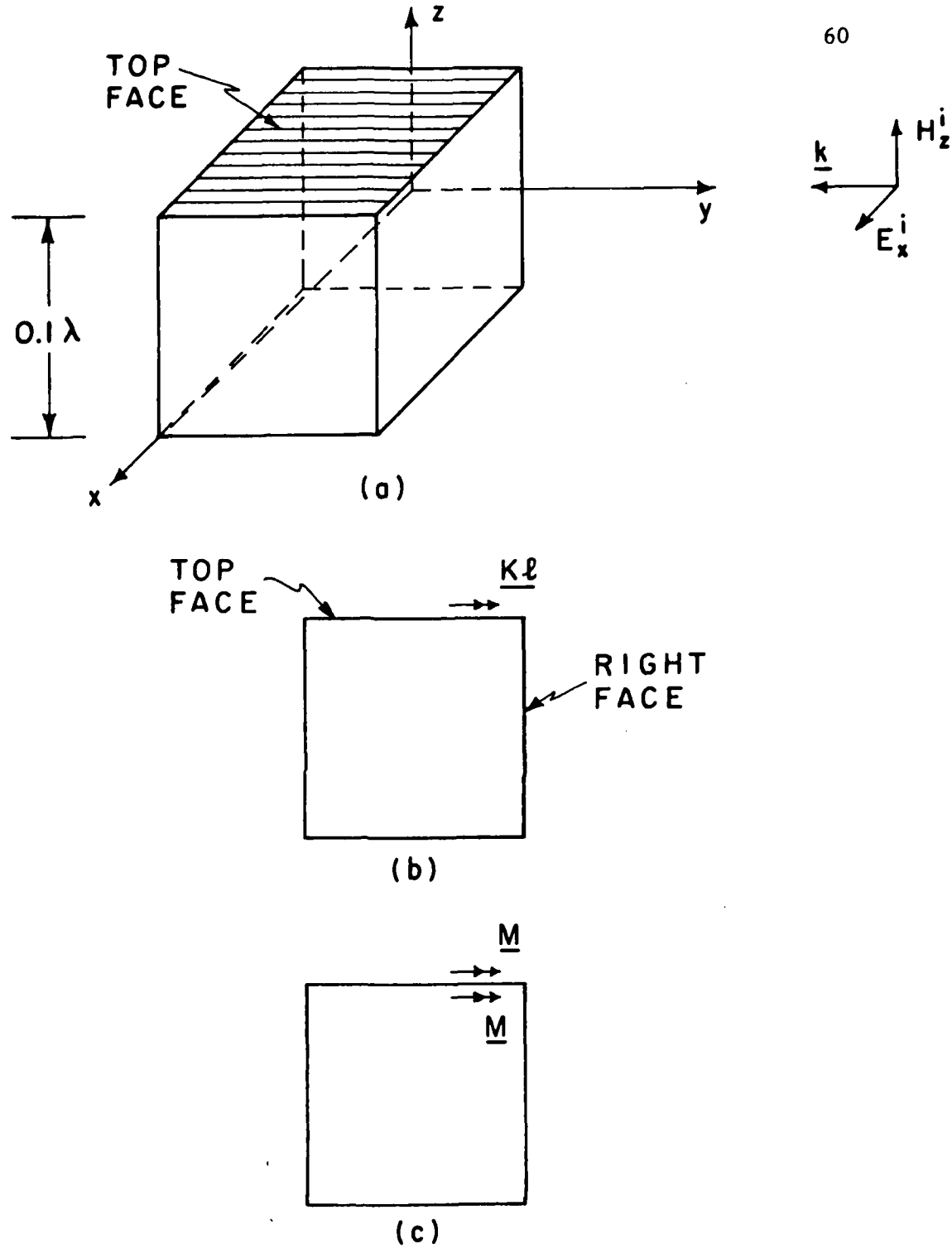

Fig. 3.17. a)Plane wave normally incident on a small conducting cube. b)An oscillating magnetic dipole on the top surface of the cube. c) Equivalent magnetostatic problem for part (b) ; A pseudo-image magnetic dipole is placed just inside the cube, below the source dipole M.

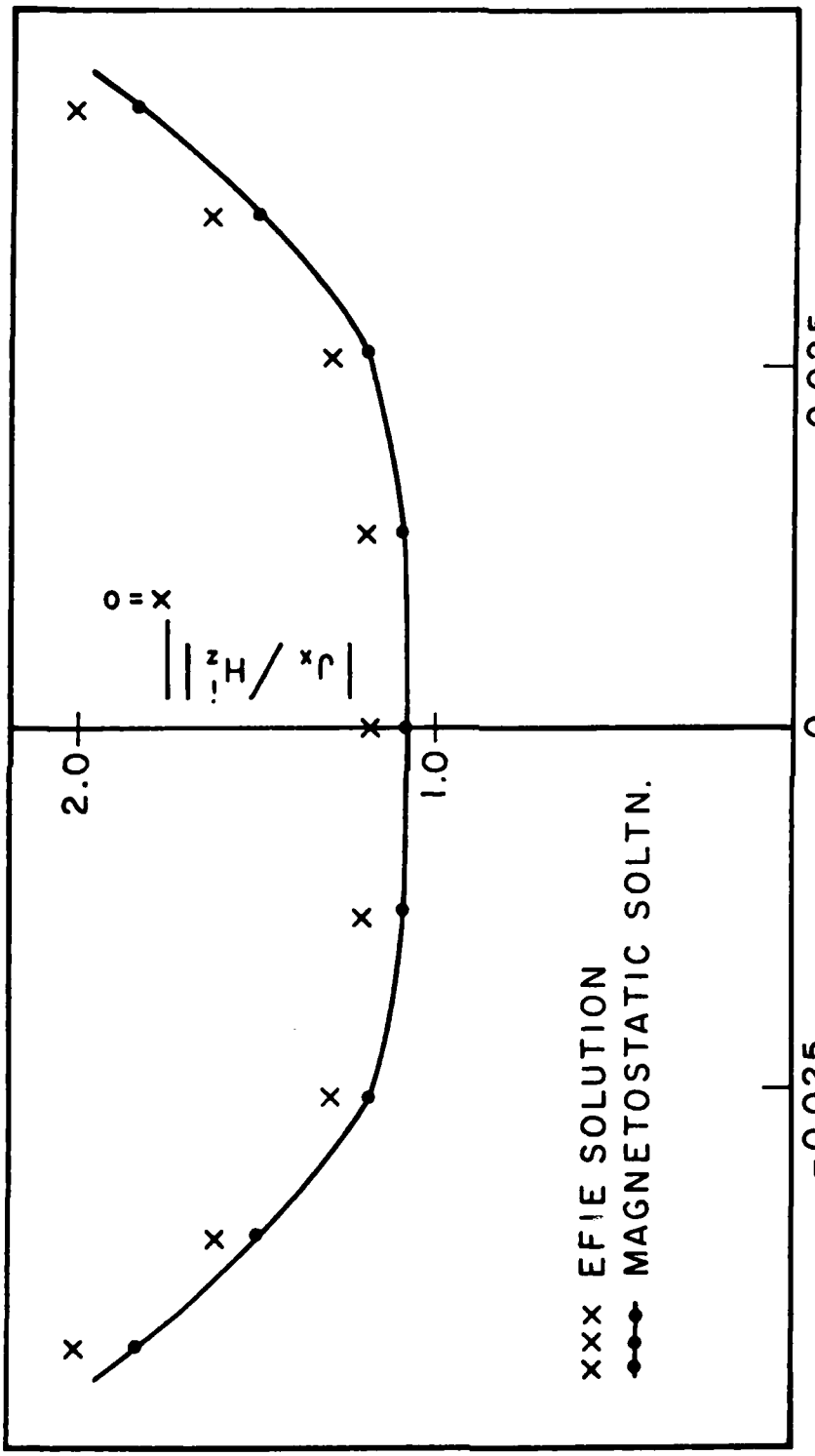

Fig. 3.18. The induced current on the right face (y=0.05λ) of the cube of Fig. 3.17a.

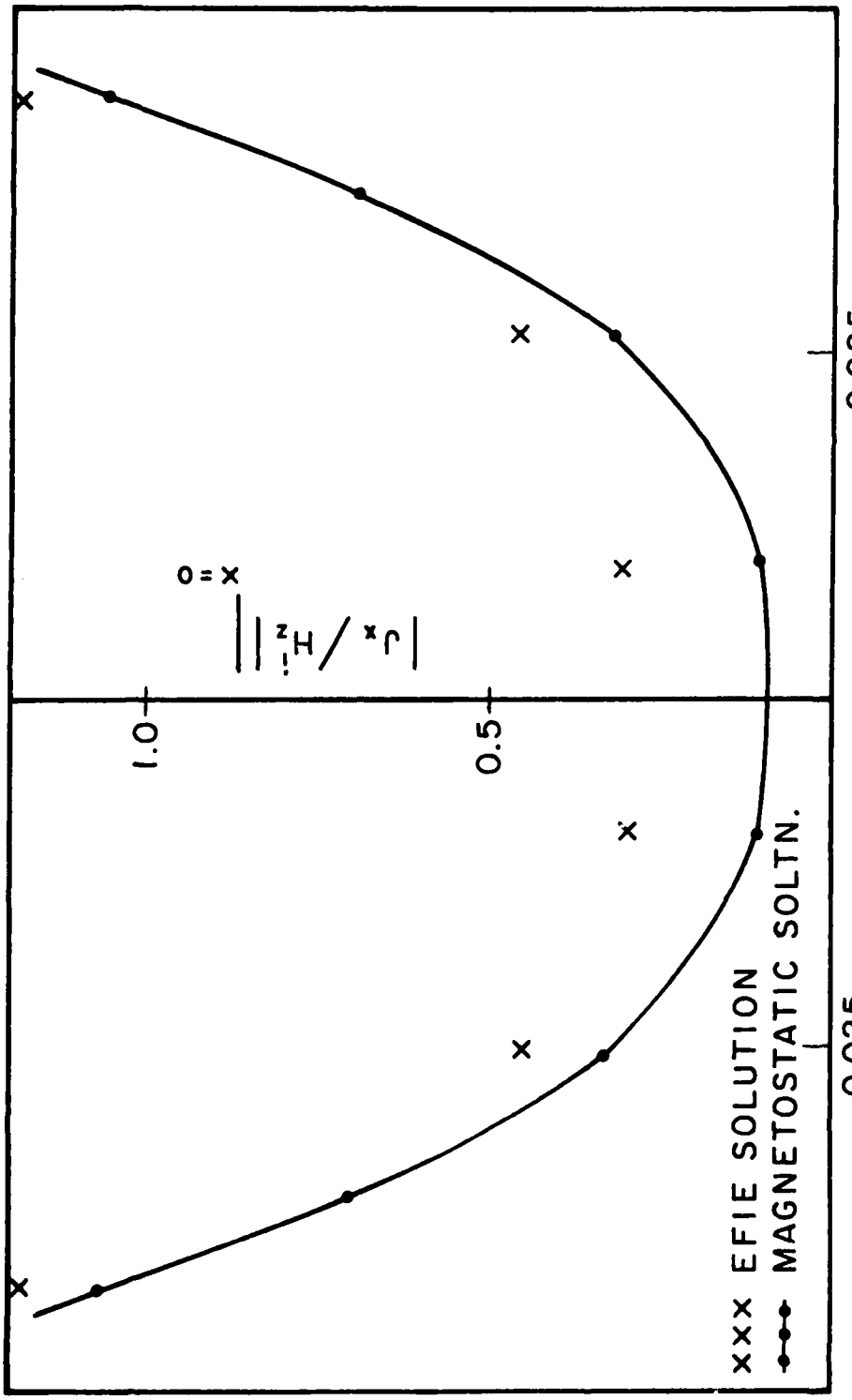

Fig. 3.19. The induced current on the top face of the cube of Fig. 3.17a.

We have also observed that the induced dipole moments for the cube are slightly larger than the ones obtained for the sphere, provided the incident field is the same and the volumes of the sphere and the cube are equal.

3.5.2) A Magnetic Dipole on the Cube

Consider a cube with some internal sources and a small narrow slot on one face. The problem is to compute the fields transmitted through the slot. If the cube is small, then an approximate equivalent problem is shown in Fig. 3.17b. Here we have a magnetic dipole $\underline{K\ell}$ placed tangentially on the cube at the position of the slot, and the slot is shorted. To solve the corresponding magnetostatic problem, we use the pseudo-image technique to obtain the problem depicted in Fig. 3.17c. An image dipole is placed just below the original one, inside the cube. Hence the normal (tangential) component of the total magnetic (electric) field produced by the two dipoles is zero on the face. At any other point on the cube surface the field is twice that produced by the original dipole $\underline{K\ell}$ alone. Because of the singularity problem mentioned in Section 3.2.2, we use (3-18) for the excitation vector.

The center of the cube is placed at the origin of a Cartesian coordinate system. The side length is assumed to be 1 meter. The point ($x = 0$, $y = 0$, $z = 0.5$) defines the center of the top face. The source dipole is taken to be $\underline{M} = 1\hat{\underline{x}}$ (A-m^2). Table 3.6 shows the computed induced dipole moment, as the position (x_o, y_o, z_o) of the source dipole $\underline{M}$ is changed. From the table we conclude that a narrow slot at the center of a face of the cube transmits energy outside less efficiently than a slot closer to the edges of the face.

Finally we have the following observations: i) As the size of the cube is changed keeping the source dipole at the same relative position , the induced dipole moment does not change. For plane wave incidence the induced dipole moments are proportional to the volume of the cube. ii) When a magnetic dipole $\underline{M}$ is placed tangentially at the center of a face of the cube, the computed induced dipole moment is 0.15 $\underline{M}$. This is about three times smaller than the induced magnetic dipole moment if $\underline{M}$ were placed tangentially on a sphere. To see the effect of an electric dipole $\underline{P}$ placed normally at the center of a face of the cube, we compute the induced dipole moment. The computed induced electric dipole moment is 0.65 $\underline{P}$. This also is about three times smaller than the induced electric dipole moment when $\underline{P}$ is placed normally on a sphere.

Table 3.6. Induced magnetic dipole moment due to a tangential magnetic dipole $\underline{M} = 1\ \hat{\underline{x}}$ (A-m^2) on the top face of a cube. The top face is at $z = 0.5$. $\underline{M}$ is at $(x_o, y_o, 0.5)$.

x_o	y_o	Induced Dipole $\underline{M}^{ind}$
0	0	$0.15\ \hat{\underline{x}}$
0.2	0	$0.18\ \hat{\underline{x}} - 0.237\ \hat{\underline{z}}$
0.3	0	$0.22\ \hat{\underline{x}} - 0.406\ \hat{\underline{z}}$
0.45	0	$0.36\ \hat{\underline{x}} - 0.716\ \hat{\underline{z}}$
0	0.2	$0.164\ \hat{\underline{x}}$
0	0.3	$0.204\ \hat{\underline{x}}$
0	0.45	$0.507\ \hat{\underline{x}}$
0.3	0.3	$0.244\ \hat{\underline{x}} - 0.33\ \hat{\underline{y}} - 0.382\ \hat{\underline{z}}$
0.45	0.45	$0.8\ \hat{\underline{x}} - 0.49\ \hat{\underline{y}} - 0.57\ \hat{\underline{z}}$

Chapter 4

LOW FREQUENCY SCATTERING IN THE PRESENCE OF A GROUND PLANE

Figure 4.1a represents an electrically small conducting body B1, above an infinite ground plane, illuminated by an electromagnetic source S1. Using the method of images, we obtain the equivalent problem shown in Fig. 4.1b. Here we have two bodies B1 and B2 and two sources S1 and S2. The ground plane is removed and the space surrounding the bodies is characterized by (ε,μ). B2 is the mirror image of the true body B1, and S2 is the image of the true source S1. To use our low-frequency approximation technique, we assume that the true body B1 is close to the ground plane in Fig. 4.1a. More precisely, it is assumed that we can inscribe the true body B1 and its image B2 (Fig. 4.1b) in a sphere of diameter d. Then, provided d is much less than the wavelength of the incident wave, we can approximate the low-frequency problem shown in Fig. 4.1b by the corresponding electrostatic and magnetostatic problems. The method described in Chapter 2 can directly be applied to the two body problem of Fig. 4.1b to compute the induced charge, current and dipole moments. However this leads to unnecessarily large matrices. In this chapter we describe how to avoid these large matrices and formulate the problem in terms of moment matrices which have the same sizes as if the true body B1 were in free space. The elements of the matrices are, of course, more complicated.

4.1. The Electrostatic Problem in the Presence of a Ground Plane

The problem here consists of finding the induced static charge distribution on the conducting bodies B1 and B2 of Fig. 4.1b when the incident

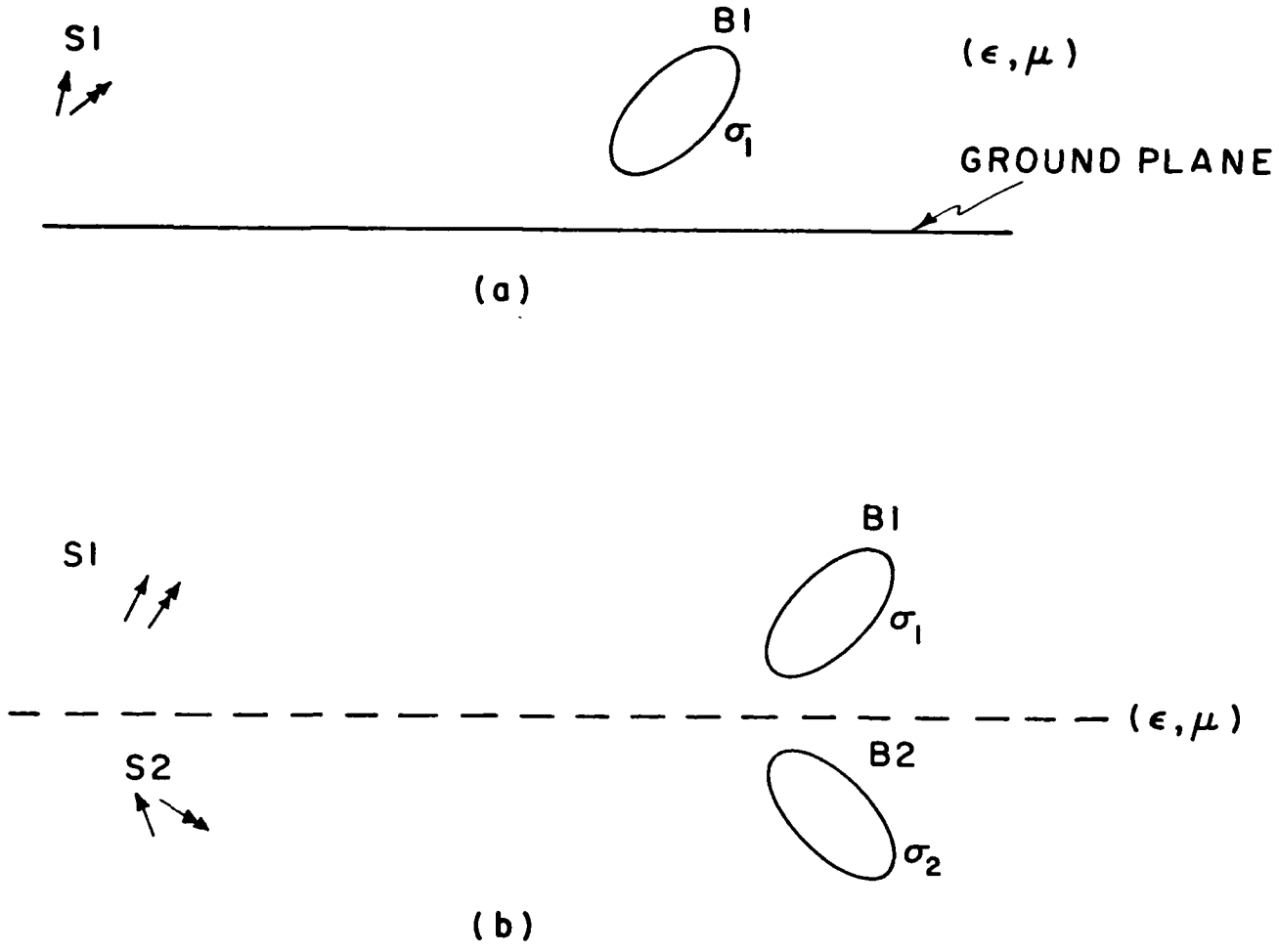

Fig. 4.1. a)A small conducting body B1 over a ground plane. The external source is S1. b) The equivalent problem obtained by the method of images. B2 is the mirror image of B1, and S2 is the image of S1.

electric field due to S1 and S2 is replaced by its electrostatic limit. Assume for the moment that the true body B1 is strictly above the ground plane in the original problem, is isolated,and has an initial charge Q on it. Then the net charge on B2 of Fig. 4.1b is equal to -Q. If the total potential produced by the sources S1, S2,and the induced charges σ_1 and σ_2 is V1 on B1, then it is -V1 on B2. (Here σ_1 and σ_2 are, respectively, the induced charge densities on B1 and B2.) In other words we have the following conditions to be satisfied by the induced charges:

$$\phi^{S1}(\underline{r}) + \phi^{S2}(\underline{r}) + \iint_{S_{B1}} \frac{\sigma_1(\underline{r}')\, ds'}{4\pi\epsilon|\underline{r}-\underline{r}'|} + \iint_{S_{B2}} \frac{\sigma_2(\underline{r}')ds'}{4\pi\epsilon|\underline{r}-\underline{r}'|} = \begin{cases} V1, & \underline{r} \text{ on } S^{B1} \\ -V1, & \underline{r} \text{ on } S^{B2} \end{cases} \tag{4-1}$$

$$\iint_{S_{B1}} \sigma_1(\underline{r})ds' = -\iint_{S_{B2}} \sigma_2(\underline{r})ds' = Q \tag{4-2}$$

Here $\phi^{S1}(\underline{r})$ and $\phi^{S2}(\underline{r})$ denote the potentials produced at a point $\underline{r}$ by the true source S1 and the image source S2, respectively. The integrals in (4-1) represent the potentials produced by the induced sources, and S_{B1} and S_{B2} denote the surfaces of B1 and B2, respectively. As in Chapter 2, we assume that S_{B1} is modeled by N triangular patches and the charge density on the nth patch is a constant σ_n. Then S_{B2}, being the mirror image of S_{B1}, is represented by N triangular patches, and the charge density on the n'th patch (which is the image of the nth patch on S_{B1}) is $-\sigma_n$. Hence, following the same steps used in Section 2.1, we reduce the integral equation (4-1) to the following set of linear equations:

$$
\begin{array}{cccccccccc|c|l}
K_{11} & K_{12} & \cdots & K_{1N} & K_{11'} & K_{12'} & \cdots & K_{1N'} & -1 & \sigma_1 & -4\pi\varepsilon(\phi_1^{S1} + \phi_1^{S2}) \\
K_{21} & K_{22} & \cdots & K_{2N} & K_{21'} & K_{22'} & & K_{2N'} & -1 & \sigma_2 & -4\pi\varepsilon(\phi_2^{S1} + \phi_2^{S2}) \\
\vdots & & & & & & & & & \vdots & \\
K_{N1} & K_{N2} & \cdots & K_{NN} & K_{N1'} & K_{N2'} & \cdots & K_{NN'} & -1 & \sigma_N & -4\pi\varepsilon(\phi_N^{S1} + \phi_N^{S2}) \\
\hline
K_{1'1} & K_{1'2} & \cdots & K_{1'N} & K_{1'1'} & K_{1'2'} & \cdots & K_{1'N'} & +1 & -\sigma_1 & -4\pi\varepsilon(\phi_{1'}^{S1} + \phi_{1'}^{S2}) \\
K_{2'1} & K_{2'2} & \cdots & K_{2'N} & K_{2'1'} & K_{2'2'} & \cdots & K_{2'N'} & +1 & -\sigma_2 & -4\pi\varepsilon(\phi_{2'}^{S1} + \phi_{2'}^{S2}) \\
\vdots & & & & & & & & & \vdots & \\
K_{N'1} & K_{N'2} & \cdots & K_{N'N} & K_{N'1'} & K_{N'2'} & \cdots & K_{N'N'} & +1 & -\sigma_N & -4\pi\varepsilon(\phi_{N'}^{S1} + \phi_{N'}^{S2}) \\
 & & & & & & & & & 4\pi\varepsilon V1 &
\end{array}
\qquad (4-3)
$$

Here each subscripted K denotes the potential produced by a constant charge density of $4\pi\varepsilon$ coulomb per square meter lying on a triangular patch designated by the second subscript, at the centroid of the triangular patch designated by first subscript. For example $K_{57'}$ denotes the potential at the centroid of the fifth triangle produced by the constant charge density over the 7'th triangle. The 7'th triangle is on S_{B2}, and is the image of the 7th triangle on S_{B1}. ϕ_m^{S1} denotes the potential produced by the true source S1 at the centroid of the mth triangle. Similarly, ϕ_m^{S2} is the potential due to image source S2 at the centroid of the mth triangle. Observe that

$$K_{mn} = K_{m'n'} \tag{4-4}$$

$$K_{mn'} = K_{m'n} \tag{4-5}$$

and

$$\phi_m^{S1} + \phi_m^{S2} = -(\phi_{m'}^{S1} + \phi_{m'}^{S2}) \tag{4-6}$$

Then it is obvious that (4-3) represents the same N equations written twice. We approximate (4-2) by

$$T^1\sigma_1 + T^2\sigma_2 + \ldots + T^N\sigma_N = Q \tag{4-7}$$

and combine (4-7) with the first N equations of (4-3) to obtain the following:

$$\left[\begin{array}{cccc|c|c} K_{11}-K_{1'1} & K_{12}-K_{1'2} & \cdots & K_{1N}-K_{1'N} & -1 & \sigma_1 \\ K_{21}-K_{2'1} & K_{22}-K_{2'2} & \cdots & K_{2N}-K_{2'N} & -1 & \sigma_2 \\ \vdots & & & & \vdots & \vdots \\ K_{N1}-K_{N'1} & K_{N2}-K_{N'2} & \cdots & K_{NN}-K_{N'N} & -1 & \sigma_N \\ \hline T^1 & T^2 & \cdots & T^N & 0 & 4\pi\varepsilon V_1 \end{array}\right] = \left[\begin{array}{c} -4\pi\varepsilon(\phi_1^{S1}+\phi_1^{S2}) \\ -4\pi\varepsilon(\phi_2^{S1}+\phi_2^{S2}) \\ \vdots \\ -4\pi\varepsilon(\phi_N^{S1}+\phi_N^{S2}) \\ \hline Q \end{array}\right] \tag{4-8}$$

In matrix notation this is

$$[PG]\ [\vec{\Sigma}G] = [\vec{\Phi}G] \tag{4-9}$$

where the moment matrix PG is the square matrix of order (N+1) × (N+1) on the left-hand side of (4-8), $\vec{\Sigma}G$ is the column vector on the left-hand side of (4-8), and $\vec{\Phi}G$ is the column vector on the right-hand side of (4-8). The solution of (4-9) gives both the induced charge density σ and the potential V_1 of the true body B1 above the ground plane (Fig. 4.1a). Notice that the entry in the last row and the last column of the inverse of the matrix PG is equal to $4\pi\varepsilon$ times the reciprocal of the capacitance of the true body above the ground plane.

Observe that the number of equations to be solved in (4-9) is the same as the number of equations in (2-12) where we had no ground plane. However, the matrix elements and the excitation vector elements in (4-9) are more complicated. Once the charge density is computed, we use (2-16) to compute the induced electric dipole moment. Note that in this case the induced dipole radiates in the presence of the ground plane.

Figure 4.2a shows the computed capacitance of a sphere of 1m radius, the center of which is a distance d above the ground plane. Also shown are the exact results [12,Eq.(4-42)]. The agreement is good. We see that the computed results are less than (at most by four percent) the exact values. The reason for this is that the patched surface is taken to be an inscribed model of the actual spherical surface. As the number of patches is increased, the triangulated model represents the actual surface more closely, and the computed capacitance approaches the exact value. This can be observed from Figure 4.2b, which shows the computed capacitance versus the number of patches for the case d = 2 meters.

We note in passing that the condition that the true body B1 be close to the ground plane is necessary only if we use the present procedure to

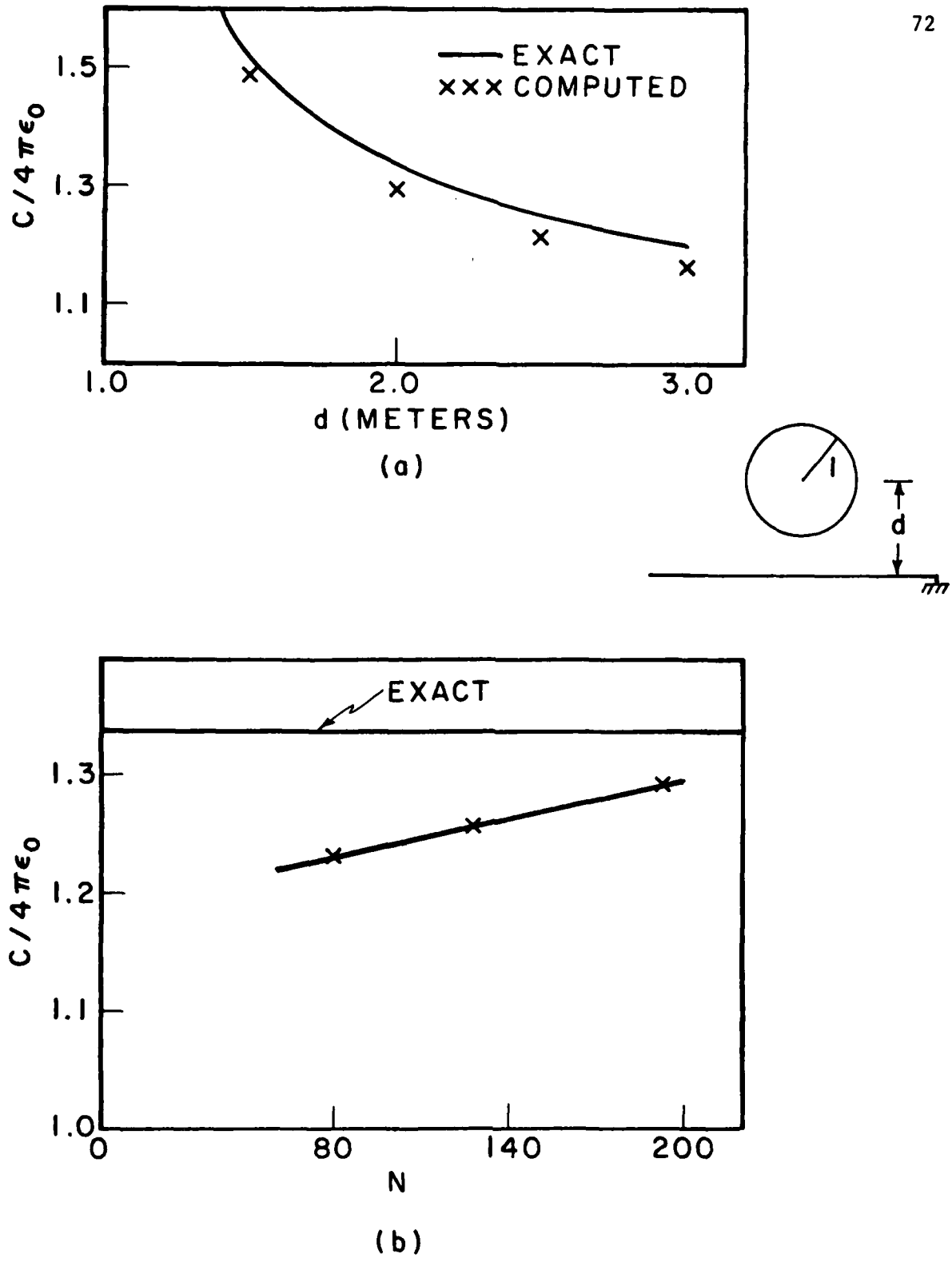

Fig. 4.2. a) The capacitance of a sphere above a ground plane. b) The computed capacitance vs. the number of patches for d=2 m.

approximate a low frequency scattering problem. Obviously, if we are interested in strictly electrostatic results, that condition is no longer necessary.

4.2. The Magnetostatic Problem in the Presence of a Ground Plane

Here the problem consists of computing the induced current distribution $\underline{J}_t$ on the true body B1 of Figure 4.1a when the incident magnetic field due to source S1 is replaced by its magnetostatic limit. We again assume that B1 is strictly above the ground plane. We first formulate the problem as a two body magnetostatic problem, using the procedure of Section 2.2, and then use the information provided by the method of images to reduce the number of equations by a factor of two. For the two body problem shown in Fig. 4.1b, the boundary condition to be satisfied is that the normal component of total magnetic field produced by the sources S1 and S2 plus the induced currents on B1 and B2 must be zero on both S_{B1} and S_{B2}. The condition that the induced currents on both bodies are charge-free is automatically satisfied by the choice of expansion functions, described in Section 2.2.2.

Assume that S_{B1} is patched so that it has N^b interior nodes. Then S_{B2}, being the mirror image of S_{B1}, has N^b interior nodes. (For closed bodies, N^b represents the total number of nodes minus one.) We have N^b expansion functions on each of S_{B1} and S_{B2}. Then, corresponding to (2-33), we have the following set of linear equations for this two body problem:

$$\begin{bmatrix}[ZBB] & [ZBI] & [\vec{I}B] \\ & & [\vec{I}I] \end{bmatrix} = [\vec{V}B] \qquad (4\text{-}10a)$$

$$\begin{bmatrix}[ZIB] & [ZII] & [\vec{I}B] \\ & & [\vec{I}I] \end{bmatrix} = [\vec{V}I] \qquad (4\text{-}10b)$$

Here ZBB, ZBI, ZIB, and ZII are $N^b \times N^b$ square matrices; $\vec{IB}$, $\vec{II}$, $\vec{VB}$, and $\vec{VI}$ are $N^b \times 1$ column vectors . ZBB(j,i) is the normal component of the magnetic field produced by the ith expansion function attached to the ith node on the true body, tested over the domain of the jth expansion function on the true body, as given by (2-34) and (2-46). Similarly, ZBI(j,i) represents the field produced by the image of the ith expansion function tested over the domain of the jth expansion function. ZIB(j,i) is the field produced by the ith expansion function tested over the domain of the image of the jth expansion function, and finally ZII(j,i) represents the field of the image of the ith expansion function tested over the domain of the image of the jth expansion function. The ith element of $\vec{IB}$ is the expansion coefficient of the ith expansion function, and the ith element of $\vec{II}$ is the coefficient of the image of the ith expansion function. The kth element of $\vec{VB}$ is the negative of the normal component of the total impressed magnetic field (produced by S1 and S2) tested over the domain of the kth expansion function, as given by (2-36). Similarly , the kth element of $\vec{VI}$ is the negative of the impressed field tested over the domain of the image of the kth expansion function. Since S_{B2} and S2 are the images of S_{B1} and S1, and due to (2-46) and (2-49), it is not difficult to see that

$$IB(i) = II(i) \qquad i = 1,2,\ldots,N^b, \tag{4-11}$$

$$VB(k) = VI(k) \qquad k = 1,2,\ldots,N^b, \tag{4-12}$$

and

$$ZBB(j,i) + ZBI(j,i) = ZIB(j,i) + ZII(j,i) \tag{4-13}$$

Hence, (4-10a) and (4-10b) represent the same set of equations. (This is to be expected, since satisfying the boundary condition mentioned earlier on S_{B1} , (4-10a), automatically satisfies the same condition on S_{B2} , (4-10b)). We rewrite (4-10a) in matrix notation as

$$[ZG]\ [\vec{IG}] = [\vec{VG}] \tag{4-14}$$

where ZG is a square matrix of order $N^b \times N^b$ such that

$$ZG(j,i) = ZBB(j,i) + ZBI(j,i) \tag{4-15}$$

$\vec{IG}$ and $\vec{VG}$ are column vectors which are the same as $\vec{IB}$ and $\vec{VB}$ of (4-10a), respectively. The term ZBB(j,i) in (4-15) is equal to Z(j,i) of (2-46), and ZBI(j,i) is given by the following:

$$ZBI(j,i) = -\frac{1}{4\pi} \sum_{m=1}^{t_j} T_{jm}\, \underline{J}_{jm} \cdot \left(\sum_{\ell=1}^{t_i} \underline{J}'_{i\ell}\, K(jm, i'\ell) \right) \tag{4-16}$$

Here $\underline{J}'_{i\ell}$ represents the value of the image of ith expansion function on the ℓth triangle attached to node i, and K(jm,i'ℓ) represents an element of the matrix on the left-hand side of (4-3). The row and column of this element are defined by two triangular surfaces. The row is defined by the mth triangle attached to node j, and the column is defined by the image of the ℓth triangle attached to node i.

Figure 4.3 illustrates the expansion function $\underline{J}_i$, together with its image $\underline{J}'_i$. Here we have three surfaces attached to node i. It is seen that the z component of the expansion function is the same on each surface and its image. However the x and y components (which are parallel to the ground plane) are reversed in direction. Keeping this in mind, we have the following expression for ZG(j,i).

$$ZG(j,i) = -\frac{1}{4\pi} \sum_{m=1}^{t_j} T_{jm}\, \underline{J}_{jm} \cdot \sum_{\ell=1}^{t_j} (K(jm, i\ell) - K(jm, i'\ell))$$

$$(\hat{\underline{x}}(\hat{\underline{x}} \cdot \underline{J}_{i\ell}) + \hat{\underline{y}}(\hat{\underline{y}} \cdot \underline{J}_{i\ell})) + (K(jm, i\ell) + K(jm, i'\ell))\ \hat{\underline{z}}(\hat{\underline{z}} \cdot \underline{J}_{i\ell})]$$

But from (4-5) we have

$$K(jm, i'\ell) = K(j'm, i\ell)\ . \tag{4-17}$$

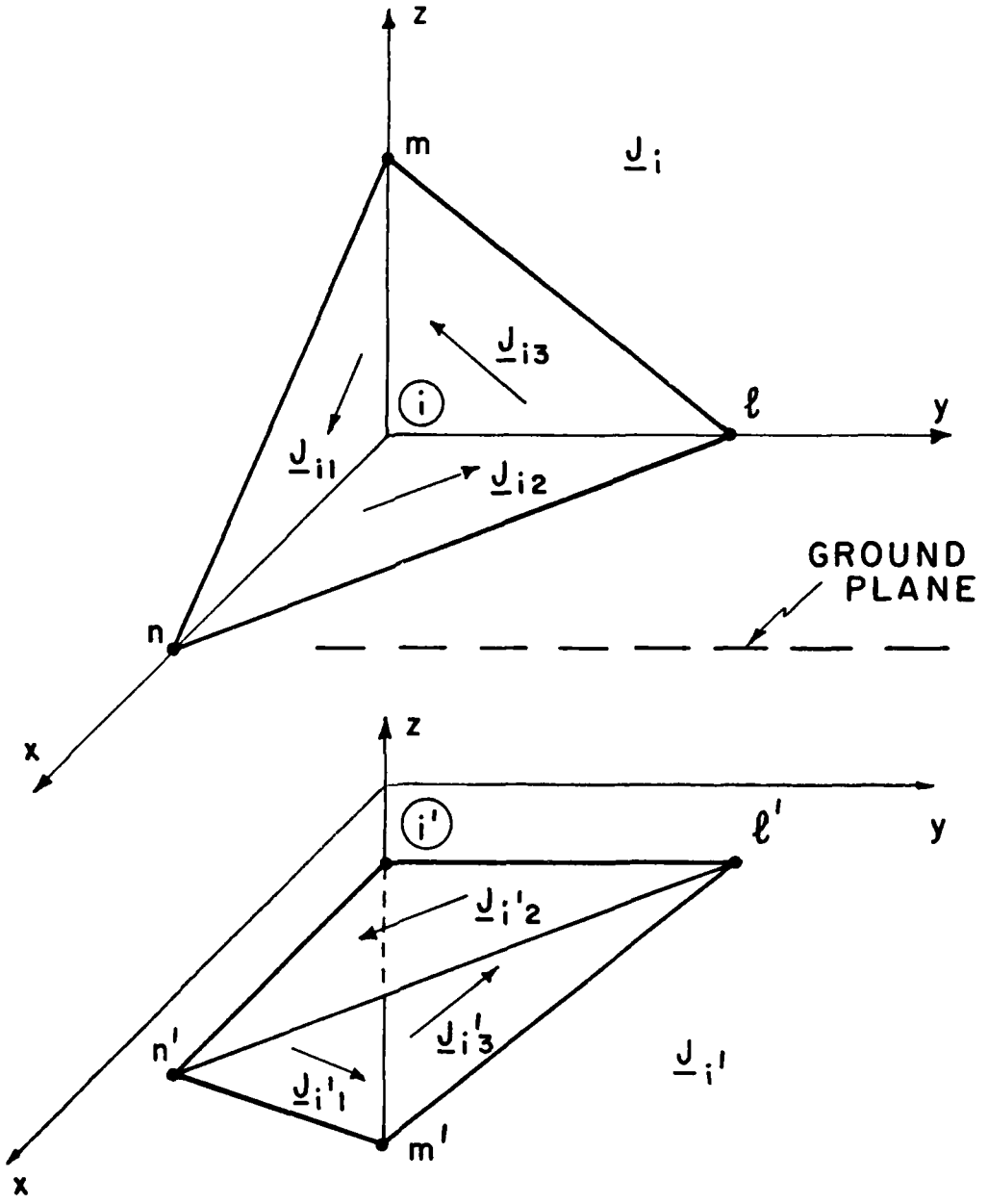

Fig. 4.3. Expansion function $\underline{J}_i$ associated with node i and its image $\underline{J}_{i'}$.

Hence,

$$ZG(j,i) = -\frac{1}{4\pi} \sum_{m=1}^{t_j} T_{jm} \underline{J}_{jm} \cdot \sum_{\ell=1}^{t_i} \{ PG(jm,i\ell)[\hat{\underline{x}}(\hat{\underline{x}} \cdot \underline{J}_{i\ell}) + \hat{\underline{y}}(\hat{\underline{y}} \cdot \underline{J}_{i\ell})]$$

$$+ [K(jm, i\ell) + K(j'm, i\ell)] (\hat{\underline{z}} \cdot \underline{J}_{i\ell})\hat{\underline{z}}\} \qquad (4\text{-}18)$$

Here PG(jm, iℓ) is an element of matrix PG in (4-9). The row of this element is defined by the mth triangular surface attached to node j, and the column is defined by the ℓth triangle attached to node i.

Hence, we use the electrostatic matrix PG to compute the magnetostatic matrix ZG. We also need the sum K(jm, iℓ) + K(j'm, iℓ), but we do not perform any integration to find this sum, because both of its terms are by-products of the calculation of PG.

The jth element of $\vec{V}G$ is the same as (2-49), with one exception. The exception is that the term $H_n^{imp}(\underline{r}_{cjm})$ is now taken to mean the normal component of the total impressed field (i.e., produced by the true source plus its image) at $\underline{r}_{cjm}$.

Once the current distribution is solved for using (4-14), the induced magnetic dipole is computed using (2-52). This dipole replaces the body and, strictly speaking, it is above the ground plane. Since the distance between the ground plane and the body is assumed to be small, we place the dipole on the ground plane and use image theory to remove the ground plane.

Figure 4.4 shows the induced current density on a square plate which is vertical to, and 1 cm above, the ground plane. The plate is 1 meter by 1 meter and is placed in the yz plane. The ground plane is defined by z = 0. The incident field (in the presence of the ground plane and in the absence of the plate) is a z-polarized, y-traveling, plane wave (grazing incidence) with $\underline{H}^{imp} = 1\ \hat{\underline{x}}$ Ampere/meter. Comparing the result with Fig. 3.15 ($\theta = 90^\circ$ case), which represents the current when the plate is in free space, we observe that the presence of the ground plane destroys

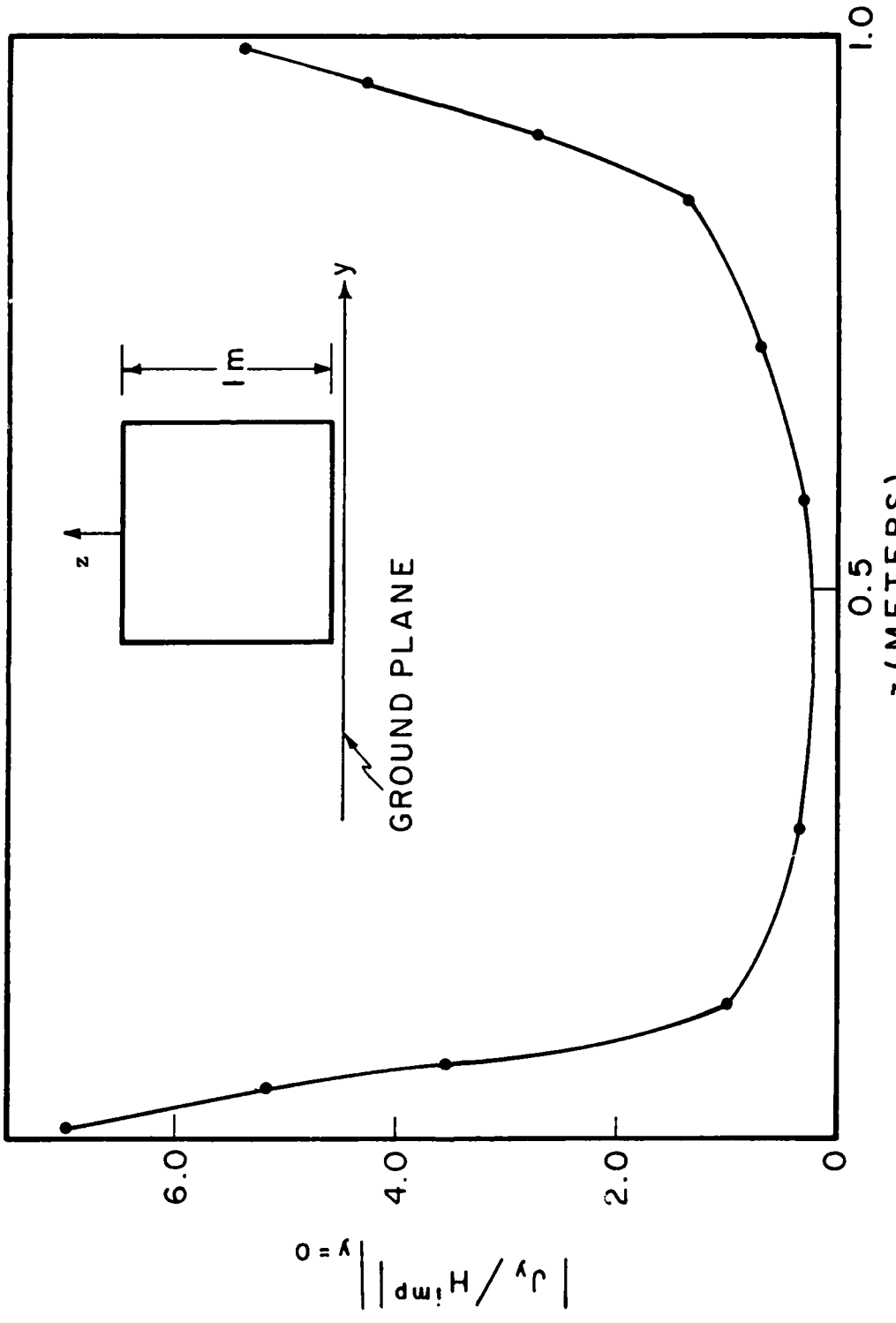

Fig. 4.4. Current on a square plate 1 cm. above a ground plane. No. of unknowns=25.

the symmetry about the center of the plate, as expected. The current is bigger near the edge close to the ground plane. The computed induced magnetic dipole is $\underline{M}^{ind} = -0.455\ \hat{\underline{x}}$, which is about nine percent bigger (in magnitude) than the induced dipole moment in the free space case ($-0.418\ \hat{\underline{x}}$). Since the former dipole is above the ground plane, we can conclude the following using image theory: The magnetic (electric) polarizability of two such square plates (apertures in an infinite conducting screen) is larger by about nine percent than the sum of their individual polarizabilities.

Consider a small cube of side length 1 meter, placed a distance of 0.5 meter above a ground plane. The ground plane is at $z = 0$, and the top face of the cube is at $z = 1.5$ meters. When a magnetic dipole is placed tangentially on any surface of the cube, we use the pseudo-image method described in Section 3.5.2 to compute the induced magnetic dipole moment. For excitation vector elements, we use (3-18). However in this case $\underline{E}^{imp}$ of (3-18) is produced by four dipoles; the original source dipole, the pseudo-image of the original dipole just inside the cube, and the images of these two dipoles below the ground plane. Figure 4.5 illustrates the problem when the source dipole is perpendicular to the ground plane. When an x-directed magnetic dipole of moment $M_x = 1$ is placed at the center of the top face of the cube at the point $x = 0$, $y = 0$, and $z = 1.5$, the computed induced dipole is given by $M_x^{ind} = 0.18$. If the source dipole is placed at the center of the right face at the point $x = 0$, $z = 1.0$, and $y = 0.5$, the induced dipole moment is $M_x^{ind} = 0.2$. If a z-directed magnetic dipole of moment $M_z = 1$ is placed at the center of the right face, the induced dipole moment is $M_z^{ind} = 0.21$. These dipoles represent the cube

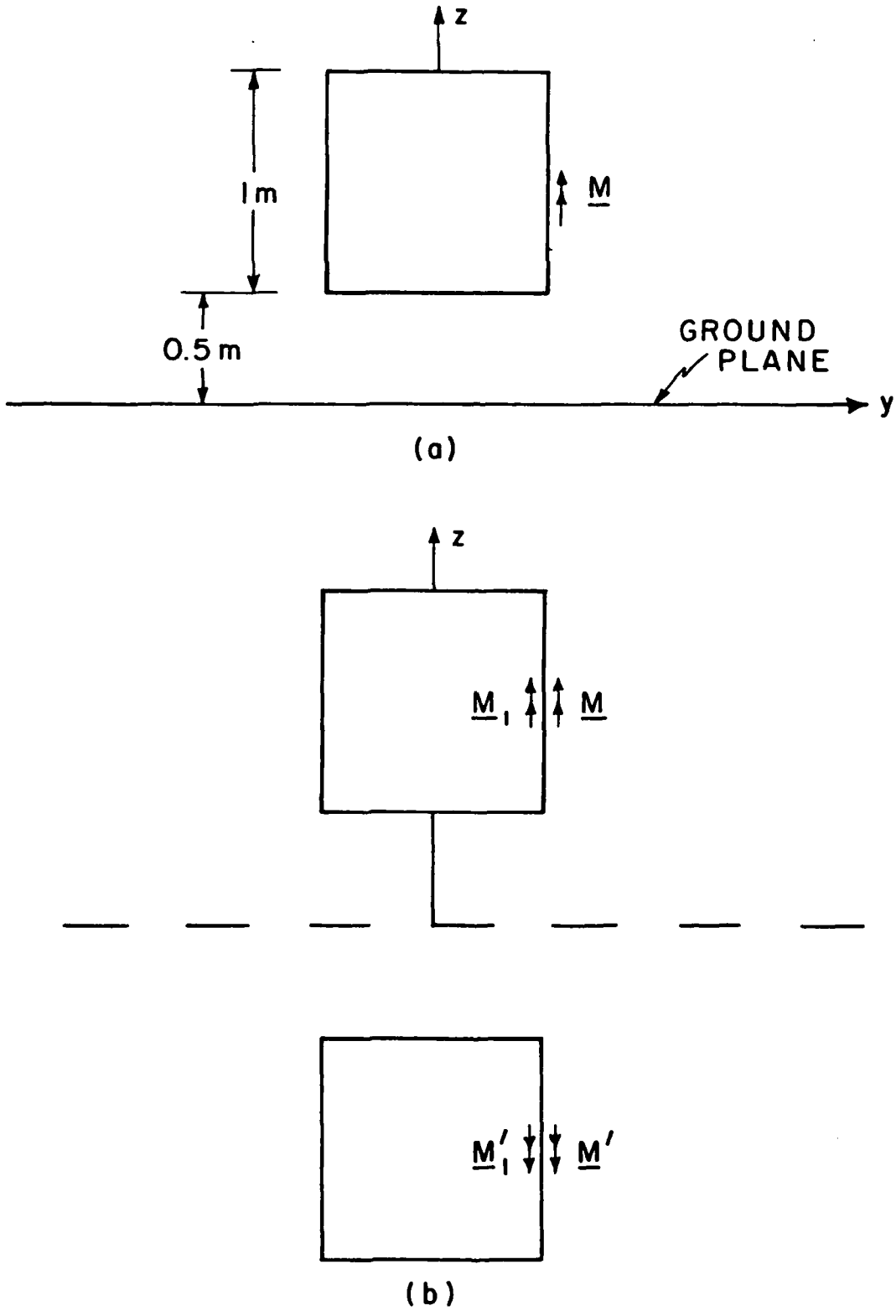

Fig. 4.5. a) Original problem : A magnetic dipole $\underline{M}$ is placed tangentially on the right face of a cube above a ground plane. b) Equivalent problem: $\underline{M}_1$ is the pseudo-image of $\underline{M}$. $\underline{M}'$ and $\underline{M}_1'$ are the images of $\underline{M}$ and $\underline{M}_1$, respectively.

above the ground plane. Since a z-directed magnetic dipole has an image in the negative z direction, we conclude that, at distances large compared to the size of the cube, the scattered field will be smallest for the last case considered. In other words, to prevent radiation from sources inside the cube to the outside region, a narrow slot vertical to the ground plane is better than a slot parallel to the ground plane.

4.3 Conducting Box on a Ground Plane

Electronic equipment is usually contained in a conducting box which has several apertures for input-output connections and for ventilation purposes. It is desirable to keep the radiation through these apertures as low as possible. To investigate the effect of these apertures, test measurements are done in an anechoic chamber with the box usually placed on a ground plane. In this section, we study the problem of a box on a ground plane. The box is assumed to have a narrow slot, and, for computational purposes, this slot is represented by a magnetic dipole tangent to the box. Also, plane wave scattering from the box is studied.

4.3.1) The Electrostatic Problem.

The electrostatic problem in this case is the same as the case considered in Section 4.1 with two exceptions. Now the potential is zero, and the net charge is unknown. Hence the moment equation for this case can be written as

$$\begin{bmatrix} K_{11} - K_{1'1} & K_{12} - K_{1'2} \cdots & K_{1N} - K_{1'N} \\ K_{21} - K_{2'1} & K_{22} - K_{2'2} \cdots & K_{2N} - K_{2'N} \\ \vdots & & \\ K_{N1} - K_{N'1} & K_{N2} - K_{N'2} \cdots & K_{NN} - K_{N'N} \end{bmatrix} \begin{bmatrix} \sigma_1 \\ \sigma_2 \\ \\ \sigma_N \end{bmatrix} = \begin{bmatrix} -4\pi\varepsilon(\phi_1^{S1} + \phi_1^{S2}) \\ -4\pi\varepsilon(\phi_2^{S1} + \phi_2^{S2}) \\ \\ -4\pi\varepsilon(\phi_N^{S1} + \phi_N^{S2}) \end{bmatrix} \tag{4-19}$$

where all quantities appearing in this equation are the same as those in (4-8).

Note that in patching the box surface the bottom face (the part of the surface on the ground plane) is not considered. Hence, the patched surface will be an open one. For a rectangular box, the boundary of this open surface is a rectangle on the ground plane. The image of the patched surface is also an open surface with the same boundary. Hence, the patched surface together with its image forms a closed surface. It represents a box of twice the height of the original box.

4.3.2) The Magnetostatic Problem

The moment equation for this problem is the same as (4-14), but we have the following modification for some expansion functions. Since the patched surface together with its image represents a closed surface, all the nodes are considered to be interior nodes. Hence, we associate an expansion function with each node but one . The image of a node on the boundary is itself. The expansion function associated with such a node cannot complete a loop around the node. However, this expansion function together with its image forms a loop around the node. This is illustrated in Fig. 4.6. This shows the expansion function associated with node L, which is assumed to be on the ground plane. An expansion function associated with a node not on the ground plane is the same as the one illustrated in Fig. 2.2.

Consider a cube of side length 1m placed on a ground plane at z = 0. The top face of the cube is at z = 1m, and the right face is at y = 0.5m. For a plane wave at grazing incidence with E_z^i = 377 (V/m) and H_x^i = 1 (A/m), the computed induced dipole moments are $\underline{P}^{ind}=0.865\times10^{-8}\ \hat{z}$ and $\underline{M}^{ind}=-1.32\ \hat{x}$. (The scattered fields can be computed by placing these dipoles on the ground plane.)

We have considered three magnetic dipole excitations for three different boxes on the ground plane . First , we place a magnetic dipole with dipole moment $\underline{M} = 1\ \hat{x}$ ($A\text{-}m^2$) at the center of the top

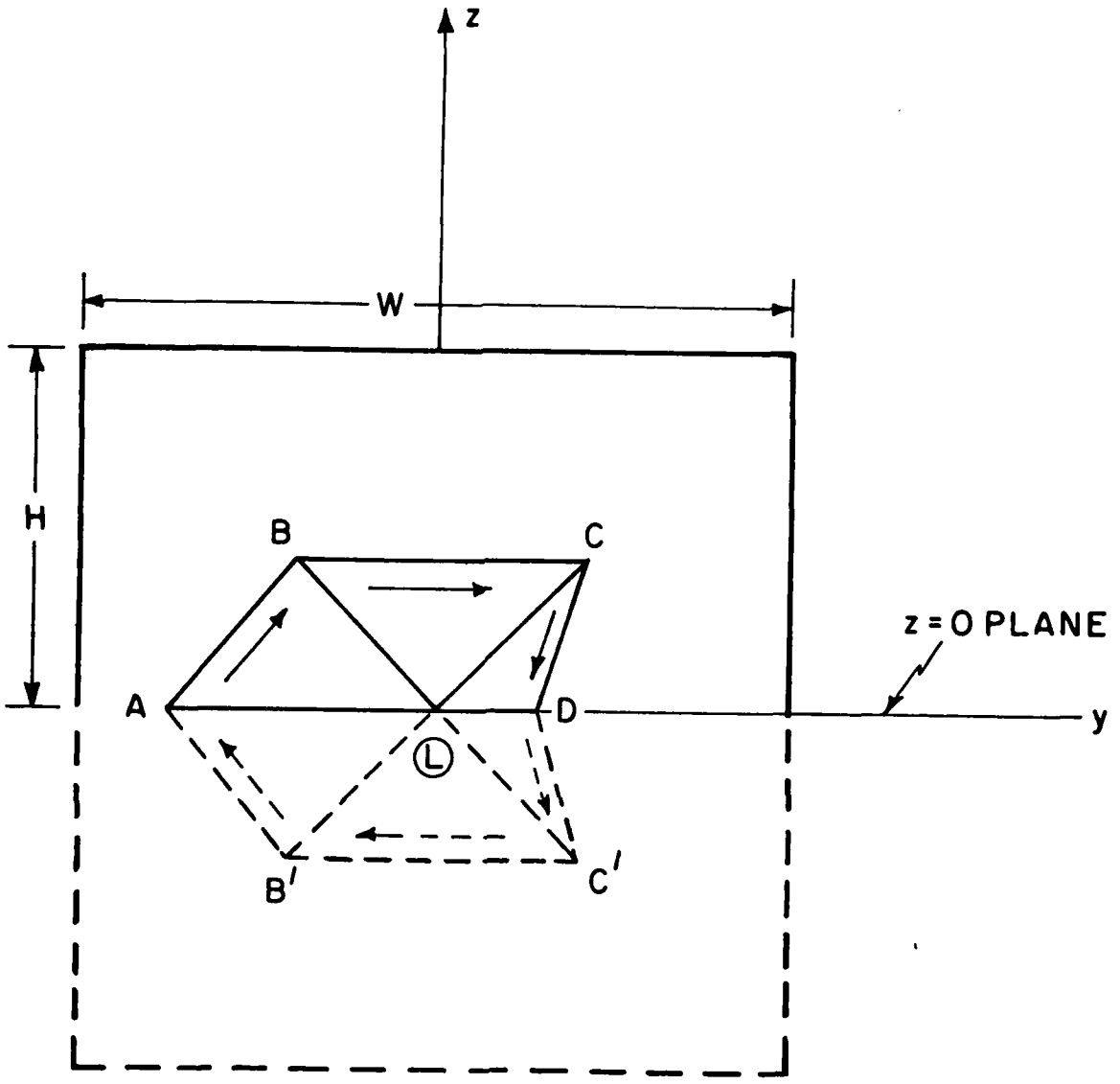

Fig. 4.6. A face of a conducting rectangular box together with its image in a ground plane. (The ground plane is at z=0.) The solid arrows indicate the expansion function associated with node L. The dashed arrows represent the image of the expansion function. The unprimed capital letters denote the nodes and the primed capital letters denote the images of the nodes in the ground plane. The expansion function together with its image completes a loop around the node L.

face of the box . This is referred to as "first excitation." Secondly, we place $\underline{M} = 1\ \hat{\underline{x}}$ at the center of the right face, and thirdly we place $\underline{M} = 1\ \hat{\underline{z}}$ at the center of the right face. The boxes considered are i) a cube (W = L = H = 1 m), ii) a tall box (W = L = 0.9 m, H = 1.25 m), and iii) a short box (W = L = 1.2 m, H = 0.7 m). The volumes of the three boxes are almost identical. Table 4.1 summarizes the computed induced magnetic dipole moments obtained for these three boxes with each of the three excitations.These dipoles radiate in the presence of the ground plane.

Table 4.1. The induced magnetic dipole moment due to a tangential magnetic dipole on a face of a box.

Box Shape \ Excitation	First Excitation	Second Excitation	Third Excitation
Cube	$0.21\ \hat{\underline{x}}$	$0.25\ \hat{\underline{x}}$	$-0.18\ \hat{\underline{y}} + 0.31\ \hat{\underline{z}}$
Tall box	$0.25\ \hat{\underline{x}}$	$0.30\ \hat{\underline{x}}$	$-0.122\ \hat{\underline{y}} + 0.20\ \hat{\underline{z}}$
Short box	$0.18\ \hat{\underline{x}}$	$0.15\ \hat{\underline{x}}$	$-0.28\ \hat{\underline{y}} + 0.56\ \hat{\underline{z}}$

APPENDIX A

APPROXIMATION OF THE LOW FREQUENCY SCATTERING PROBLEM

In this appendix we describe how to approximate the problem of low frequency electromagnetic scattering by the corresponding electrostatic and magnetostatic problems. The procedure is explained in [1] and is summarized here for quick reference. An example is given to illustrate the ideas developed.

Consider a perfectly conducting body placed in an unbounded homogeneous medium characterized by (ε,μ). Let the body be illuminated by an incident electromagnetic field $(\underline{E}^i,\underline{H}^i)$ whose wavelength is much larger than the maximum linear dimension of the body. The problem consists of determining the scattered fields $(\underline{E}^s,\underline{H}^s)$ such that

$$\nabla \times \underline{E}^s = - j\eta k \underline{H}^s \quad ; \quad \nabla \times \underline{H}^s = j \frac{k}{\eta} \underline{E}^s \tag{A-1}$$

$$\nabla \cdot \underline{E}^s = 0 \quad ; \quad \nabla \cdot \underline{H}^s = 0 \tag{A-2}$$

$$\hat{n} \times \underline{E}^s\Big|_S = - \hat{n} \times \underline{E}^i\Big|_S \quad ; \quad \hat{n} \cdot \underline{H}^s\Big|_S = - \hat{n} \cdot \underline{H}^i\Big|_S \tag{A-3}$$

$$\lim_{r\to\infty} \underline{r} \times (\nabla \times \underline{E}^s) - jkr\underline{E}^s = 0 \quad ; \quad \lim_{r\to\infty} \underline{r} \times (\nabla \times \underline{H}^s) - jkr\underline{H}^s = 0 \tag{A-4}$$

where

$\eta = \sqrt{\mu/\varepsilon}$,

$k = \omega \sqrt{\mu\varepsilon}$,

ω = angular frequency of the incident wave,

S denotes the surface of the body, and $\hat{n}$ is the unit outward normal vector to S.

Note that in (A-3) the boundary condition on $\underline{E}^s$ implies the boundary condition on $\underline{H}^s$.

It is known that all field quantities may be written as convergent power series in k, provided k is sufficiently small, that is,

$$\underline{E}^{s,i} = \sum_{m=0}^{\infty} (jk)^m \underline{E}_m^{s,i} \quad ; \quad \underline{H}^{s,i} = \sum_{m=0}^{\infty} (jk)^m \underline{H}_m^{s,i} \tag{A-5}$$

The mth terms in these expansions may be found by substituting (A-5) into (A-1)-(A-3) and equating the coefficients of like powers of k. We find that the first terms, $\underline{E}_o^s$ and $\underline{H}_o^s$, satisfy

$$\underline{\nabla} \times \underline{E}_o^s = 0 \qquad ; \qquad \underline{\nabla} \times \underline{H}_o^s = 0 \tag{A-6}$$

$$\underline{\nabla} \cdot \underline{E}_o^s = 0 \qquad ; \qquad \underline{\nabla} \cdot \underline{H}_o^s = 0 \tag{A-7}$$

$$\hat{\underline{n}} \times \underline{E}_o^s\Big|_S = -\hat{\underline{n}} \times \underline{E}_o^i\Big|_S \quad ; \quad \hat{\underline{n}} \cdot \underline{H}_o^s\Big|_S = -\hat{\underline{n}} \cdot \underline{H}_o^i\Big|_S \tag{A-8}$$

In addition to these we have the following equations

$$\lim_{r\to\infty} r\, \underline{E}_o^s = 0 \quad ; \quad \lim_{r\to\infty} r\, \underline{H}_o^s = 0 \tag{A-9}$$

These equations were first used by Rayleigh [2] and subsequently verified by Stevenson [20] and Kleinman [21].

Note that the boundary conditions in (A-8) are now independent. This is due to the fact that equations (A-6) are decoupled. Equation (A-6) implies that there exists a scalar function ϕ_o^s such that

$$\underline{E}_o^s = -\underline{\nabla}\phi_o^s \tag{A-10}$$

Then the left equations in (A-7) - (A-9) are satisfied if

$$\nabla^2 \phi_o^s = 0 \tag{A-11}$$

$$- \hat{n} \times \underline{\nabla} \phi_o^s \Big|_S = - \hat{n} \times \underline{E}_o^i \Big|_S \tag{A-12}$$

and

$$\lim_{r \to \infty} r \frac{\partial \phi_o^s}{\partial r} = 0 \tag{A-13}$$

It is obvious that (A-11)-(A-13) define a standard electrostatic Dirichlet potential problem for the surface S except for a minor detail. The exception being that the boundary condition in (A-12) may be shown to specify the boundary values of ϕ_o^s within an arbitrary additive constant. But this constant can be evaluated by employing the condition that there is no net charge on the surface of the body, i.e.,

$$\iint_S \hat{n} \cdot \underline{E}_o^s \, ds = 0 \tag{A-14}$$

If we replace ($\underline{E}^s$, $\underline{H}^s$) by ($\underline{E}^i$, $\underline{H}^i$) in (A-1) and use (A-5), we have

$$\underline{\nabla} \times \underline{E}_o^i = 0 \tag{A-15}$$

so that

$$\underline{E}_o^i = - \underline{\nabla} \phi_o^i \tag{A-16}$$

where ϕ_o^i is a scalar function. Then (A-12) implies that

$$\phi_o^s + \phi_o^i = V_o \qquad \text{on} \quad S \tag{A-17}$$

where V_o is a constant.

We can think of the problem defined by (A-11), (A-13), (A-14) with $\underline{E}_o^s$ replaced by $-\underline{\nabla}\phi_o^s$, and (A-17) in the following way. A perfectly conducting isolated body (with net charge Q = 0) is placed in an impressed electrostatic potential ϕ_o^i and a surface charge density σ_o is induced on the surface

of the body. This charge produces ϕ_o^s. The body, being a perfect conductor, is an equipotential surface at an unknown total potential V_o, i.e.,

$$\phi_o^s(\sigma_o) + \phi_o^i = V_o \qquad \text{on} \quad S \tag{A-18}$$

This represents an integral equation for σ_o. Once it is solved we can obtain ϕ_o^s at an arbitrary point $\underline{r}$ by

$$\phi_o^s = \frac{1}{4\pi\varepsilon} \iint_S \frac{\sigma_o(\underline{r}')}{|\underline{r} - \underline{r}'|}\, ds' \tag{A-19}$$

and $\underline{E}_o^s$ is given by (A-10). The induced electric dipole moment can be obtained by

$$\underline{P}^{ind} = \iint_S \sigma_o(\underline{r})\underline{r}\, ds \tag{A-20}$$

In a similar fashion we can interpret the right set of equations in (A-6) to (A-9) as follows. A perfectly diamagnetic body is placed in an impressed static field $\underline{H}_o^i$ and a surface current $\underline{J}_o$ is induced on it, which in turn produces $\underline{H}_o^s$ such that the normal component of the total magnetic field is zero on the surface, i.e.,

$$\hat{\underline{n}} \cdot (\underline{H}_o^i + \underline{H}_o^s(\underline{J}_o)) = 0 \qquad \text{on} \quad S \tag{A-21}$$

This represents an integral equation for the induced surface current $\underline{J}_o$. Additional information about $\underline{J}_o$ can be obtained as follows. Consider the continuity equation

$$\underline{\nabla}_s \cdot \underline{J}^{ind} = -jkc\,\sigma^{ind} \tag{A-22}$$

where $c = 1/\sqrt{\mu\varepsilon}$ is the speed of light in the surrounding medium, and $\underline{J}^{ind}$ and σ^{ind} are respectively the current and charge density induced on the

surface of the scatterer due to the incident field $(\underline{E}^i, \underline{H}^i)$. $\underline{\nabla}_s \cdot$ denotes the surface divergence operator. The induced sources $\underline{J}^{ind}$ and σ^{ind} are the sources of $\underline{E}^s$ and $\underline{H}^s$ of (A-1) to (A-4). Since $\underline{J}^{ind}$ and σ^{ind} are related (on S) to the total fields $\underline{H}^i + \underline{H}^s$ and $\underline{E}^i + \underline{E}^s$, one can argue that $\underline{J}^{ind}$ and σ^{ind} can be expanded into convergent series of the form given in (A-5) if k is sufficiently small. Then (A-22) gives

$$\underline{\nabla}_s \cdot \sum_{m=0}^{\infty} (jk)^m \underline{J}_m^{ind} = - jkc \sum_{m=0}^{\infty} (jk)^m \sigma_m^{ind} \tag{A-23}$$

Equating the coefficients of like powers of k, we obtain

$$\underline{\nabla}_s \cdot \underline{J}_o^{ind} = 0 \tag{A-24}$$

$$\underline{\nabla}_s \cdot \underline{J}_1^{ind} = - c \sigma_o^{ind} \tag{A-25}$$

etc.

Since $\underline{J}_o$ of (A-21) must represent $\underline{J}$ in the limit as $k \to 0$ and since

$$\underline{J}_o^{ind} = \lim_{k \to 0} \underline{J}^{ind} \tag{A-26}$$

we conclude that $\underline{J}_o = \underline{J}_o^{ind}$ and hence

$$\underline{\nabla}_s \cdot \underline{J}_o = 0 \tag{A-27}$$

This is the property of stationary currents. That is why we call the problem defined by (A-21) and (A-27) a quasi-stationary magnetic problem or simply a magnetostatic problem. Once $\underline{J}_o$ is solved for using (A-21) and (A-27) the scattered field $\underline{H}_o^s$ can be computed using the Biot-Savart law. The induced magnetic dipole is given by

$$\underline{M}^{ind} = \frac{1}{2} \iint_S \underline{r} \times \underline{J}_o(\underline{r}) ds \tag{A-28}$$

Following the same argument that led us to (A-27) we conclude that σ_o of (A-18) and σ_o^{ind} of (A-25) are identical.

At distances small compared with the wavelength, the scattered field $(\underline{E}^s, \underline{H}^s)$ is approximately $(\underline{E}_o, \underline{H}_o)$ where $\underline{E}_o$ is the quasi-static electric field due to σ_o and $\underline{H}_o$ is the quasi-static magnetic field due to $\underline{J}_o$. At distances that are appreciable compared with the wavelength, $(\underline{E}^s, \underline{H}^s)$ can not be approximated by $(\underline{E}_o, \underline{H}_o)$ because $(\underline{E}_o, \underline{H}_o)$ is not a propagating field. Now, $(\underline{E}^s, \underline{H}^s)$ is the field radiated by $\underline{J}^{ind}$. In Appendix B, it is shown that, at distances large compared with the maximum dimension of a small surface, the field radiated by an arbitrary current distribution $\underline{J}$ on that surface is the field of the combination of the electric and magnetic dipole moments of $\underline{J}$. Therefore, at distances large compared with the maximum dimension of the scatterer, $(\underline{E}^s, \underline{H}^s)$ is the field radiated by the combination of the electric and magnetic dipole moments of $\underline{J}^{ind}$. In the limit as $k \to 0$, these dipole moments approach $\underline{P}^{ind}$ of (A-20) and $\underline{M}^{ind}$ of (A-28).

Notice that depending on the structure of the scatterer and the polarization of the incident wave $\underline{P}^{ind}$ and/or $\underline{M}^{ind}$ may vanish. For example, if a plane wave impinges on a plate with $\underline{E}^i$ ($\underline{H}^i$) being perpendicular (tangential) to the surface then $\underline{P}^{ind}$ ($\underline{M}^{ind}$) is zero.

We now illustrate the ideas developed in this appendix by the example of plane wave scattering from a small conducting sphere. Figure A.1 represents a conducting sphere of radius a illuminated by an incident plane wave. Take the incident wave to be x-polarized and z-traveling, that is,

$$\underline{E}^i = E_o e^{-jkz}\, \hat{x} \tag{A-29}$$

$$\underline{H}^i = \frac{E_o}{\eta}\, e^{-jkz}\, \hat{y} \tag{A-30}$$

where

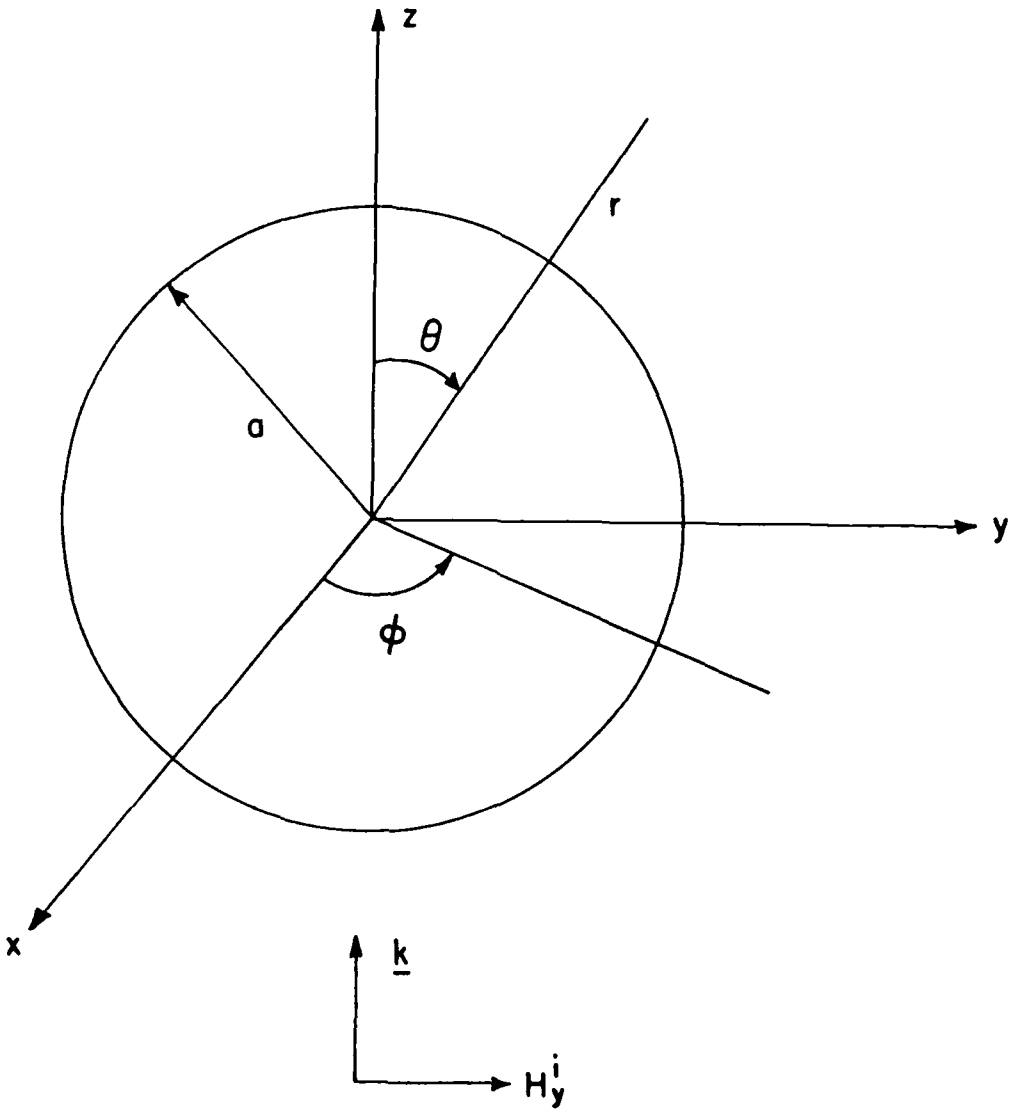

Fig. A.1. Plane wave incident on a conducting sphere.

$$\eta = \sqrt{\mu_o/\varepsilon_o} = 120\pi ,$$

$k = 2\pi/\lambda$ = wave number of the incident wave, and E_o is a constant.

The exact results are taken from [4].

$$J_\theta = \frac{jE_o}{\eta}\frac{\cos\phi}{ka}\sum_{n=1}^{\infty} a_n \left[\frac{\sin\theta\, P_n^{1'}(\cos\theta)}{\hat{H}_n^{(2)'}(ka)} + j\,\frac{P_n^1(\cos\theta)}{\sin\theta\,\hat{H}_n^{(2)}(ka)}\right] \tag{A-31}$$

$$J_\phi = \frac{jE_o}{\eta}\frac{\sin\phi}{ka}\sum_{n=1}^{\infty} a_n \left[\frac{P_n^1(\cos\theta)}{\sin\theta\,\hat{H}_n^{(2)'}(ka)} + j\,\frac{\sin\theta\, P_n^{1'}(\cos\theta)}{\hat{H}_n^{(2)}(ka)}\right] \tag{A-32}$$

$$E_r^s = -\frac{jE_o\cos\phi}{(kr)^2}\sum_{n=1}^{\infty} b_n n(n+1)\,\hat{H}_n^{(2)}(kr)\,P_n^1(\cos\theta) \tag{A-33}$$

$$E_\theta^s = -\frac{E_o\cos\phi}{kr}\sum_{n=1}^{\infty}\left[c_n\frac{\hat{H}_n^{(2)}(kr)\,P_n^1(\cos\theta)}{\sin\theta} - jb_n\,\hat{H}_n^{(2)'}(kr)P_n^{1'}(\cos\theta)\sin\theta\right] \tag{A-34}$$

$$E_\phi^s = -\frac{E_o\sin\phi}{kr}\sum_{n=1}^{\infty}\left[c_n\,\hat{H}_n^{(2)}(kr)\,\sin\theta\,P_n^{1'}(\cos\theta) - jb_n\frac{\hat{H}_n^{(2)'}(kr)P_n^1(\cos\theta)}{\sin\theta}\right] \tag{A-35}$$

$$\sigma = -\frac{E_o}{\eta}\frac{\cos\phi}{c(ka)^2}\sum_{n=1}^{\infty}\frac{j^{-n}(2n+1)}{\hat{H}_n^{(2)'}(ka)}P_n^1(\cos\theta) \tag{A-36}$$

where

J_θ and J_ϕ denote the θ and ϕ-components of the induced surface current density respectively,

E_r^s, E_θ^s, E_ϕ^s denote the r, θ, and ϕ components of the scattered electric field respectively,

σ is the induced surface charge density, and c is the speed of light.

$$a_n = \frac{j^{-n}(2n+1)}{n(n+1)} \tag{A-37}$$

$$b_n = - a_n \frac{\hat{J}_n'(ka)}{\hat{H}_n^{(2)'}(ka)} \tag{A-38}$$

$$c_n = - a_n \frac{\hat{J}_n(ka)}{\hat{H}_n^{(2)}(ka)} \tag{A-39}$$

$$\hat{J}_n(x) = x\, j_n(x) \tag{A-40}$$

$$\hat{H}_n^{(2)}(x) = x\, h_n^{(2)}(x) \tag{A-41}$$

Here, j_n and $h_n^{(2)}$ denote the spherical Bessel function and the spherical Hankel function of the second kind respectively.

The distant scattered field is given by

$$E_\theta^s \xrightarrow[kr\to\infty]{} \frac{jE_o}{kr} e^{-jkr} \cos\phi \sum_{n=1}^{\infty} j^n [b_n \sin\theta\, P_n^{1'}(\cos\theta) - c_n \frac{P_n^1(\cos\theta)}{\sin\theta}] \tag{A-42}$$

$$E_\phi^s \xrightarrow[kr\to\infty]{} \frac{jE_o}{kr} e^{-jkr} \sin\phi \sum_{n=1}^{\infty} j^n [b_n \frac{P_n^1(\cos\theta)}{\sin\theta} - c_n \sin\theta\, P_n^{1'}(\cos\theta)] \tag{A-43}$$

Now if we assume that k is small such that $(ka) \ll 1$, then we have

$$\begin{aligned} \underline{E}^i &= \hat{x}\, E_o (1 - jkz + (jk)^2 \frac{z^2}{2} + \ldots) \\ \underline{H}^i &= \hat{y} \frac{E_o}{\eta} (1 - jkz + (jk)^2 \frac{z^2}{2} + \ldots) \end{aligned} \tag{A-44}$$

Comparing (A-44) and (A-5) we have

$$\underline{E}_o^i = \hat{x}\, E_o = - \nabla(-x\, E_o) \tag{A-45}$$

$$\underline{H}_o^i = \hat{y}\, E_o/\eta \tag{A-46}$$

From (A-16) and (A-45) we have

$$\phi_o^i = - x E_o \tag{A-47}$$

Similarly for small (ka) we obtain

$$J_\theta \cong \frac{E_o}{\eta} \cos \phi [- \frac{3}{2} + (jk) \frac{7a}{3} \cos \theta + \ldots] \tag{A-48}$$

$$J_\phi \cong \frac{E_o}{\eta} \sin \phi [\frac{3}{2} \cos \theta - (jk)a (\frac{3}{2} + \frac{5}{6} \cos 2\theta) + \ldots] \tag{A-49}$$

$$c\sigma \cong \frac{E_o}{\eta} \sin \theta \cos \phi [3 - (jk) \frac{5a}{2} \cos \theta + \ldots] \tag{A-50}$$

Comparing (A-48) - (A-50) with the series representations of $\underline{J}^{ind}$ and σ^{ind} in (A-23), we obtain

$$\underline{J}_o^{ind} = \frac{3}{2} \frac{E_o}{\eta} [- \cos \phi \, \underline{\hat{\theta}} + \cos \theta \sin \phi \, \underline{\hat{\phi}}] , \tag{A-51}$$

$$\underline{J}_1^{ind} = \frac{E_o a}{\eta} [\frac{7}{3} \cos \phi \cos \theta \, \underline{\hat{\theta}} - \sin \phi \, (\frac{3}{2} + \frac{5}{6} \cos 2\theta) \, \underline{\hat{\phi}}], \tag{A-52}$$

and

$$\sigma_o^{ind} = \frac{E_o}{\eta c} 3 \sin \theta \cos \phi \tag{A-53}$$

The symbols $\underline{\hat{\theta}}$ and $\underline{\hat{\phi}}$ denote the unit vectors in the θ and ϕ directions respectively.

Note that

$$\underline{\nabla}_s \cdot \underline{J}_o^{ind} = 0 \tag{A-54}$$

and

$$\underline{\nabla}_s \cdot \underline{J}_1^{ind} = - c\sigma_o^{ind} \tag{A-55}$$

in agreement with (A-24) and (A-25). Observe that σ_o^{ind} of (A-53) is the static charge distribution induced on the sphere due to the impressed static electric field given in (A-45). Using $\underline{J}_o^{ind}$ and σ_o^{ind} given above we compute the induced dipole moments to obtain

$$\underline{P}^{ind} = \iint_{sphere} \sigma_o^{ind}(\underline{r})\, \underline{r}\, ds = \hat{x}\, \frac{E_o}{\eta c}\, 4\pi\, a^3$$

so that

$$\underline{I}\ell = j\omega \underline{P}^{ind} = \hat{x}\, j\, \frac{4\pi\, E_o (ka)^3}{\eta\, k^2} \tag{A-56}$$

and

$$\underline{M}^{ind} = \frac{1}{2} \iint_{sphere} \underline{r} \times \underline{J}_o^{ind}(\underline{r}) ds$$

$$= -\, 2\pi\, a^3\, \frac{E_o}{\eta}\, \hat{y}$$

so that

$$\underline{K}\ell = j\omega\mu_o\, \underline{M}^{ind} = \hat{y}\, \frac{2\pi\, E_o}{jk^2}\, (ka)^3 \tag{A-57}$$

Now consider the distant scattered field. For small (ka), (A-42) and (A-43) reduce to

$$E_\theta^s \xrightarrow[ka\to 0]{kr\to\infty} E_o\, \frac{e^{-jkr}}{kr}\, (ka)^3 \cos\phi\, (\cos\theta - 1/2) \tag{A-58}$$

$$E_\phi^s \xrightarrow[ka\to 0]{kr\to\infty} E_o\, \frac{e^{-jkr}}{kr}\, (ka)^3 \sin\phi\, (\tfrac{1}{2}\cos\theta - 1) \tag{A-59}$$

The field given by (A-58) and (A-59) is the far field of the combination of the dipoles (A-56) and (A-57). This is in agreement with the fact that the scattered far field of a small body can be expressed in terms of an electric and/or a magnetic dipole.

Now consider the expressions given in (A-33) - (A-34). Assume ka is small enough such that

$$b_n \xrightarrow[ka\to 0]{} -\frac{n+1}{n} c_n \xrightarrow[ka\to 0]{} \left[\frac{2^n(n-1)!}{(2n)!}\right]^2 \frac{(ka)^{2n+1}}{j^{n+1}} \qquad \text{(A-60)}$$

Then it is easy to show that for any kr the first term in (A-33) is the field of $\underline{I}^{\ell}$ in (A-56). Hence as ka→0, E_r^s is determined by $\underline{I}^{\ell}$ only. Figure A.2 shows the scattered field E_{θ}^s for the case ka = 0.2. The solid curves represent the exact solution which was obtained by summing the first six terms of (A-34). The dashed curves represent the field of the two dipoles given in (A-56) and (A-57) placed at the origin. The fields are normalized with respect to $E_o \cos \phi$. It is seen from the figure that the exact fields and the dipole fields are in close agreement even at a distance equal to twice the radius. We believe this is due to the symmetrical structure of the sphere.

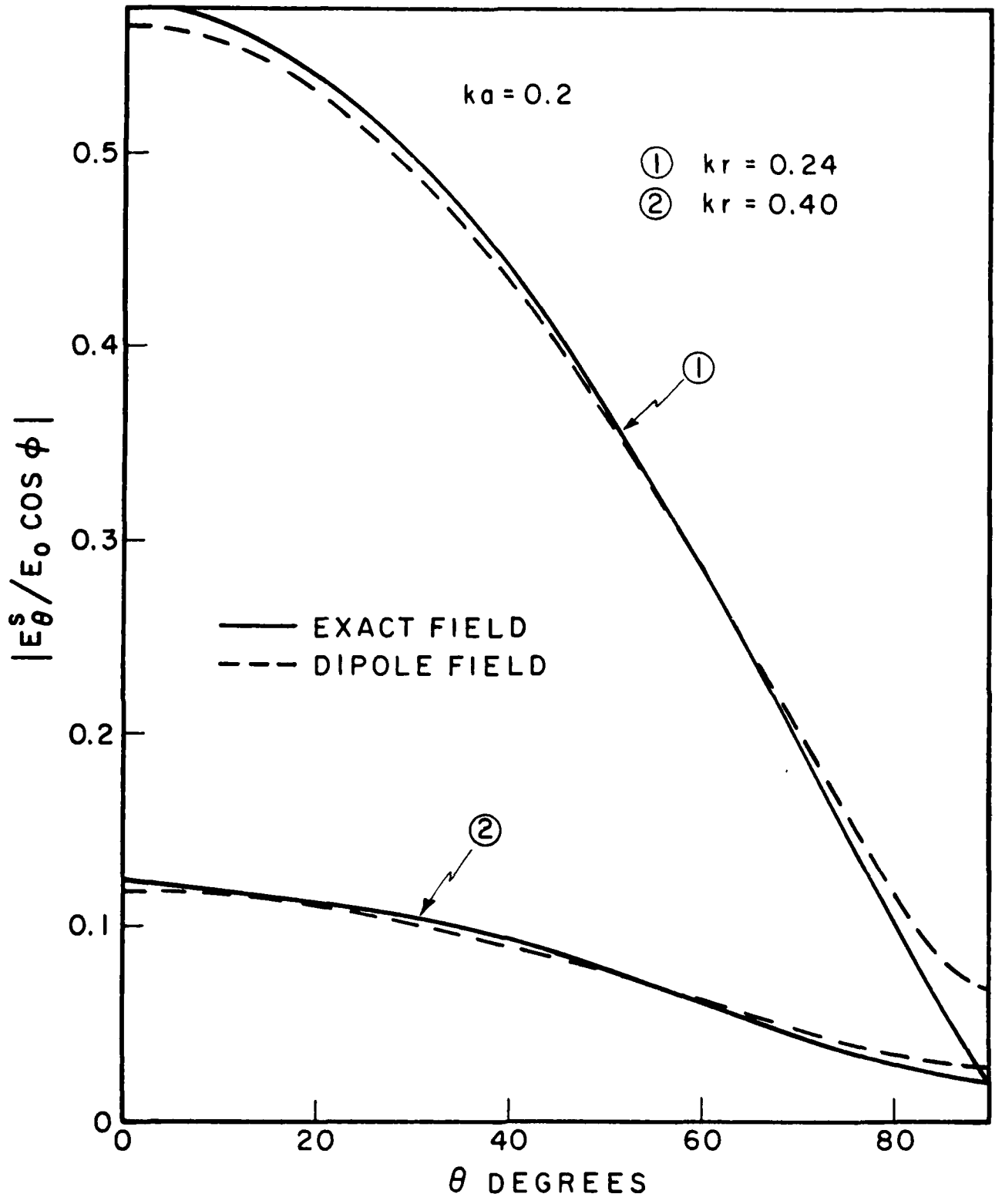

Fig. A.2. Plane wave scattering from a small sphere.

APPENDIX B

DIPOLE REPRESENTATION OF THE FIELDS DUE TO ELECTRIC AND MAGNETIC CURRENTS FLOWING ON A SMALL SURFACE

Consider a time-harmonic surface density of electric current $\underline{J}$ on the surface S whose maximum dimension D is appreciably smaller than the wavelength. This electric current produces an electromagnetic field $(\underline{E}^s,\underline{H}^s)$. For convenience, the coordinate origin is chosen such that the distance r' from the origin to any point on S is less than D. In Appendix B, it is shown that, whenever the distance r to the point of observation of $(\underline{E}^s,\underline{H}^s)$ is large compared with D, $(\underline{E}^s,\underline{H}^s)$ reduces to the electromagnetic field of the combination of an electric dipole and a magnetic dipole, both dipoles being located at the origin. From inspection of this dipole representation of the electromagnetic field $(\underline{E}^s,\underline{H}^s)$ due to the electric current $\underline{J}$, a dipole representation of the electromagnetic field $(\underline{E}^{sm},\underline{H}^{sm})$ due to a magnetic surface current $\underline{J}^m$ on S is easily obtained.

Jones [22, pp. 530-532] has shown that the dipole representation is valid under the more restrictive conditions that S is closed and perfectly conducting and that r is not only large compared with D but also large compared with the wavelength. Not assuming that S is perfectly conducting but assuming that S is closed, Kleinman [23,24], in a long but straightforward presentation, has obtained a dipole representation for the electric field $\underline{E}^s$ far outside S due to an electromagnetic field $(\underline{E},\underline{H})$ existing on S. According to the equivalence principle [4, Sec. 3-5], this $\underline{E}^s$ can be viewed as the electric field due to the combination of the electric surface current $\underline{n} \times \underline{H}$ and the magnetic surface current $\underline{E} \times \underline{n}$ where $\underline{n}$ is the unit vector

which points outward from S. In order to obtain his final result [24, Eqs. (16)-(18)], Kleinman had to assume that r is large compared with the wavelength.

The dipole representations of Appendix B are obtained without assuming that S is perfectly conducting and without assuming that S is closed. These representations are valid whenever r is large compared with D, no matter how r compares with the wavelength.

In search of the dipole representation for the electric field $\underline{E}^s$ due to the electric current $\underline{J}$, we write [4, Eqs. (3-63)]

$$\underline{E}^s = \frac{1}{j\omega\epsilon} (\nabla(\nabla \cdot \underline{A}) + k^2 \underline{A}) \tag{B-1}$$

$$\underline{A} = \frac{1}{4\pi} \iint_S \frac{\underline{J}(\underline{r}') \, e^{-jk|\underline{r}-\underline{r}'|}}{|\underline{r}-\underline{r}'|} \, ds' \tag{B-2}$$

In (B-2), $\underline{r}'$ is the radius vector (from the origin) to the point at which the differential element of area ds' is located and $\underline{r}$ is the radius vector to the point at which $\underline{A}$ is evaluated.

Since $\underline{r}'$ is on S,

$$r' < D \tag{B-3}$$

where r' is the length of the vector $\underline{r}'$. If it is assumed that r, the length of $\underline{r}$, satisfies

$$r >> D \tag{B-4}$$

then

$$r' << r \tag{B-5}$$

Thanks to (B-5), we obtain

$$|\underline{r} - \underline{r}'| \simeq r - \underline{\hat{r}} \cdot \underline{r}' \tag{B-6}$$

$$\frac{1}{|\underline{r} - \underline{r}'|} \simeq \frac{1}{r} \left(1 + \frac{\underline{\hat{r}} \cdot \underline{r}'}{r}\right) \tag{B-7}$$

where $\underline{\hat{r}}$ is the unit vector in the $\underline{r}$ direction. Substitution of (B-6) and (B-7) into (B-2) gives

$$\underline{A} = \frac{e^{-jkr}}{4\pi r} \iint_S \underline{J}(\underline{r}')(1 + \frac{\hat{\underline{r}} \cdot \underline{r}'}{r}) e^{jk\, \hat{\underline{r}} \cdot \underline{r}'}\, ds' \qquad \text{(B-8)}$$

Because D was assumed to be appreciably smaller than the wavelength, it is evident from (B-3) that

$$kr' << 1 \qquad \text{(B-9)}$$

Equation (B-9) authorizes the approximation

$$e^{jk\hat{\underline{r}} \cdot \underline{r}'} \approx 1 + jk\, \hat{\underline{r}} \cdot \underline{r}' \qquad \text{(B-10)}$$

Substituting (B-10) into (B-8) and neglecting the second order term, we obtain

$$\underline{A} = \frac{e^{-jkr}}{4\pi r} \left[\iint_S \underline{J}(\underline{r}')ds' + (jk + \frac{1}{r}) \iint_S (\hat{\underline{r}} \cdot \underline{r}')\, \underline{J}(\underline{r}')ds'\right] \qquad \text{(B-11)}$$

The first integral in (B-11) is called $\underline{I}_1$.

$$\underline{I}_1 = \iint_S \underline{J}(\underline{r}')ds' \qquad \text{(B-12)}$$

The dot product of (B-12) with an arbitrary constant vector $\underline{a}$ is

$$\underline{a} \cdot \underline{I}_1 = \iint_S \underline{a} \cdot \underline{J}(\underline{r}')ds' \qquad \text{(B-13)}$$

Now,

$$\underline{a} = \nabla'(\underline{a} \cdot \underline{r}') \qquad \text{(B-14)}$$

where ∇' is the ∇ operator with respect to the coordinates of $\underline{r}'$. Substitution of (B-14) into (B-13) gives

$$\underline{a} \cdot \underline{I}_1 = \iint_S (\nabla'(\underline{a} \cdot \underline{r}')) \cdot \underline{J}(\underline{r}')ds' \tag{B-15}$$

The form of the integrand in (B-15) suggests the identity [8, Eq. (A-1)]

$$\iint_S \underline{W} \cdot \nabla'\phi ds' = - \iint_S \phi(\nabla'_s \cdot \underline{W})ds' + \int_C \phi(\underline{W} \cdot \underline{u}_b)d\ell' \tag{B-16}$$

In (B-16), $\underline{W}$ is tangent to S, and $\nabla'_s \cdot$ is the surface divergence on S with respect to the coordinates of $\underline{r}'$. If S is closed, the integral over C is to be deleted from (B-16). If S is open, C is the contour that bounds S, $d\ell'$ is the differential element of length along C, and $\underline{u}_b$ is the unit vector tangent to S and normal to C. The direction of $\underline{u}_b$ is away from S. Application of (B-16) to the integral on the right-hand side of (B-15) gives

$$\underline{a} \cdot \underline{I}_1 = - \iint_S (\underline{a} \cdot \underline{r}')\nabla'_s \cdot \underline{J}(\underline{r}')ds' + \int_C (\underline{a} \cdot \underline{r}')(\underline{J}(\underline{r}') \cdot \underline{u}_b)d\ell' \tag{B-17}$$

Since no line charge can exist on C, it follows that

$$\underline{J}(\underline{r}') \cdot \underline{u}_b = 0 \quad \text{on} \quad C \tag{B-18}$$

In view of (B-18) and the fact that $\underline{a}$ is arbitrary, (B-17) implies that

$$\underline{I}_1 = - \iint_S \underline{r}' \nabla'_s \cdot \underline{J}(\underline{r}')ds' \tag{B-19}$$

The second integral in (B-11) is called $\underline{I}_2$.

$$\underline{I}_2 = \iint_S (\hat{\underline{r}} \cdot \underline{r}')\underline{J}(\underline{r}')ds' \tag{B-20}$$

The identity formed by substituting (B-12) for $\underline{I}_1$ in (B-19) is also valid with $\underline{J}(\underline{r}')$ replaced by $(\hat{\underline{r}} \cdot \underline{r}')\underline{J}(\underline{r}')$. As a result,

$$\underline{I}_2 = - \iint_S \underline{r}' \nabla_s' \cdot ((\hat{\underline{r}} \cdot \underline{r}')\underline{J}(\underline{r}'))ds' \tag{B-21}$$

The $\nabla_s' \cdot$ term in (B-21) suggests the identity [8, Eq. (A-4)].

$$\nabla_s' \cdot (\phi \underline{W}) = \underline{W} \cdot \nabla_s' \phi + \phi \nabla_s' \cdot \underline{W} \tag{B-22}$$

In (B-22), $\underline{W}$ is tangent to S, and ∇_s' is the surface gradient on S with respect to the coordinates of $\underline{r}'$. Application of (B-22) to the integrand on the right-hand side of (B-21) gives

$$\underline{I}_2 = - \iint_S \underline{r}'(\underline{J}(\underline{r}') \cdot \nabla_s'(\hat{\underline{r}} \cdot \underline{r}'))ds' - \iint_S \underline{r}'(\hat{\underline{r}} \cdot \underline{r}') \nabla_s' \cdot \underline{J}(\underline{r}')ds' \tag{B-23}$$

Since $\underline{J}(\underline{r}')$ is tangent to S, the surface gradient ∇_s' in (B-23) can be replaced by the ordinary gradient ∇'. Using (B-14) with $\underline{a}$ replaced by $\hat{\underline{r}}$ to simplify this gradient, we obtain

$$\underline{I}_2 = - \iint_S \underline{r}'(\underline{J}(\underline{r}') \cdot \hat{\underline{r}})ds' - \iint_S \underline{r}'(\hat{\underline{r}} \cdot \underline{r}') \nabla_s' \cdot \underline{J}(\underline{r}')ds' \tag{B-24}$$

Next, $\underline{I}_2$ is expressed as half of the sum of the right-hand sides of (B-20) and (B-24).

$$\underline{I}_2 = \frac{1}{2} \iint_S ((\hat{\underline{r}} \cdot \underline{r}')\underline{J}(\underline{r}') - \underline{r}'(\underline{J}(\underline{r}') \cdot \hat{\underline{r}}))ds' - \frac{1}{2} \iint_S \underline{r}'(\hat{\underline{r}} \cdot \underline{r}')\nabla_s' \cdot \underline{J}(\underline{r}')ds' \tag{B-25}$$

Thanks to the vector identity [4, last of Eqs. (A-13)], the integrand of the first integral on the right-hand side of (B-25) is $-\hat{\underline{r}} \times (\underline{r}' \times \underline{J})$. As a result, (B-25) becomes

$$\underline{I}_2 = -\frac{1}{2}\,\hat{\underline{r}} \times \iint_S \underline{r}' \times \underline{J}(\underline{r}')ds' - \frac{1}{2}\iint_S \underline{r}'(\hat{\underline{r}} \cdot \underline{r}')\nabla_s' \cdot \underline{J}(\underline{r}')ds' \tag{B-26}$$

The equation of continuity is

$$\nabla_s' \cdot \underline{J}(\underline{r}') = -j\omega\sigma(\underline{r}') \tag{B-27}$$

where σ is the surface density of electric charge on S. In view of (B-27), substitution of (B-19) and (B-26) into (B-11) gives

$$\underline{A} = \frac{e^{-jkr}}{4\pi r}\left[j\omega \iint_S \underline{r}'\,\sigma(\underline{r}')(1 + \frac{1}{2}(jk + \frac{1}{r})(\hat{\underline{r}} \cdot \underline{r}'))ds' - \right.$$

$$\left.(jk + \frac{1}{r})\,\hat{\underline{r}} \times \frac{1}{2}\iint_S \underline{r}' \times \underline{J}(\underline{r}')ds'\right] \tag{B-28}$$

It is evident from (B-5) and (B-9) that

$$\left|\frac{1}{2}\,(jk + \frac{1}{r})(\hat{\underline{r}} \cdot \underline{r}')\right| << 1 \tag{B-29}$$

As a result, (B-28) reduces to

$$\underline{A} = \frac{e^{-jkr}}{4\pi r}\left[j\omega \iint_S \underline{r}'\sigma(\underline{r}')ds' - (jk + \frac{1}{r})\hat{\underline{r}} \times \frac{1}{2}\iint_S \underline{r}' \times \underline{J}(\underline{r}')ds'\right] \tag{B-30}$$

If $kr >> 1$, (B-30) reduces to the electric and magnetic dipole terms in [25, Eq. (14) without the factor μ_o]. Expression (B-30) can be rewritten as

$$\underline{A} = \frac{e^{-jkr}}{4\pi r}\,j\omega \iint_S \underline{r}'\,\sigma(\underline{r}')ds' + (\nabla\,\frac{e^{-jkr}}{4\pi r}) \times \frac{1}{2}\iint_S \underline{r}' \times \underline{J}(\underline{r}')ds' \tag{B-31}$$

Thanks to the vector identity [4, sixth of Eqs. (A-14)], (B-31) becomes

$$\underline{A} = \hat{\underline{A}} + \frac{1}{j\omega\mu} \nabla \times \hat{\underline{F}} \tag{B-32}$$

where

$$\hat{\underline{A}} = \frac{e^{-jkr}}{4\pi r} j\omega \iint_S \underline{r}' \, \sigma(\underline{r}')ds' \tag{B-33}$$

$$\hat{\underline{F}} = \frac{e^{-jkr}}{4\pi r} \frac{j\omega\mu}{2} \iint_S \underline{r}' \times \underline{J}(\underline{r}')ds' \tag{B-34}$$

Substituting (B-32) for $\underline{A}$ in (B-1), we obtain

$$\underline{E}^s = \frac{1}{j\omega\varepsilon} (\nabla(\nabla \cdot \hat{\underline{A}}) + k^2\hat{\underline{A}}) - \nabla \times \hat{\underline{F}} \tag{B-35}$$

According to [4, first of Eqs. (3-83)], the right-hand side of (B-35) is the electric field of the combination of the magnetic vector potential $\hat{\underline{A}}$ and the electric vector potential $\hat{\underline{F}}$. Now, (B-33) can be expressed as

$$\hat{\underline{A}} = \underline{I\ell} \frac{e^{-jkr}}{4\pi r} \tag{B-36}$$

where

$$\underline{I\ell} = j\omega \iint_S \underline{r}' \, \sigma(\underline{r}')ds' \tag{B-37}$$

Since $\hat{\underline{A}}$ is a magnetic vector potential, $\underline{I\ell}$ can be viewed as an electric current element located at the origin. Equation (B-34) is recast as

$$\hat{\underline{F}} = \underline{K\ell} \frac{e^{-jkr}}{4\pi r} \tag{B-38}$$

where

$$\underline{K\ell} = \frac{j\omega\mu}{2} \iint_S \underline{r}' \times \underline{J}(\underline{r}')ds' \tag{B-39}$$

Since $\hat{\underline{F}}$ is an electric vector potential, $\underline{K\ell}$ can be viewed as a magnetic current element located at the origin.

Substituting (B-36) and (B-38) for $\hat{\underline{A}}$ and $\hat{\underline{F}}$ in (B-35), we obtain

$$\underline{E}^s = \frac{1}{4\pi j\omega\epsilon}\left(\nabla\left(\nabla\cdot\frac{\underline{I\ell}\ e^{-jkr}}{r}\right) + k^2\frac{\underline{I\ell}\ e^{-jkr}}{r} - j\omega\epsilon\nabla\times\frac{\underline{K\ell}\ e^{-jkr}}{r}\right) \qquad \text{(B-40)}$$

When the differential operations in (B-40) are performed, (B-40) expands to

$$\underline{E}^s = \frac{e^{-jkr}}{4\pi j\omega\epsilon r}\left[k^2(\hat{\underline{r}}\times\underline{I\ell})\times\hat{\underline{r}} + \left(\frac{jk}{r}+\frac{1}{r^2}\right)(3(\underline{I\ell}\cdot\hat{\underline{r}})\hat{\underline{r}}-\underline{I\ell}) + j\omega\epsilon\left(jk+\frac{1}{r}\right)(\hat{\underline{r}}\times\underline{K\ell})\right] \qquad \text{(B-41)}$$

According to (B-35), the electric field $\underline{E}^s$ due to $\underline{J}$ is the electric field due to the combination of $\hat{\underline{A}}$ and $\hat{\underline{F}}$. Hence, the magnetic field $\underline{H}^s$ due to $\underline{J}$ must be the magnetic field due to the combination of $\hat{\underline{A}}$ and $\hat{\underline{F}}$. This magnetic field is given by [4, second of Eqs. (3-83)]

$$\underline{H}^s = \frac{1}{j\omega\mu}\left(\nabla(\nabla\cdot\hat{\underline{F}}) + k^2\hat{\underline{F}}\right) + \nabla\times\hat{\underline{A}} \qquad \text{(B-42)}$$

Substituting (B-36) and (B-38) for $\hat{\underline{A}}$ and $\hat{\underline{F}}$ in (B-42), we obtain

$$\underline{H}^s = \frac{1}{4\pi j\omega\mu}\left(\nabla\left(\nabla\cdot\frac{\underline{K\ell}\ e^{-jkr}}{r}\right) + k^2\frac{\underline{K\ell}\ e^{-jkr}}{r} + j\omega\mu\nabla\times\frac{\underline{I\ell}\ e^{-jkr}}{r}\right) \qquad \text{(B-43)}$$

Since (B-43) is similar to (B-40), it is evident from inspection of (B-41) that (B-43) expands to

$$\underline{H}^s = \frac{e^{-jkr}}{4\pi j\omega\mu r}\left[k^2(\hat{\underline{r}}\times\underline{K\ell})\times\hat{\underline{r}} + \left(\frac{jk}{r}+\frac{1}{r^2}\right)(3(\underline{K\ell}\cdot\hat{\underline{r}})\hat{\underline{r}}-\underline{K\ell}) - j\omega\mu\left(jk+\frac{1}{r}\right)(\hat{\underline{r}}\times\underline{I\ell})\right] \qquad \text{(B-44)}$$

An electric charge dipole $\underline{P}$ is implicitly defined in terms of $\underline{I\ell}$ by

$$\underline{I\ell} = j\omega\underline{P} \qquad \text{(B-45)}$$

The factor $j\omega$ appears in (B-45) because electric current is the product of $j\omega$ with electric charge. For brevity, $\underline{P}$ is called an electric dipole.

Alternatively, $\underline{P}$ can be called the electric dipole moment of the electric current $\underline{J}$. Comparison of (B-45) with (B-37) gives

$$\underline{P} = \iint_S \underline{r}' \, \sigma(\underline{r}')ds' \tag{B-46}$$

where σ is the electric charge associated with $\underline{J}$.

A magnetic pole charge dipole $\underline{M}$ is implicitly defined in terms of $\underline{K\ell}$ by

$$\underline{K\ell} = j\omega\mu \, \underline{M} \tag{B-47}$$

Magnetic pole charge is magnetic charge divided by μ. The factor $j\omega\mu$ appears in (B-47) because magnetic current is the product of $j\omega\mu$ with magnetic pole charge. For brevity, $\underline{M}$ is called a magnetic dipole. Alternatively, $\underline{M}$ can be called the magnetic dipole moment of the electric current $\underline{J}$. Comparison of (B-47) with (B-39) gives

$$\underline{M} = \frac{1}{2} \iint_S \underline{r}' \times \underline{J}(\underline{r}')ds' \tag{B-48}$$

Consider a surface density of magnetic current $\underline{J}^m$ on S. The electric field $\underline{E}^{sm}$ due to $\underline{J}^m$ is given by [4, Eqs. (3-4) and (3-5)]

$$\underline{E}^{sm} = -\nabla \times \underline{F} \tag{B-49}$$

$$\underline{F} = \frac{1}{4\pi} \iint_S \frac{\underline{J}^m(\underline{r}') \, e^{-jk|\underline{r}-\underline{r}'|}}{|\underline{r}-\underline{r}'|} ds' \tag{B-50}$$

On the other hand, the magnetic field $\underline{H}^s$ due to the electric current $\underline{J}$ is given by [4, Eqs. (3-4) and (3-5)]

$$\underline{H}^s = \nabla \times \underline{A} \tag{B-51}$$

where $\underline{A}$ is given by (B-2). The pair of equations (B-49) and (B-50) is similar to the pair of equations (B-51) and (B-2). If the $\underline{E}^{sm}$ in (B-49)

and (B-50) is called $\underline{E}^{sm}(\underline{J}^m)$ and if the $\underline{H}^s$ in (B-51) and (B-2) is called $\underline{H}^s(\underline{J})$, then

$$\underline{E}^{sm}(\underline{J}^m) = - \underline{H}^s(\underline{J}^m) \tag{B-52}$$

Directed by (B-52), we reverse the sign of the right-hand side of (B-44) and replace $\underline{J}$ by $\underline{J}^m$ therein to obtain

$$\underline{E}^{sm} = \frac{e^{-jkr}}{4\pi j\omega\varepsilon r}\left[k^2(\hat{r}\times \underline{I\ell}^m)\times\hat{r} + (\frac{jk}{r}+\frac{1}{r^2})(3(\underline{I\ell}^m\cdot\hat{r})\hat{r} - \underline{I\ell}^m) + j\omega\varepsilon(jk+\frac{1}{r})(\hat{r}\times\underline{K\ell}^m)\right] \tag{B-53}$$

where

$$\underline{I\ell}^m = - \frac{j\omega\varepsilon}{2}\iint_S \underline{r}'\times\underline{J}^m(\underline{r}')ds' \tag{B-54}$$

$$\underline{K\ell}^m = j\omega\iint_S \underline{r}'\,\sigma^m(\underline{r}')ds' \tag{B-55}$$

In (B-55), σ^m is the surface density of magnetic charge associated with $\underline{J}^m$.

$$\nabla_s'\cdot\underline{J}^m(\underline{r}') = - j\omega\sigma^m(\underline{r}') \tag{B-56}$$

Note that $\underline{E}^{sm}$ of (B-53) is $\underline{E}^s$ of (B-41) with $\underline{I\ell}$ and $\underline{K\ell}$ replaced by $\underline{I\ell}^m$ and $\underline{K\ell}^m$, respectively. Hence, the magnetic field $\underline{H}^{sm}$ due to $\underline{J}^m$ can be obtained from inspection of (B-44).

$$\underline{H}^{sm} = \frac{e^{-jkr}}{4\pi j\omega\mu r}\left[k^2(\hat{r}\times\underline{K\ell}^m)\times\hat{r} + (\frac{jk}{r}+\frac{1}{r^2})(3(\underline{K\ell}^m\cdot\hat{r})\hat{r} - \underline{K\ell}^m) - j\omega\mu(jk+\frac{1}{r})(\hat{r}\times\underline{I\ell}^m)\right] \tag{B-57}$$

An electric charge dipole $\underline{P}^m$ is implicitly defined in terms of $\underline{I\ell}^m$ by

$$\underline{I\ell}^m = j\omega\underline{P}^m \tag{B-58}$$

Comparison of (B-58) with (B-54) gives

$$\underline{P}^m = -\frac{\varepsilon}{2} \iint_S \underline{r}' \times \underline{J}^m(\underline{r}')ds' \tag{B-59}$$

A magnetic pole charge dipole $\underline{M}^m$ is implicitly defined in terms of $\underline{K\ell}^m$ by

$$\underline{K\lambda}^m = j\omega\mu \, \underline{M}^m \tag{B-60}$$

Comparison of (B-60) with (B-55) shows that

$$\underline{M}^m = \frac{1}{\mu} \iint_S \underline{r}' \, \sigma^m(\underline{r}')ds' \tag{B-61}$$

REFERENCES

[1] R. E. Kleinman, "The Rayleigh Region ," Proc. IEEE, vol. 53, pp. 848-856, August 1965.

[2] Lord Rayleigh, "On the Incidence of Aerial and Electric Waves upon Small Obstacles in the Form of Ellipsoids or Elliptic Cylinders, and on the Passage of Electric Waves through a Circular Aperture in a Conducting Screen," Phil. Mag., vol. 44, pp. 28-52, 1897.

[3] C. J. Bouwkamp, "Diffraction Theory," Rep. Prog. Phys., vol. 17, pp. 35-100, 1954.

[4] R. F. Harrington, Time Harmonic Electromagnetic Fields, McGraw-Hill, New York, 1961.

[5] R. E. Collin, Field Theory of Guided Waves, McGraw-Hill, New York, pp. 294-298, 1960.

[6] H. A. Bethe, "Theory of Diffraction by Small Holes," Phys. Rev., vol. 66, pp. 163-182, 1944.

[7] R. F. Harrington, Field Computation by Moment Methods, Macmillan Company, New York, 1968.

[8] J. R. Mautz and R. F. Harrington, "A New E-field Solution for a Conducting Surface Small or Comparable to the Wavelength," Tech. Rept., ECE Dept., Syracuse University, September 1982.

[9] S. M. Rao, A. W. Glisson, D. R. Wilton, and B. Vidula, "A Simple Numerical Solution Procedure for Statics Problems Involving Arbitrary-shaped Surfaces," IEEE Trans. AP, vol. AP-27, pp. 604-608, Sept. 1979.

[10] E. E. Okon and R. F. Harrington, "The Polarizabilities of Electrically Small Apertures of Arbitrary Shape," IEEE Trans. EMC, vol. EMC-23, pp. 359-366, November 1981.

[11] F. De Meulenaere and J. Van Bladel, "Polarizability of Some Small Apertures," IEEE Trans. AP, vol. AP-25, March 1977.

[12] P.Lorrain and D. Corson, Electromagnetic Fields and Waves, W. H. Freeman and Company, San Francisco, 1970.

[13] W. H. Eggimann, "Higher-Order Evaluation of Electromagnetic Diffraction by Circular Disks," IRE Trans. MTT, vol. MTT-9, pp.408-418, Sept. 1961.

[14] S. M. Rao, D. R. Wilton, and A. W. Glisson, "Electromagnetic Scattering by Surfaces of Arbitrary Shape," IEEE Trans. AP, vol. AP-30, pp. 409-418, May 1982.

[15] J. A. Stratton, Electromagnetic Theory, McGraw-Hill, New York, 1941.

[16] J. J. Bowman, T. B. A. Senior, and P.L.E. Uslenghi, Electromagnetic and Acoustic Scattering by Simple Shapes, Amsterdam: North-Holland. 1969.

[17] K. A. Lur'e, "Diffraction of a Plane Electromagnetic Wave on an Ideally Conducting Circular Disc," Tech. Phys. Soviet Phys., pp. 1313-1325, June 1960.

[18] Chang-Yu Wu, "Field Distribution Inside a Box with Aperture," Ph. D. Dissertation, ECE Dept., Syracuse University, 1977.

[19] J. J. Wang and C. J. Drane, "Numerical Analysis of Arbitrarily Shaped Bodies Modeled by Surface Patches," IEEE Trans. MTT,vol. MTT-30, pp. 1167-1173, August 1982.

[20] A. F. Stevenson, "Solution of Electromagnetic Scattering Problems as Power Series in the Ratio (Dimension of Scatterer)/Wavelength," J. Appl. Phys., vol. 24, pp. 1134-1142, 1953.

[21] R. E. Kleinman, "Low Frequency Solution of Electromagnetic Scattering Problems," in Electromagnetic Wave Theory (Delft Symposium), Pergamon Press, Oxford, pp. 891-905, 1967.

[22] D. S. Jones, The Theory of Electromagnetism, Pergamon Press, New York, 1964.

[23] R. E. Kleinman, "Far Field Scattering at Low Frequencies," Appl. Sci. Res., vol. 18, pp. 1-8, August 1967.

[24] R. E. Kleinman, "Dipole Moments and Near Field Potentials," Appl. Sci. Res., vol. 27, pp. 335-340, April 1973.

[25] J. Van Bladel, "The Multipole Expansion Revisited," AEU, vol. 31, pp. 407-411, October 1977.